January 2015

Critical Evaluations Of Modis And Misr Satellite Aerosol Products For Aerosol Modeling Applications

Yingxi Shi

CRITICAL EVALUATIONS OF MODIS AND MISR SATELLITE
AEROSOL PRODUCTS FOR AEROSOL MODELING
APPLICATIONS

by

Yingxi Shi
Bachelor of Science, Sun Yat-sen University, 2006
Master of Science, University of North Dakota, 2009

A Dissertation
Submitted to the Graduate Faculty

of the

University of North Dakota

in partial fulfillment of the requirements

for the degree of

Doctor of Philosophy

Grand Forks, North Dakota
December
2015

This dissertation, submitted by Yingxi Shi in partial fulfillment of the requirements for the Degree of Doctor of Philosophy from the University of North Dakota, has been read by the Faculty Advisory Committee under whom the work has been done and is hereby approved.

_____
Jianglong Zhang
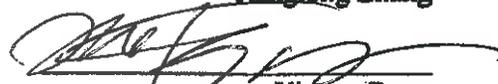
_____
Xiquan Dong

_____
. Mark A. Askelson
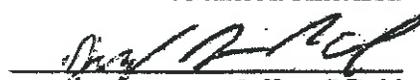
_____
Jeffrey S Reid

_____
N. Christina Hsu

_____
Yun Ji

This dissertation is being submitted by the appointed advisory committee as having met all of the requirements of the School of Graduate Studies at the University of North Dakota and is hereby approved.

_____
Dean of the Graduate School: Wayne Swisher

_____
December 14, 2015
Date

iii

PERMISSION

Title   Critical Evaluations of MODIS and MISR Satellite Aerosol Products for Aerosol Modeling Applications

Department   Atmospheric Sciences

Degree   Doctor of Philosophy

      In presenting this dissertation in partial fulfillment of the requirements for a graduate degree from the University of North Dakota, I agree that the library of this University shall make it freely available for inspection. I further agree that permission for extensive copying for scholarly purposes may be granted by the professor who supervised my dissertation work or, in his absence, by the chairperson of the department or the dean of the Graduate School. It is understood that any copying or publication or other use of this dissertation or part thereof for financial gain shall not be allowed without my written permission. It is also understood that due recognition shall be given to me and to the University of North Dakota in any scholarly use which may be made of any material in my dissertation.

Signature   _____

                                  Yingxi Shi

Date   _____

                           December 1st 2015

TABLE OF CONTENTS

LIST OF FIGURES

LIST OF TABLES

ACKNOWLEDGEMENTS

This work would never have been completed without the guidance from my committee members, assistance from individuals outside the university, and support from my family. First and foremost, I want to thank my advisor, Dr. Jianglong Zhang for his excellent guidance. Jianglong was a caring mentor who went above and beyond to help me become an independent researcher. His hard work and attention to detail influenced me greatly. He was extremely patient with me, especially through versions of writings and corrections. Jianglong also taught me the importance of networking as he provided me as many chances as possible to interact with other scientists and made it possible for me to complete my work at the University of Washington. Beyond that, he also encouraged me to pursue a work-life-balance. Without his support, I would not have been able to reach so many milestones in my life during my PhD study.

I would also like to thank my dissertation committee of Dr. Jeffrey Reid, Dr. Christina Hsu, Dr. Xiquan Dong, Dr. Mark Askelson, and Dr. Yun Ji. Dr. Reid envisioned the direction of my research and provided insightful advice throughout the course of my work. Dr. Dong, along with Dr. Baike Xi, treated me as his own student from the beginning and believed in me when I was at the lowest point of my life. I will always remember the holidays that I spent in Xiquan's and Baike's houses, which were much-needed breaks from the intense work, not to mention the opportunities to taste delicious homemade food. Dr. Hsu hosted my visit in Goddard for two summers,

ABSTRACT

The study of uncertainties in satellite aerosol products is essential to aerosol data assimilation and modeling efforts. In this study, with the assistance of ground-based observations, uncertainties in Moderate Resolution Imaging Spectroradiometer (MODIS) collection 5 Deep Blue (DB), Multi-Angle Imaging Spectroradiometer (MISR) version 22 aerosol products, and the newly released collection 6 Dark Target over-ocean and DB products were evaluated. For each product, systematic biases were analyzed against observing conditions. Empirical correction procedures and data filtering steps were generated to develop noise and bias reduced DA-quality aerosol products for modeling related applications.

Special attention was also directed at the potential low bias in satellite aerosol optical depth (AOD) climatology due to misclassification of aerosols as clouds over Asia. A heavy aerosol identifying system (HAIS) was developed through the combined use of the Ozone Monitoring Instrument (OMI) and Cloud-Aerosol Lidar with Orthogonal Polarization (CALIOP) products for detecting heavy smoke aerosol plumes. Upon extensive evaluation, HAIS was applied to one year of collocated OMI, CALIOP, and MODIS data to study the misclassifications related low bias. This study suggests that the misclassification of heavy smoke aerosol plumes by MODIS is rather infrequent and thus introduces an insignificant low bias to its AOD climatology. Still, this study confirms that misclassification happens in both active- and passive-based satellite aerosol products and needs to be studied for forecasting these events.

CHAPTER I

INTRODUCTION

Atmospheric aerosols, which are small particles in air, can affect atmospheric radiation in the short-wave and long-wave spectrums (Kaufman et al., 2002). As of which, the study of atmospheric aerosol properties and their spatial and temporal distributions is of an interest to both the climate and visibility forecasting communities. Aerosols take a multitude of forms, from mostly naturally generated aerosols such as sea salt, desert dust, and microbial particles to anthropogenic aerosols such as sulfate aerosols and smoke from agriculture burning and fossil fuel consumption. Aerosol particles, based on their formation, can also be separated into primary aerosol particles, which are emitted directly into the atmosphere, and secondary aerosol particles, which undergo gas to particle formation. The global distribution of aerosol particles depends highly on their source region due to their relatively short lifetime ranging from one to several days (Blifford et al., 1952; Haxeland Schumann, 1955; Balkanski et al., 1993; Rodhe 1999; Giorgi and Chameides, 1986; Williams et al., 2002). However, studies have shown that aerosol particles can be transported a long distance such as from Asia to North America (VanCuren and Cahill, 2002; Husar et al., 2001; Jaffe et al., 1999; Duce et al., 1980). Volcanic aerosols are a significant exception, however. Once the volcanic aerosol particles get inserted into the stratosphere, it can take up to four years for the aerosol concentrations in the stratosphere to return to their background value (Minnis et al.,

1993; McCormick et al., 1995). Thus, currently, satellite remote sensing is the only means that can provide contemporary global aerosol observation with good spatial and temporal data coverage.

In the past, spatial distributions of atmospheric aerosol particles have been studied using both passive-based and active-based satellite observations such as those from the Advanced Very High Resolution Radiometer (AVHRR), the Geostationary Operational Environmental Satellite system (GOES), the Total Ozone Mapping Spectrometer (TOMS), the Sea-viewing Wide Field-of-View Sensor (SeaWiFS), the Moderate Resolution Imaging Spectraradiometer (MODIS), the Multi-angle Imaging Spectralradiometer (MISR), the Ozone Monitoring Instrument (OMI), the Cloud-Aerosol Lidar and Infrared Pathfinder Satellite Observations (CALIPSO), and the newly launched Visible Infrared Imaging Radiometer Suite (VIIRS). Among these sensors, three satellite aerosol products from MODIS and MISR are widely used among the community, including the MODIS Dark Target (DT), MODIS Deep Blue (DB), and the MISR aerosol products, due to their consistent data quality and their ability to provide global data coverage on a daily to weekly basis.

Using aerosol products from MODIS and MISR, various researchers have attempted to investigate aerosol direct and indirect climate effects. For example, utilizing collocated broadband observations from the Clouds and the Earth's Radiant Energy System (CERES) and/or MODIS DT aerosol products, clear sky aerosol direct radiative effects (DRE) have been studied over global oceans (e.g. Loeb and Manalo-Smith, 2005; Zhang et al., 2005a, b; Bellouin et al., 2005; Zhang and Christopher, 2003). Studies have also been conducted in which both satellite

observations and model simulations are used to estimate direct aerosol forcing (e.g. Yu et al., 2006). Some researchers have extended satellite-based aerosol forcing studies to estimate the anthropogenic portion of aerosol radiative effects (e.g. Kaufman et al., 2005; Christopher et al., 2006). Satellite aerosol data have also been used to study aerosol indirect effects, which involve changing cloud properties due to aerosol particle interactions (e.g. Quaas et al., 2008; Quaas et al., 2006; Lohmann and Feichter, 2005; Sekiguchi et al., 2003).

Using near real time satellite aerosol data, and especially aerosol products from MODIS and MISR, efforts have also been directed at assimilating these data into numerical models to improve atmospheric aerosol forecasts through either variation-based or ensemble-based methods. For example, schemes/methods have been developed for directly assimilating satellite aerosol optical depth (AOD, τ) (e.g., Zhang et al., 2008a; Yu et al., 2003); aerosol vertical profiles from lidar instruments (e.g., Uno et al., 2008; Sekiyama et al., 2010; Zhang et al., 2011), and multi-wavelength corrected top of atmosphere radiances into these models (Weaver et al., 2007). In particular, due to their relative simplicity in application, level 2 aerosol products have been used widely in operational centers for aerosol forecasts (e.g. Zhang et al., 2008a; Benedetti et al., 2009). Still, these level 2 satellite aerosol products do have errors. Kahn et al. (2010) and Shi et al. (2011a) show that large discrepancies exist between collection 5 (c5) DT and MISR version 22 (v22) operational aerosol products, which, as mentioned before, are the two most popular satellite aerosol products.

Efforts have been directed at exploring differences between the MISR and MODIS aerosol products (e.g. Kahn et al, 2009; Shi et al., 2011b) and further understanding uncertainties associated within each product. Zhang and Reid (2006) first explored uncertainties within the collection 4 (c4) DT over-ocean products as functions of observational conditions. Extending the effort from Zhang and Reid (2006), this author evaluated the level-2 c5 DT over-ocean aerosol product, and developed a data-assimilation quality (DA-quality) c5 DT level 3 over-ocean product. This product has been used operationally in the Navy's aerosol forecasting system (Shi et al., 2011a). Hyer et al. (2011) studied the c5 DT over-land product and found that complex surface features and regional biases in aerosol microphysical properties are the main sources of uncertainties for the operational DT aerosol products, whereas uncertainties due to viewing geometry and snow contamination are also noticeable. Kahn et al. (2009 and 2010) determined that biases and uncertainties in MISR v22 AOD values are associated with cloud contamination, lower boundary conditions in some locations, and lack of an aerosol model to represent the regions where dust and smoke mixtures are present.

While previous research efforts have focused on understanding major bias in MODIS c4 and c5 DT aerosol products, efforts are also needed to evaluate MODIS DB and MISR aerosol products for their applications in aerosol data assimilation. Also, the collection 6 (c6) DT and DB aerosol products were released recently with new changes applied. Thus, it is also necessary to revisit the DT/DB product-based analysis. This effort focuses on critically evaluating uncertainties within the MODIS and MISR satellite aerosol products and generating bias-reduced and further quality

controlled aerosol products for applications that require high quality aerosol satellite data. In sequence, the collection 5.1 (referred to c5 DB afterwards) and c6 DB over land product and the MISR aerosol products were studied. As an overview, the problematic regions were identified through the inter-comparisons between MODIS and MISR products within and outside of ground truth sites. For each product, potential uncertainty sources were then analyzed against observational conditions in order to discover systematic biases. Based on these analyses, empirical correction procedures and several noisy-data filters were generated in order to develop the corresponding Data Assimilation (DA)-quality aerosol products. At last, these data were aggregated into a level-3 product for modeling applications. These products, although aimed for aerosol DA uses, are suitable for other aerosol related studies that require quality-assured data. After generating the individual global level-3 aerosol products, as the last part of this study an investigation of heavily polluted regions such as Asia was performed. This was conducted to estimate the under-sampling of heavy aerosol events using combined active and passive observations.

A total of eight chapters are included in this dissertation. Chapter II introduces datasets that are used in this study. Chapter III highlights issues in MODIS and MISR aerosol products through inter-comparisons of collocated MODIS and MISR aerosol products. Chapters IV through VI provide detailed analyses of c5.1 and c6 DB, and v22 MISR aerosol products. In Chapter VII, the impact of misclassification of aerosol plumes as clouds is evaluated over Asia. The results are summarized in Chapter VIII.

CHAPTER II

DATASET

This section contains detailed discussions of the data that are used in this study. The operational level 2 MODIS and MISR aerosol products that were studied and analyzed include MODIS c5 and c6 Dark Target over ocean and over land, MODIS c5 and c6 Deep Blue, and MISR v22 over land and ocean. To assist the analysis, additional datasets are also used, which include the AERONET aerosol product, MODIS cloud mask products, OMIUV aerosol index data, CALIOP level 1B data and aerosol profile products, and NOGAPS modeled wind speed data.

2.1 MODIS Aerosol Products

Both Aqua and Terra satellites carry the MODIS instrument. With a total of 36 spectral channels that have spatial resolutions ranging from 250 m to 1 km, observations from MODIS can be used for studying aerosols and clouds. Currently there are two operational MODIS aerosol products (DT and DB) available for climate and modeling applications. The DT algorithm is applicable over visibly dark surfaces such as oceans, and low albedo land surfaces. The original DB algorithm, by taking advantage of relatively dark surface reflectivity at the blue channel, provides retrievals over bright surfaces such as desert regions. Both MODIS level 2.0 DT and DB aerosol products have a spatial resolution of 10 kilometers. In this study, only

DT over-ocean and DB over-land products were evaluated. The evaluation of over-land DT products was performed by a separate study (Hyer et al., 2011).

In 2000, the first version of the DT aerosol product was released for public access, after which improvements to the retrieval algorithms have been made continually (Kaufman et al., 1997; Tanré et al., 1997). MODIS c5 DT and DB products were released in 2007 (Remer et al., 2005) and possibly are the most widely used versions to date. A portion of MODIS c6 DT and DB products were released in late 2014 and the remaining portions were released early this year (Levy et al., 2013). Thus, both c5 and c6 MODIS DT and DB data were used in this study.

2.1.1 MODIS DT Over-ocean Aerosol Products

The DT over ocean aerosol retrieval algorithm is applied when all observations within a 10×10 km grid are marked as ocean pixels. Pixels that are not suitable for retrievals are removed, including those flagged as cloudy, or within glint regions (within 40° glint angle) (Levy et al., 2003). To exclude cloudy pixels, the MODIS cloud mask product (Platnick et al., 2003; Gao et al., 2002) is used with additional spatial variability based cloud screening steps (Remer et al., 2005). After excluding cloudy pixels and those within glint regions, the top and bottom 25% of pixels based on brightness at 0.86 μm are removed. If there are at least 10 pixels left within a 10×10 km grid after the filtering steps, then inversion is performed based on the look-up table (LUT) method using radiance observations from six wavelengths ranging from 0.47 to 2.13 μm. The LUT was generated by tabulating simulated satellite radiances as functions of aerosol microphysical properties, such as aerosol effective radius, single scattering albedo, asymmetry factor, phase function and AOD,

and observing conditions, such as viewing geometries. The retrieval process is then performed by choosing the best fit of the calculated LUT radiances with those observed at top of atmosphere (TOA).

There are nine standardized aerosol models used in the c5 over-ocean retrieval algorithm: four fine modes and five coarse modes (Remer et al., 2005). One fine and one coarse model are selected during the retrieval process when the minimum difference between LUT and observed radiances is achieved. This approach is based on the assumption that aerosol particles are in a bi-model distribution. Uncertainties occur when inaccurate representations of aerosol microphysical properties are used following this assumption. There are other assumptions that can introduce uncertainties within the aerosol products. For example, in the c5 DT over-ocean algorithm, all radiances within the LUT are calculated using a 6 m s^{-1} near-surface wind speed (Remer et al., 2005). The wind speed alters the ocean surface reflectance, which ultimately influences the estimation of the radiance contribution from aerosols. One major update in the c6 DT over-ocean aerosol product is that the wind dependency of surface reflectance is taken into account (Levy et al., 2010). Incremental adjustments are also made to thresholds and formulas for cloud screening in the c6 DT algorithm. Adjustments in selecting the clear sky pixels have been implemented in the c6 MODIS cloud mask product (Personal communication with Dr. Levy, 2013). Thus, corresponding adjustments are made in the DT aerosol retrieval algorithm to mediate this change in the c6 MODIS cloud mask product.

Corrections were applied to level 1B Terra MODIS data to account for calibration drift, especially for the blue and red bands (Sayer et al., 2015). The

changes in upstream radiance data will inevitably affect aerosol retrievals. For example, Levy et al. (2013) reported an increase in over-land AOD of 0.02 and an increase of 0.004 for over-ocean AODs due to this change in radiance calibration.

The ultimate output parameters from the inversion are AODs (at 7 wavelengths, including the commonly used AOD at 0.55 μm) and the fine mode fraction (η), which denotes the percentage of contribution from retrieved fine and coarse mode aerosols. The reported uncertainties of the DT AOD data are 0.03 ± 0.05 × τ over ocean and 0.05 ± 0.15 × τ over land for both c5 and c6 DT products when validated against AERONET (Remer et al., 2005; Levy et al., 2013).

Other than AOD, MODIS DT aerosol products also contain ancillary variables including observation conditions and a quality control (QC) flag. The QC flag provides information regarding retrieval confidence and can be used to identify data that are retrieved under not-so-favorable conditions (Levy et al., 2003; Tanré et al., 1997). Other parameters that could be used in QA/QC steps include "Average Cloud Distance Land Ocean," which measures the distance of a retrieval from the nearest cloudy region and could be used in detecting cloud contaminated retrievals.

2.1.2 MODIS DB Aerosol Products

The DB algorithm is used to retrieve AOD and other ancillary parameters over visibly bright surfaces, utilizing the facts that surface albedo is relatively dark at blue channels (0.412, 0.47 μm) and dust absorption is weak at the red channel (0.65 μm) (Hsu et al., 2004). In the c5 DB algorithm, a pre-calculated clear sky surface albedo database for arid and semi-arid areas is used in the retrieval process (Hsu et al., 2006). These surface albedo data, combined with a set of models describing aerosols with

different optical properties, are used as inputs to a radiative transfer simulation to generate LUT entries, which tabulate the simulated satellite radiances at 0.412, 0.47, and 0.65 μm as functions of AOD (at 0.55 μm), aerosol type, and surface albedo. Using a maximum likelihood method, the optimal combination of aerosol models is selected by matching the observed radiances at 1 km resolution with the LUT values.

For pure dust aerosol cases, AOD and single scattering albedo are reported at 0.412 and 0.47 μm, while for mixed aerosol cases, AOD and Angström exponent values are reported (Hsu et al., 2004). The DB algorithm is applied to 1 km cloud-free MODIS pixels, which are then aggregated into 10 km resolution data (Hsu et al., 2004). This is different from the standard MODIS products, where radiances are aggregated to a 10 × 10 km spatial resolution first, and then the retrieving processes are applied. In the c5 DB algorithm, basic cloud screening is accomplished using the MODIS cloud mask product. To further reduce cloud contamination, spatial variances of TOA reflectance (at 0.412 μm) are computed for every 3 × 3 pixels and are used to remove potential cloud-contaminated pixels. The DB absorbing aerosol index AI is also used to retain pixels with thick dust loading that are misidentified as cloudy pixels by the MODIS cloud masks (Hsu et al., 2004). The DB absorbing aerosol index AI detects changes in wavelength-dependent reflectance from Rayleigh scattering due to aerosol absorption (Hsu et al., 2004), and thus can be used to discriminate heavy UV-absorbing aerosol plumes from clouds.

The DB data includes a three-category quality assurance (QA) flag: "none," "good," and "very good." Also included are other ancillary parameters such as

viewing/scattering angles, solar zenith and azimuth angles, surface albedo, and the number of pixels used, all of which are used for evaluation purposes.

The spatial coverage of c5 DB data includes North Africa, the Arabian Peninsula, parts of Central Asia, India, Australia, the Western US, and the Andes Mountains. The spatial resolution of the data is 10 km at nadir and the revisit time is about one to two days. Compared to MISR, which is also used to retrieve aerosol properties over bright surfaces, DB has a much wider spatial coverage and a more frequent revisiting time. The uncertainties in DB AOD retrievals are listed as $\pm 0.03 \pm 20\% \times \tau_{AERONET}$ for c5 and $\pm 0.03 \pm 20\% \times \tau_{DB}$ for c6 (Hsu et al., 2006; Sayer et al., 2013).

A climatological surface albedo database is used in the c5 DB retrieval algorithm, which, as discussed in CHAPTER I, introduces retrieval uncertainties and limits the usage of the DB algorithm to vegetated surfaces. A hybrid method of estimating surface reflectance, which uses seasonal surface reflectance data and the normalized difference vegetation index (NDVI) products, is applied in the c6 DB algorithm. The new c6 DB surface reflectance database extends the data coverage to all "cloud-free and snow free" land masses (Hsu et al., 2013). A more sophisticated global surface reflectance database was generated using seven years of data and is built as a function of NDVI. This is used for retrieving aerosols over arid and semi-arid regions. Surface reflectance of naturally vegetated regions is calculated using linear relations between surface reflectance at 0.47 and 0.65 μm and the TOA reflectance at 2.1 μm (Hsu et al., 2013). For urban and agricultural regions, a hybrid

11

method that takes into account the effects of the bidirectional reflectance distribution function (BRDF) is used (Hsu et al., 2013).

Another major change in the c6 DB algorithm is in the cloud screening procedures. In the c5 DB algorithm, the spatial homogeneity of TOA reflectance at 0.412 μm is used as the primary cloud-screening check, and 1.38 μm data are used for detecting cirrus contamination. This approach masks out both regions with "highly variable" surface characteristics and masks out non-existent cirrus clouds over arid areas due to the high sensitivity of 1.38 μm to water vapor (Hsu et al., 2013). The updated cloud masking procedures include tests using brightness temperature (BT) at 11 μm, BT differences between 11 μm and 12 μm, and total precipitable water, which results in more cloud-free pixels that are suitable for aerosol retrievals (Hsu et al., 2013).

2.2 MISR Aerosol Products

On board the Terra satellite, MISR measures radiances at 4 spectral channels (446.4 nm, 557.5 nm, 671.7 nm, and 866.4 nm) and at nine different viewing angles (nadir, ±26.1, ±45.6, ±60.0, and ±70.5 degrees) with a swath of 360 km. Derived from MISR TOA radiances measured in 1.1 km sub-regions, the MISR level 2 aerosol products have a spatial resolution of 17.6 × 17.6 km (Martonchik et al., 1998, 2002, 2009). Two separate retrieval systems were applied over dark water and heterogeneous land surface (a 3-stage retrieval process). Stage one involves pre-processing, which includes radiance calibration, ozone and water vapor corrections, and removal of radiances that are not suitable for retrievals. During this stage, pixels

that are influenced by cloud, glint, complex terrain, and low solar zenith are filtered out. Stage two determines the surface type of a scene, including dark water and heterogeneous land. For over-land retrievals, an empirical orthogonal function analysis is used to separate the surface contribution of TOA radiances from that from the atmosphere (Martonchik et al., 1998). Stage three is the inversion step. During this step, the averaged reflectance of the red and near-infrared band is used primarily for dark-water retrievals when AOD is smaller than 0.5 at 0.558 μm. The core retrieval strategy is based on an LUT method similar to that previously described. Instead of using coarse and fine mode aerosol models, five natural aerosol types are used, including sea salt, pollution, dust, biogenic particles and urban soot. The physical and chemical properties of the five aerosol species are obtained from previous field campaigns (Diner et al., 1998; Diner et al., 2001).

To exclude cloudy pixels, the MISR cloud team has developed three independent cloud detection methods: Radiometric Camera-by-Camera Cloud Mask (RCCM), Stereoscopically Derived Cloud Mask (SDCM), and Angular Signature Cloud Mask (ASCM) (Diner et al., 1998; Martonchik et al., 2009). RCCM is based on a radiance threshold technique and produces cloud masks for each of the nine camera angles at a 1.1 km spatial resolution. The SDCM method is designed to retrieve the reflecting layer height and is used in combination with the RCCM method to indicate the confidence level regarding clouds presence near or above a surface. The ASCM method utilizes differences in angular-dependent Rayleigh scattering in the blue and red or near-IR channels at forward-scattering directions between high clouds and the surface. It is designed for detecting high clouds and clouds over icy

and snowy surfaces. Over land, ASCM is currently only applied over the icy and snowy surfaces with static thresholds. A sensitivity study showed that the ASCM method is not sensitive to cirrus clouds that have optical depths less than 0.5 (Di Girolamo and Davies, 1994). Besides these three primary cloud detection methods, two additional data-filtering procedures including angle-to-angle smoothness and correlation evaluation along with a brightness test, are also used to remove possible contaminated observations for aerosol retrievals by the MISR aerosol team (Diner et al., 2001; Martonchik et al., 2002). Both methods are designed to eliminate pixels with large radiance variations within each camera angle and among the nine angles.

Kahn et al. (2005, 2010) showed that approximately one standard deviation of uncertainty in MISR-retrieved AOD is on the order of 0.05 or $0.2 \times \tau$, whichever is larger. Biases and uncertainties in MISR AOD values are associated with cloud contamination and lower boundary conditions in some locations (Kahn et al., 2010). Uncertainties are also present over regions that have mixtures of dust and smoke, as only a limited number of aerosol models are used in the retrieval process. Specific biases have been identified for retrievals with AOD values lower than 0.025 or higher than 0.5 (Kahn et al., 2010). Besides AOD, the MISR aerosol product also reports constraints on particle shape, size, and absorption.

2.3 Aerosol Robotic NETwork (AERONET) Observations

AERONET is a global aerosol-monitoring network that contains more than 200 sun photometers. Each photometer is designed to measure attenuated solar energy at eight spectral bands from 0.34 μm – 1.64 μm that can be used to derive

aerosol optical properties (Holben et al., 1998). The sun photometers measure attenuated solar energy through two scanning modes: direct sun measurement and sky measurement (Holben et al., 1998). For the direct sun measurement mode, a photometer points directly at the sun and measures solar radiation every 15 minutes. The Rayleigh and gas-absorption-adjusted radiance measurements are used to calculate the spectral AODs following Beer-Bouguer's Law. Sky measurements are used to derive aerosol inversion products, which include aerosol microphysical properties such as particle size distribution and phase function (Dubovik et al., 2000). There are two types of sky measurements: the "almucantar plane" and the "principal plane" modes. Both include series of measurements that point away from the sun following sequences of azimuth or scattering angles (Holben et al., 1998).

Level 2.0 aerosol AOD products include extensive cloud masking and quality assurance procedures (Smirnov et al., 2000). Two temporal variation tests are performed to remove potential cloud contamination within the aerosol products. First, triplet measurements of AOD collected in 1 minute intervals need to be smaller than 0.02 for AOD smaller than 0.67. If AOD is greater than 0.67, then the threshold of the triplet test is set to $0.03 \times \tau$. The continuity test is a spike filter that is applied to the second order time-series derivative of spectral AODs. Other quality assurance steps include exclusion of specific channels with large calibration changes, exclusion of AOD retrieved at 1.02 μm when temperature measurements are unreliable, and exclusion of data anomalies that are obvious artifacts. Besides spectral AODs, the aerosol size parameter, called the Angström Exponent, is derived for AOD values

ranging from 0.44 to 0.87 μm (O'Neil et al., 2003). Lastly, the reported uncertainty in spectral AODs is on the order of ~0.01–0.02 (Eck et al., 1999).

2.4 MODIS Cloud Mask Product

In this study, attempts have been made to use the MODIS cloud mask for cloud clearing of the MISR aerosol product. With additional channels centered at IR and the 1.375-μm channel, MODIS, in comparison with MISR, has an enhanced capability of detecting clouds, especially thin cirrus (Ackerman et al., 1998). The MODIS cloud mask products provide levels of confidence regarding how unobstructed the satellite field of view is at the pixel level. A combination of 19 visible and infrared spectral bands is used to perform a series of threshold and consistency tests to detect clouds. The MODIS MOD35 cloud mask indicates cloud status with one of four values at a 1 km resolution: "cloudy" (CD), "uncertain clear" (UC), "probably clear" (PC), and "confidently clear" (CC) (Frey et al., 2008). The MODIS cloud mask products also include other ancillary information regarding items such as thin cirrus and high clouds, surface shadow, cloud adjacency, sea ice, snow, and sun glint. In this study, the 1 km resolution cloud screening flags from the MODIS cloud mask are used for cloud clearing of MISR scene-AOD after collocated with the MISR aerosol products. The thin cirrus cloud flag, derived primarily from the 1.375-μm water vapor sensitive band (Gao et al., 2002; Gao and Kaufman, 2003), is also used in this study for detecting thin cirrus clouds. Ackerman et al. (2008) showed that cloudy/clear areas from the MODIS cloud mask agree with lidar data about 85% of the time with a cloud optical depth sensitivity of 0.4. Uncertainties in

the MODIS cloud mask products, as well as the complicated nature of near-cloud aerosols, contribute to the complexity of the cloud clearing issue. For example, particle hydration (Tackett and Di Girolamo, 2009) and/or cloud particle detrainment might occur near clouds, which infuses ambiguity into discriminating clouds and aerosols.

2.5 OMI AI Product

The Ozone Monitoring Instrument (OMI), installed on the Aura satellite, has a broad swath of 2600 km with a spectral coverage from ultraviolet (UV) to visible (0.264 to 0.504 μm) and a spatial resolution of 13 × 24 km at nadir (Levelt et al., 2006). Due to the curvature of the Earth, a pixel size at the extreme edge of the swath can be as large as 28 × 150 km (Levelt et al., 2006). Aura is a part of the Aqua constellation with an Equator crossing time of 13:45, 15 minutes behind Aqua. In this study, the aerosol index (AI) from the OMI OMAERUV product is used. The OMI AI is defined as

$$AI = -100 \log_{10} \left[\frac{I_{354}^{obs}}{I_{354}^{calc} \left(R_{354}^{*} \right)} \right]$$

(1)

where I_{354}^{obs} is the observed radiance at 0.354 μm, I_{354}^{calc} is the calculated radiance assuming a "pure Rayleigh atmosphere" (Torres et al., 2007), and R_{354}^{*} is the Lambert equivalent reflectivity that is derived from LER at 0.388 μm using a climatological database (Torres et al., 2007). Near-zero AI values indicates clouds. Positive AI values represent UV-absorbing aerosols including black carbon, mineral dust, and volcanic ash. Non UV-absorbing small aerosol particles such as sulfate aerosols

result in small negative values, but the signal is often too weak to be distinguished from the noise. Thus, in this study, AI is used to identify heavy biomass burning/smoke and dust plumes.

2.6 CALIOP Products

NASA's Cloud-Aerosol Lidar with Orthogonal Polarization (CALIOP) sensor, on board the Cloud-Aerosol Lidar and Infrared Pathfinder Satellite Observations (CALIPSO) satellite, is a multi-wavelength (0.532 and 1.064 μm) polarization-sensitive elastic backscatter lidar (Stephens et al., 2002; Winker et al., 2007; Hunt et al., 2009). As part of the A-Train constellation, the passing time of CALIPSO is only around one minute different than that of Aqua MODIS. CALIOP measures the vertical structure of aerosols and clouds in the atmosphere with a much more narrow swath of ~90m (Winker et al., 2007).

2.6.1 CALIOP Level 1B Data

The CALIOP level 1B data product provides lidar profiles of calibrated attenuated backscatter at 532 nm and 1064 nm and depolarization ratio at 532 nm. The vertical resolution of the attenuation profile is altitude dependent. The resolution from the surface to 8.3 km, where aerosol plumes are mostly located, is 30 m vertically for 532 nm, 60 m vertically for 1064 nm, and 1/3 km horizontally. The total attenuated backscattering at 532 nm, the depolarization ratio at 532 nm, and the color ratio, which is attenuated backscattering at 1064 nm over that of 532 nm, are used in this study. Other than the backscattering profiles, CALIOP level 1B data also

contains ancillary data, such as geolocation information and viewing geometries, as well as diagnostic parameters, such as observation uncertainties and QC flags.

2.6.2 CALIOP Level 3 Cloud and Aerosol Profile

CALIOP level 3 cloud and aerosol profile data are derived from the CALIOP level 1B data as well as the level 2 vertical feature mask product. The vertical feature mask reports the vertical distribution of cloud and aerosol layers along the CALIPSO track based on Feature Classification Flags (FCF). It also contains sub-types for aerosols and clouds. CALIOP cloud and aerosol products contain information regarding extinction and backscatter and other particle optical properties that are derived from these basic parameters. Only the CALIOP aerosol profile is used in this study. This product has a horizontal resolution of 5 km, with the vertical resolution dependent upon altitude. In the troposphere from 20 km to 0.5 km below the surface, the vertical resolution is 60 meter. In the stratosphere from 30 km to 20 km, the vertical resolution is 180 meters. Ancillary data, such as geolocation data, time, and data quality flags, are also included. One parameter that is used in this study is the Atmospheric Volume Description, which is a profile descriptive flag containing the FCF associated with each 5 km × 60 m (or 5 km × 180 m) range bin in the Profile Products. The FCF categorizes the atmospheric particles into cloud, aerosol, or stratospheric features. For cloud and aerosol, further identification of feature subtype is made. For example, an identified aerosol feature can be either dust, polluted dust, clean continental, polluted continental, smoke, clean marine, or other. The minimum horizontal averaging that is required for successful layer detection is also listed in the FCF.

2.7 NOGAPS Wind Speed Data

Near surface wind speed data that are used in evaluating the uncertainties within MODIS DT over-ocean products are from the Navy Operational Global Analysis and Prediction System (NOGAPS) weather forecast model (Hogan and Rosmond, 1991). The near surface wind speed is modeled with the assimilation of satellite-retrieved wind speed data and is reported four times per day on a 1° × 1° Lat/Lon grid (Zhang and Reid, 2006).

CHAPTER III

**A CRITICAL EXAMINATION OF SPATIAL BIASES BETWEEN MODIS
AND MISR AEROSOL PRODUCTS**

3.1 Introduction

The AERONET, a global scale sun photometer network, has been providing
robust aerosol optical property measurements for nearly two decades. As such, it is
often used as the primary standard for validating satellite aerosol products (e.g,
Holben et al., 1998; Kahn et al., 2010; Levy, et al., 2010; Hsu et al., 2006).
AERONET has included 443 sites globally at various times. Only 11 sites have data
records that are longer than 7 years, and 39 sites have data records that are longer
than 5 years. Field campaigns, in which extensively measurements of the
environment were collected in support of verification, have targeted specific areas of
interest, but are sporadic and short lived. This ephemeral nature of observations
suitable for satellite product characterization leads to fundamental questions about the
representativeness of available validation data sets. For example, is the distribution of
AERONET sites sufficient to cover the spatial and temporal variations of the aerosol
state globally? Are there any surface-observation-data-poor regions that clearly
require future deployments of sun photometer instruments and/or *in situ*
measurements, especially for the purpose of validating satellite observations?

Complicating matters further is the spatial correlation of bias. Typically, retrievals are underdetermined and some assumptions must be made, most typically through the lower boundary condition model, the assumed particle microphysics, or optical properties. As land features and particle properties have spatial coherence, one would expect satellite retrievals of aerosol products to share similar patterns in their biases.

Recently Shi et al. (2011a), Hyer et al. (2011) and Levy et al. (2010) published evaluations of over-water and -land MODIS DT c5 aerosol products. Over water, low and high biases are quite apparent for fine and coarse mode aerosol particles, respectively. Wind and cloud related biases are visible as well. Uncertainties are also present over coastal regions, where runoff and/or biological activity create issues for the surface boundary conditions (e.g. Kahn et al., 2010). Biases in the over-water AOD product were found to be largely correctable through alterations of model data and information contained in the retrieval (e.g., Zhang and Reid, 2006). The over-land problem, however, is much more complicated. The lower boundary condition for MODIS DT is empirical and cannot cope with all land forms everywhere. The more complicated land surface also reduces the degrees of freedom in available microphysical models that can be utilized by the retrievals. As a consequence, Hyer et al. (2011) reported many cases where correlations between satellite and AERONET AOD are good within regions, but slopes are vastly different. Such regionally correlated biases are particularly problematic for higher-level investigations that require consistent data over large areas, such as inverse modeling or lifecycle studies. Also, Kahn et al. (2010) identified MISR and MODIS DT AOD

differences over India, Eastern China, and Southeastern Asia that they attributed, in part, to dark particles absent from the current algorithm particle climatologies. They noted that a lack of mixtures containing dust and smoke optical analogs in the algorithms create AOD discrepancies over Sub-Saharan Africa and several other locations (also see Eck et al. (2010) regarding mixtures).

One way to approach spatially correlated bias is through cross-comparisons between satellite aerosol products, not only over the AERONET sites, but also over regions that may lack ground-based observations. Such methods do not specifically resolve global issues related to quantitative error characterization, but are beneficial in determining the overall scientific uncertainty of aerosol properties. Indeed, in regions with large differences among products, the data need to be understood and the causes of the discrepancies should be identified. This need motivates the current study, which aims to help direct future deployments of surface measurements to support refinement of future generations of algorithms.

Three satellite aerosol products were selected for this study: the Terra operational Moderate Resolution Imaging Spectroradiometer (MODIS) c5.1 Dark Target (DT) aerosol product, the Terra MODIS c5.1 Deep Blue (DB) aerosol product, which retrieves aerosol properties, especially but not limited to, over-bright surfaces, and the Multiangle Imaging SpectroRadiometer (MISR) version 22 aerosol product. Note that these three products were chosen because they are widely used by the community for various applications ranging from climate to air quality to real-time operational forecasts (Zhang et al., 2001; Zhang et al., 2008a,b; Kaufman et al., 2002; Remer et al., 2009; Kahn et al., 2009; Reid et al., 2009; Hsu et al., 2006; Zhang and

Reid, 2006). All three products were spatially and temporally collocated, and were used for evaluating the existing aerosol observation system. This is concluded with a discussion of regions showing clear heterogeneity between sensor retrieval results and, thus, with proposed areas that have an urgent need for additional, suborbital measurements.

3.2 Methodology

Three satellite products that are used in this study are MODIS c5.1 DT DB and MISR aerosol optical depth products. MODIS and MISR sensors have different spatial coverage and overpass times. For fair comparisons, pairs of observations from different instruments need to be collocated spatially and temporally. Since both MISR and MODIS are onboard the Terra satellite, it is possible to have near simultaneous observations overlapping the same location from both instruments. However, the two aerosol products have different spatial resolutions (10km for MODIS DT and DB, and 17.6 km for MISR). Therefore, to spatially collocate the MODIS DT (MODIS DB) products with MISR, all three products were averaged into $0.5° \times 0.5°$ (Lat/Lon) gridded products for every six hours. In the second step, the 6 hr gridded aerosol products were collocated in both space and time, and pairs of data points with valid AOD values from both MODIS DT (or MODIS DB) and MISR aerosol products were chosen for the tests described in the following section. Two comparison datasets were used in this study: (1) spatially and temporally collocated Terra c5.1 MODIS DT and MISR Version 22 aerosol products from 2005-2007 and (2) spatially and

temporally collocated Terra c5 MODIS DB and MISR Version 22 aerosol products from 2005-2007. AERONET AOD data are also used as well.

3.3 Results

First, example regressions of satellite AODto AERONET from eight important geographical regions are presented. Then, to understand the size of the bias features, the ratio of MODIS retrievals to MISR aerosol optical depth retrievals are computed and spatial patterns of different products are studied through spatially and temporally collocated comparisons. From these results, the original eight comparisons are considered and limitations in spatial coverage of the current ground-based observations for the identified problematic regions are discussed.

3.3.1 Example AERONET Comparisons

Eight AERONET sites that provide at least five-years of data and that provide representative observations for the aerosol state of a given region, were selected: Alta Floresta (for South America), Banizoumbou (for North Africa), GSFC (for the Eastern U.S.), Maricopa (for the Western U.S.), Kanpur (for India), Mongu (for South Africa), Solar Village (for Saudi Arabia) and Shirahama (for East Asia). AERONET direct sun measurements of AOD are highly accurate, with uncertainties on the order of ~0.01 in the visible and near-infrared wavelengths for the level 2 product (Eck et al., 1999). Using the standard Angstrom (linear) fit, AERONET observations from the 0.50 and 0.67µm wavelengths were used to estimate AOD values at the 0.55 (for MODIS) and 0.558 (for MISR) μ m wavelength (Shi et al., 2011). Within a 30 min temporal window and 0.1 degree spatial difference, one-to-one collocated operational

MODIS/MISR and AERONET AOD were used for the comparisons. Regressions are shown in Figure 1, with regression line parameters and r^2 values presented in Table 1. Because the behavior of satellite retrievals can change when AOD values are large, scores are provided for all data and also for $\tau < 0.5$.

Table 1. Regression coefficients for Figure 1with all AOD and satellite AOD smaller than 0.5 in parentheses.

Site	Satellite	Slope	Intercept	r^2
Alta Floresta	MISR	0.48(0.81)	0.09(0.00)	0.77(0.82)
	MODIS DT	1.33(1.01)	0.1(0.05)	0.92(0.82)
Shirahama	MISR	0.67(0.66)	0.03(0.03)	0.90(0.84)
	MODIS DT	1.01(0.85)	0.05(0.02)	0.83(0.79)
Kanpur	MISR	0.61(0.47)	0.11(0.13)	0.70(0.54)
	MODIS DT	1.06(0.54)	0.05(0.21)	0.79(0.43)
	MODIS DB	0.98(0.28)	0.04(0.19)	0.60(0.11)
Mongu	MISR	0.82(0.74)	0.03(0.04)	0.88(0.75)
	MODIS DT	0.76(0.67)	0.04(0.05)	0.83(0.71)
	MODIS DB	1.02(0.54)	0.17(0.04)	0.60(0.34)
Banizoumbou	MISR	0.51(0.33)	0.20(0.19)	0.61(0.34)
	MODIS DT	1.14(0.78)	0.13(0.01)	0.95(0.81)
	MODIS DB	0.63(0.49)	0.32(0.21)	0.81(0.50)
GSFC	MISR	0.72(0.80)	0.03(0.02)	0.87(0.90)
	MODIS DT	1.1(1.06)	0.01(0.01)	0.94(0.84)
Maricopa	MISR	0.8(0.77)	0.06(0.06)	0.35(0.39)
	MODIS DT	0.96(0.99)	0.25(0.24)	0.12(0.15)
	MODIS DB	0.82(0.82)	0.07(0.07)	0.94(0.94)
Sollar Village	MISR	0.9(0.68)	0.09(0.13)	0.74(0.66)
	MODIS DB	0.53(0.29)	0.19(0.21)	0.35(0.12)

Figure 1 shows that in most regions (the Eastern US, South America, North Africa, South Africa, East Asia and India), retrievals from the operational MODIS DT (MODIS DB) and MISR aerosol products show reasonable correlations with the collocated AERONET data. Even so, slope differences are clearly noticeable for areas dominated by different aerosol species, indicating that aerosol microphysical properties are among the sources of uncertainties in these aerosol products.

26
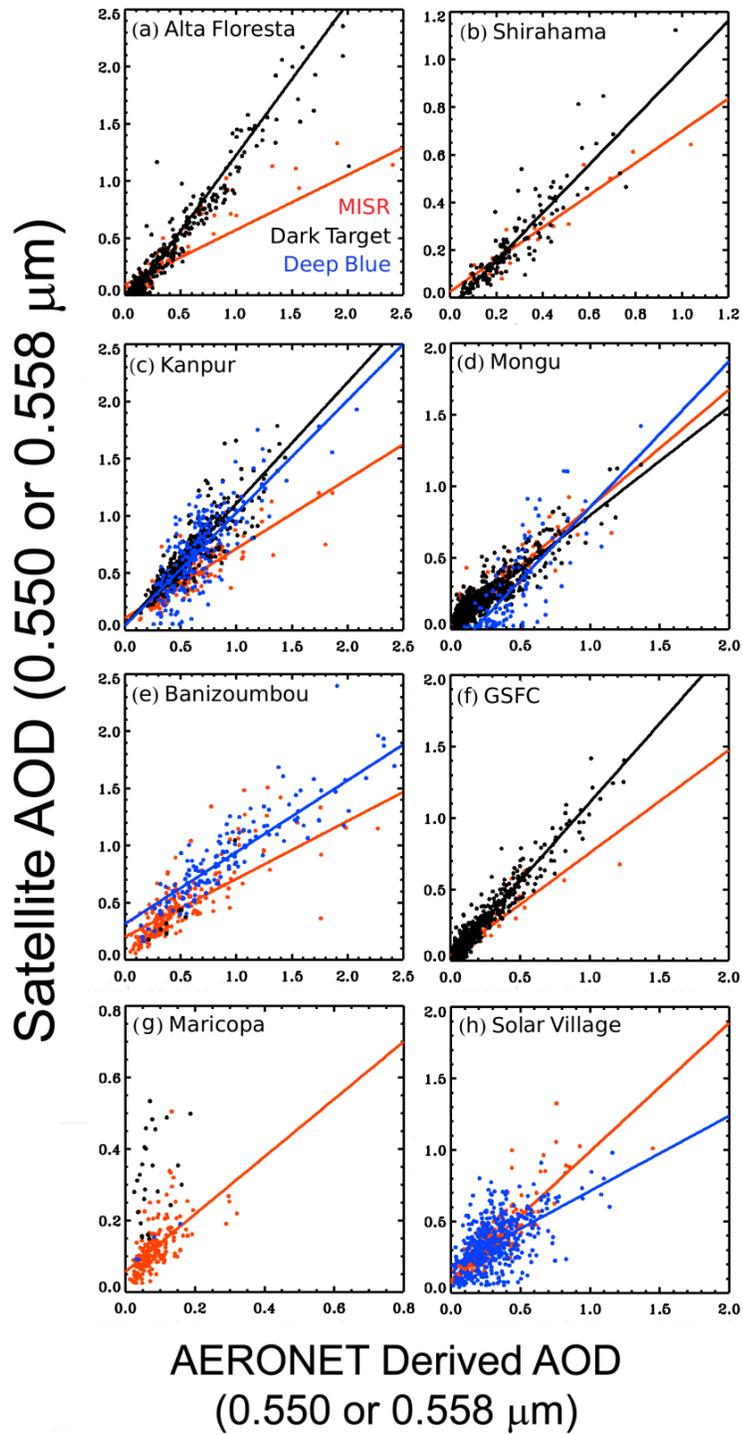
Figure 1. One to one comparisons between MODIS Dark Target (MODIS Deep Blue)/MISR and AERONET AOD at seven sites for year 2000–2008. (a) Alta Floresta, (b) Shirahama, (c) Kanpur, (d) Mongu, (e) Banizoumbou, (f) GSFC, (g) Maricopa, (h) Solar Village.

Also, although an underestimation is observed for high MISR AOD values (AOD>

0.5), in almost all regions, except Mongu (as previously reported in Kahn et al., 2010),

the influence of lower boundary conditions (generally manifested in the intercept of

the regressions) is less evident in MISR-AERONET than the MODIS-AERONET

comparisons. For example, over the Western US, where AERONET reported AOD

values are mostly smaller than 0.2, collocated AOD values from the operational

MODIS DT aerosol products show a much higher AOD range up to 0.6. Note that the

black regression line for MODIS is not provided from the Maricopa plot due to an

insufficient number of data points. Also, large intercept values are observed for the

comparisons between the MODIS DB and AERONET AOD values at the Kanpur and

Mongu sites, showing that uncertainties can exist for the MODIS DB products over

low surface albedo regions. In contrast, observations from the Banizoumbou and

Solar Village sites suggest that both the MODIS DB and MISR can retrieve aerosols

characteristics over bright surfaces.

However, point comparisons are not sufficient and may not fully represent the

performance of satellite AOD retrievals. For example, spatial comparisons between

MISR and MODIS over South Africa (see later Figure 4) indicate larger differences

than what the point comparisons show at the AERONET site. This is an issue that is

present in multiple locations, as similar trends are also present over the Arabian

Peninsula. Comparisons between satellite AOD products are therefore provided

globally henceforth.

3.3.2 Global Ratios

The regressions shown in the previous section reveal a common observation: satellite products often correlate well, but suffer from slope or Y-intercept biases. Hyer et al. (2011) reported highly variable regression slopes for different sites in the same region. The question is, then: Over what area do these regressions hold? As a first step to answering this, an examination of overall AOD for simultaneous MODIS and MISR retrievals for the 2005-2007 timeframe is provided in Figure 2. Also, as part of the supplemental materials, Figure 2 is repeated seasonally (DJF, MAM, JJA, SON).
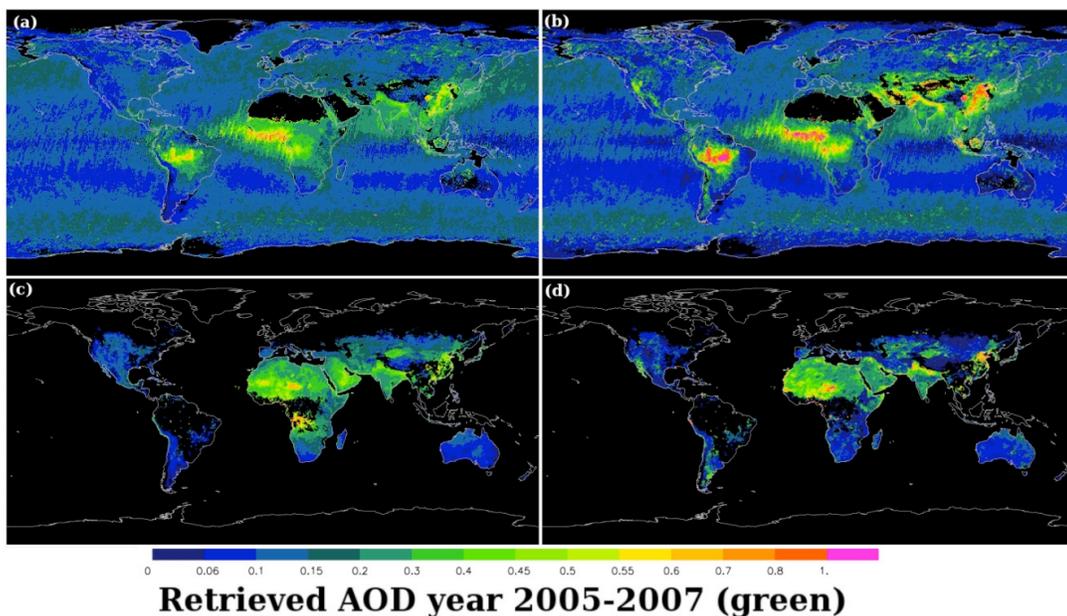
Figure 2. Average spatial distribution of MISR (0.558 μm) for 2005–2007. The MISR and operational MODIS DT/MODIS DB AOD data were first collocated both in space and time, and only collocated MISR and MODIS retrievals were used in generating this plot. Data were gridded every 0.5° × 0.5° (Lat/Lon). (a) MISR AOD that corresponds with operational MODIS DT, (b) Operational MODIS DT AOD, (c) MISR AOD that correspond with MODIS DB, and (d) MODIS DB AOD.

Figure 2 shows three-year averaged spatial plots of AOD from MISR and MODIS c5.1 retrievals. The plots were calculated pair wise; only MISR aerosol retrievals with collocated MODIS AOD retrievals (and vice versa) were used to calculate the averages. Therefore, the sampling biases in Figure 2a could be different from the three-year averaged MISR AOD plot that used all available MISR data. Shown in Figure 2a, the commonly acknowledged continental scale aerosol features are visible. Heavy smoke aerosol plumes are found over regions of South America, South Africa and Indonesia; dust aerosol plumes are visible over North Africa, and the Middle East (e.g., Husar et al., 1997). Aerosol plumes that originate from multiple aerosol sources of dust, smoke and pollutant are observable over East and South Asia (Reid et al., 2009; Eck et al., 2005). Long-range aerosol transports are shown. Asian dust plumes cross the Pacific Ocean and reach the West Coast of the US; North African dust plumes cross the Atlantic Ocean and reach the Caribbean. A high AOD band is also noticeable over high latitude southern oceans. However, this feature is probably produced by cloud artifacts (e.g. Zhang et al., 2005; Shi et al., 2011, Kahn et al., 2010; Smirnov et al., 2011).

Figure 2b shows the corresponding operational MODIS DT AOD distributions. Because only pairs of MODIS and MISR data that possess valid AOD values were used in creating Figure 2, the differences between Figure 2a and b are mostly related to the uncertainties in the retrieval processes, and sampling biases between the two products are minimized. High AOD features over the Western US, the Andes mountains, and the Namibian Desert from Figure 2b are not present in the spatially and temporally collocated MISR AOD plot in Figure 2a. Also, MODIS DT

AOD values are higher than the collocated MISR AOD values over regions such as East and Central Asia, India, Indonesia, South Africa, and South America. Note that the differences seem significant, yet could mostly be explained by the known limitations of each product. For example, for the MODIS DT aerosol product, overestimation of AOD values that are greater than 0.5 and are over sparsely vegetated land (e.g., the Andes Mountains, the Namibian Desert, and the Western US) could be due to the uncertainties in surface characteristics, which were deviating from the surface reflectance model used in the operational MODIS product. In another case, higher MODIS DT AOD values over South America, South Africa, and Central Asia could be related to the underestimation of the MISR aerosol product for high AOD (Kahn et al., 2009; Kahn et al., 2010; Personal communication with Dr. Olga Kalashnikova). This effect is present in the Alta Foresta data (Figure 1) for which the MISR retrieval underestimates aerosols generated through biomass-burning.

Figure 2c and d are structured the same as Figure 2a and b, but they show the comparison of MODIS DB and MISR aerosol products. Figure 2c shows the three-year (2005-2007) averaged spatial plot of MISR AOD (collocated with the MODIS DB product). Heavy aerosol loadings are found for dust over North Africa and the Arabian Peninsula, for smoke over South Africa, and for pollutant mixed dust over Northern India and East Asia. Figure 2d shows the corresponding MODIS DB AOD distributions. For South America, Northern India (e.g. the Kanpur site), and East Asia, higher AOD values are shown for the MODIS DB product. Conversely, Deep Blue has much lower AOD in central Africa and parts of the Arabian Peninsula. Over

desert regions, such as North Africa and the Middle East, the AOD values from the two products are consistent to a reasonable degree.

To better illustrate differences, Figure 3a and b show the spatial plots of the AOD ratio of the MODIS DT (MODIS DB) AOD divided by MISR AOD. Red colors represent regions in which MODIS retrieves higher AOD than MISR, and blue colors show the opposite. For Figure 3a, ratios larger than 1.3 are found over Western and Northeast Canada, the Western US, the Andes mountains, most of the Amazon, and Central and East Asia, indicating that the MODIS DB AOD values are much higher than the MISR AOD values over these regions. Ratios smaller than 0.75 are present over the Central US, the east coasts of South America and South Africa, and North-Central Asia. Also, even over regions like South Africa and South America, where one expects both sensors to perform better due to relatively low surface reflectivity, ratio values of 1.1–1.5 are present. Some of this behavior also appears in the sensor-AERONET comparisons for the Alta Floresta site in Figure 1. Figure 3b shows that over the Western US, Southern South America, North Africa, Central Asia, Northern India, and Eastern Australia, the ratios between MODIS DB and MISR AOD are greater than 1.3. Regions where MISR retrievals are much greater than those from MODIS DB are South Africa, the middle of the Arabian Peninsula, Mid-India, and part of Central Asia. However, the ratio plots from Figure 3a and b can be
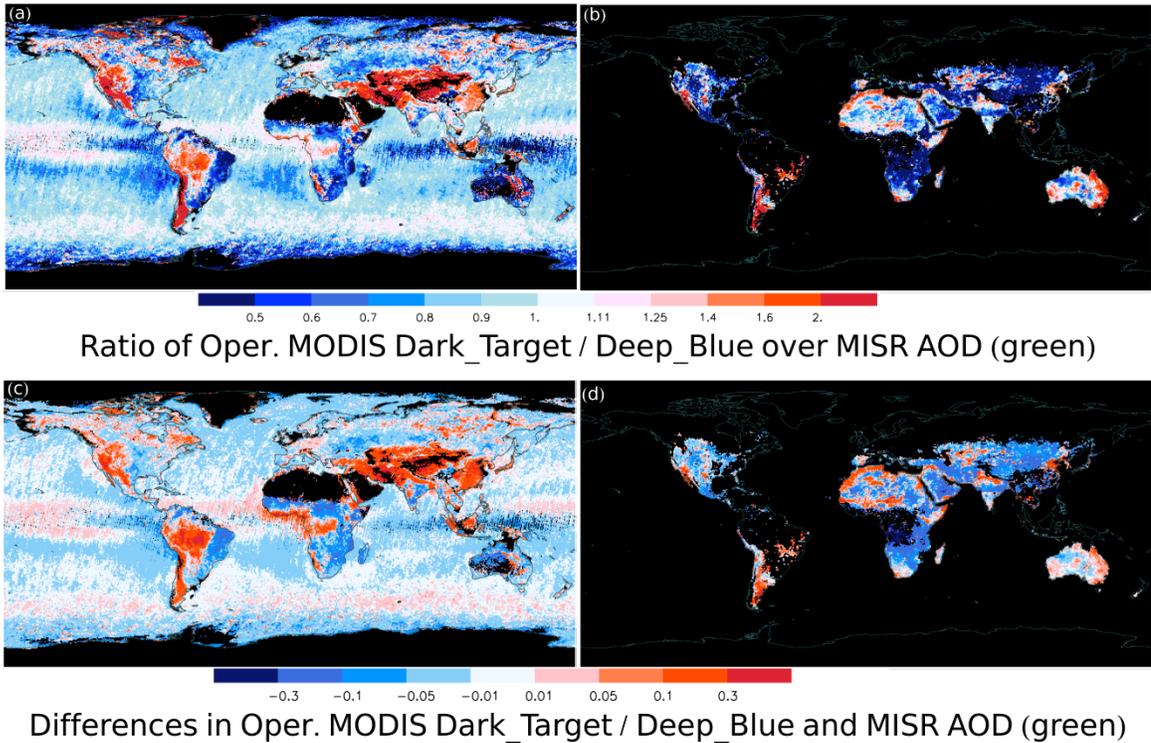
Figure 3. (a) The ratio of operational MODIS DT over MISR AOD in green channel for year 2005–2007. (b) Similar to (a) but for MODIS DB. (c) The differences between operational MODIS DT and MISR AOD in green channel for year 2005–2007, and (d) Similar to (c) but for MODIS DB. Note the color scales are different between the top and the bottom panels.

misleading, because high ratio values over regions with small AOD values can skew the picture. Therefore, the AOD differences between MODIS DT (MODIS DB) and MISR AOD at the green channel are also shown in Figure 3c and d.

The main patterns of Figure 3c and d are very similar to that of Figure 3a and b. However, regions with low AOD values and very high ratio values, such as the Western US, have AOD differences on the order of 0.1–0.3. Conversely, over Central Africa, where the ratio plot does not show a large inconsistency, Figure 3c and d highlight the regions with AOD differences larger than 0.1.

Note that Figure 3 reflects, in part, the fact that the version 22 MISR-retrieved AOD values tend to have a low bias in the high AOD regime (Kahn et al., 2010),

combined with the tendency for MODIS DT AOD values to be overestimated over bright surfaces. The uncertainties in Figure 3 due to ratios from small values of AOD are discussed in Sect. 3.4. Further, uncertainties in the microphysical models used in these retrievals are amplified when aerosol loadings reach multiple scattering regimes. Thus, as shown in Figure 4, we performed regressions between MISR and MODIS DT (MODIS DB) AOD values using collocated MODIS and MISR data that have MISR AOD values between 0 and 0.5 (MODIS = MISR × slope + interception). Figure 4a, c, and e show spatial distributions of correlation, slope, and intercept values, respectively, for the regression analysis using the collocated operational MODIS DT and MISR AOD data. Like Figure 2, seasonal regressions are included in the supplementary material. Similar to the studies of Kahn et al. (2009), correlation values greater than 0.8 are found over global oceans and most land regions. Regions with correlation values less than 0.7 are found over the Western US, the Andes Mountains, the Namibian desert, and parts of the Middle East, Central Asia, and Northern Australia. Most of the regions showing poor correlations are highlighted in intercept plot of Figure 4e as well. Regions with high intercept values are most likely attributed to surface characteristics, because all of these regions are semiarid and have relatively high surface reflectance. Also, although the correlations between MISR and MODIS DT AOD data are above 0.8 over the Amazon region, slope values of 1.2 and above are found (Figure 4c). Similar slope and correlations patterns can also be found over the middle of South Africa and Southeast Asia, suggesting potential aerosol microphysical biases over these regions. Field campaigns can help improve satellite retrievals over regions where better aerosol property information is needed.

Also, for both satellite products, high correlations of 0.8 or greater were found compared with ground-based sun photometer observations on a global basis (Shi et al., 2011a, Hyer et al., 2011), showing that:

1. There are still regions that have no or few sites that would assist in refining assumed aerosol properties for satellite retrievals.

2. Additional AERONET sites are desired for some of the regions with large MODIS/MISR ratio values, especially for regions where it is suspected that aerosol optical property assumptions have large uncertainties in satellite retrievals.

3. For regions where satellite products need better aerosol property information to constrain assumptions, field measurements can play an important role. Figure 4b, d, and f show similar spatial distributions of correlation, slope, and intercept values for the regression analysis using the collocated MODIS DB and MISR AOD data. Compared with the analyses from the collocated operational MODIS and MISR data, lower correlation, larger intercept values and lower slope values were found. However, most regions shown in Figure 4b, d, and f are either desert regions or areas with complex surface features, and therefore, lower correlations between two aerosol products are understandable due to lower sensitivity to aerosol properties over bright surfaces. Still, detailed analyses of the uncertainties for the two aerosol products over these regions, similar to the studies conducted for the MODIS DT aerosol products (e.g. Shi et al., 2011; Hyer et al., 2011), are necessary.

In summation, the areas with large disagreements between satellite retrievals can be divided into three categories:
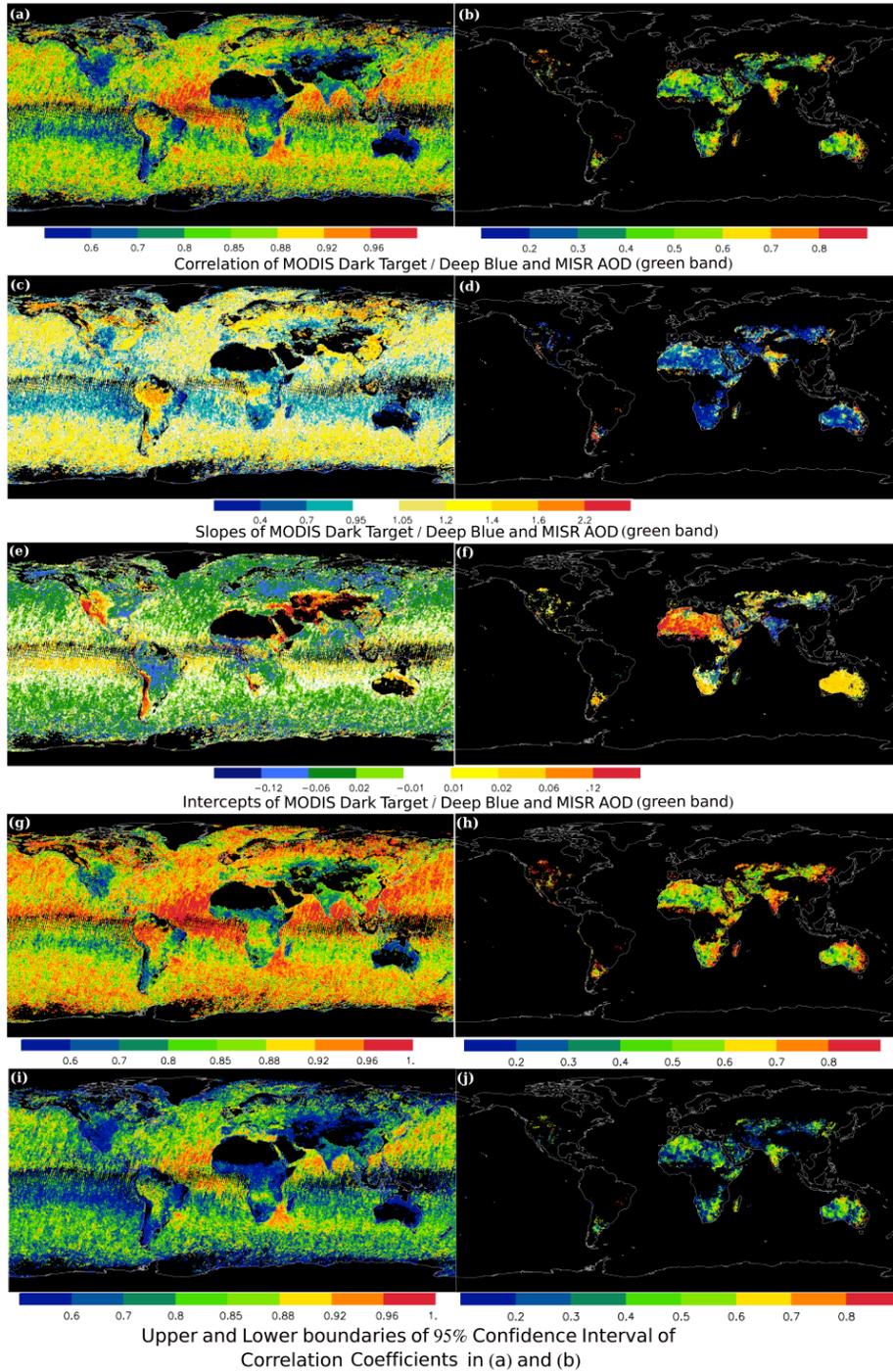
Figure 4.The regression and correlations between MISR and operational MODIS DT (right panel) / MODIS DB (left panel) for year 2005–2007 (MODIS = MISR × slope + intercept). Only collocated MODIS and MISR data that have MISR AOD values between 0–0.5 were used. (a) and(b) Correlation, (c) and (d) Slope, (e) and (f) Intercept, (g) and (h) upper boundary of the 95% confidence interval for correlation coefficient in (a) and (b), and (i) and (j) Similar to (g) and (h) but for lower boundary.

36

1. Complicated surface conditions: transition areas from bare land to areas with dense or sparse vegetation cover.

2. Complicated aerosol type: inaccurate representations of aerosol microphysics in the retrieval processes over the dark vegetation areas or dark surfaces.

3. Desert regions with very bright surfaces.

Most problematic areas belong in the first category. These regions include: the Somalia region (0-20° N, 35-50° E), the North Coast of Africa (20-35° N), the Sahel zone (~12° N across Africa), the West Coast of Africa (15-25° S), the East Coast of Africa and Madagascar (10-20° S), the East Coast of Brazil, the Andes Mountains, the East Coast of Australia, Kazakhstan, and Mongolia. The Yellow Sea region near coastal China also has a surface-type problem, as it is a region with turbid waters. Regions that fall into the second category (complicated aerosol types) include: 5° N–5° S and 10°–30° E of Africa, 20°–35° N and 100°–115° E of China and Korea, the south and north end of Japan, Malaysia, Indonesia, and the Philippines. Better agreements for aerosol retrievals among sensors are expected for the regions with low surface reflectivity at the visible spectrum. However, the AOD differences between the two products are still relatively large. This indicates that the complicated aerosol type is one of the uncertainty sources. For example, some places are known to have dark particles or mixtures of smoke or pollution and dust. Regions that fall into the third category include: Northwestern India (70° E and 35° N), Iran and Afghanistan (45°–60° E and 25°–35° N), Tibet, the East Coast of the Arabian Peninsula (45°–60° E, 10°–30° N), and high latitude areas. Also, differences in MISR and MODIS retrievals do not always point to a lack of understanding of the basic aerosol

properties in the region. Rather, they sometimes indicate satellite algorithm issues for one or both instruments. For example, regions, such as 5°−10° S and 60°−70° W of South America, where numerous field campaigns have been conducted (e.g. Reid et al, 1998, 2005, SCAR-B and SMOCC campaigns) and many AERONET data are available, may also reveal the difficulty of fully understanding aerosol properties and their spatial/temporal variations from limited ground and *in situ* observations.

3.4. Discussion: Relationship to spatial distribution of AERONET sites

Most of the problem areas listed in Sect. 3.3 are very remote and under-developed. Hence, this increases the difficulty in establishing long-term AERONET sites, which would be useful for validating the satellite aerosol retrievals over those regions. Conversely, regions with the best agreement often have the highest density of AERONET sites, even though the surrounding areas might have large inconsistencies. This is partially because the aerosol climatology used by the MODIS DT over-land algorithm is based on AERONET data (Levy et al., 2010). Also, this may, in part, be related to the concentration of sites in more developed "darker" regions where the vegetation cover is greater. The distribution of sites results in a sampling bias. The use of global statistics to measure product efficacy biases verification statistics in favor of satellite retrievals. Long-term AERONET observations greatly improve the satellite retrievals regionally by providing developers with valuable verification data that is coupled with some aerosol optical property information from sun-sky retrievals.

However, several issues were raised with the previous analysis. First, some significant differences occur in regions with existing AERONET sites, and the

differences between MISR and MODIS are due largely to the assumed aerosol properties in the satellite algorithms and/or limitations in the algorithm, such as high AOD for MISR (this is seen in Figure 1 in Amazon region with dark surfaces) or high surface reflectance for MODIS. Second, the ratio of AOD retrievals between two sensors/algorithms in regions of low AOD is not necessarily a good measure of whether errors are significant. Third, even if there are AERONET sites in high surface reflectance areas, the main issue in satellite retrievals is often the poor surface reflectance characterization, and more AERONET sites will not necessarily improve that situation.

In response to these questions, a gradient map of AOD differences (ΔAOD, MODIS DT / MODIS DB minus MISR AOD at the green wavelength) between satellite aerosol products was computed, as shown in Figure 5. Over-plotted in Figure 5 are the frequency indexes of available AERONET data. To create the gradient map of AOD bias ($\Delta\tau$), only regions with both satellite AOD values larger than 0.1 were used. The gradient is computed based on Equation 2,

$$\tau\ Error Gradient = \sqrt{\left(\frac{\partial\Delta\tau}{\partial x}\right)^2 + \left(\frac{\partial\Delta\tau}{\partial y}\right)^2} \tag{2}$$

where δx and δy (δx and δy are evaluated at half degrees Lat/Lon) represent spatial distances in west-east and south-north directions, respectively. The magnitude of the ΔAOD gradient shows the spatial variation of uncertainties in satellite aerosol products. Regions with small ΔAOD gradient values are shown in dark blue, indicating that a few AERONET sites would be sufficient to validate retrievals for the

39

whole region. Regions with large ΔAOD   gradient values are shown in lighter colors

(such as white). These regions have large spatial variance in ΔAOD, and denser
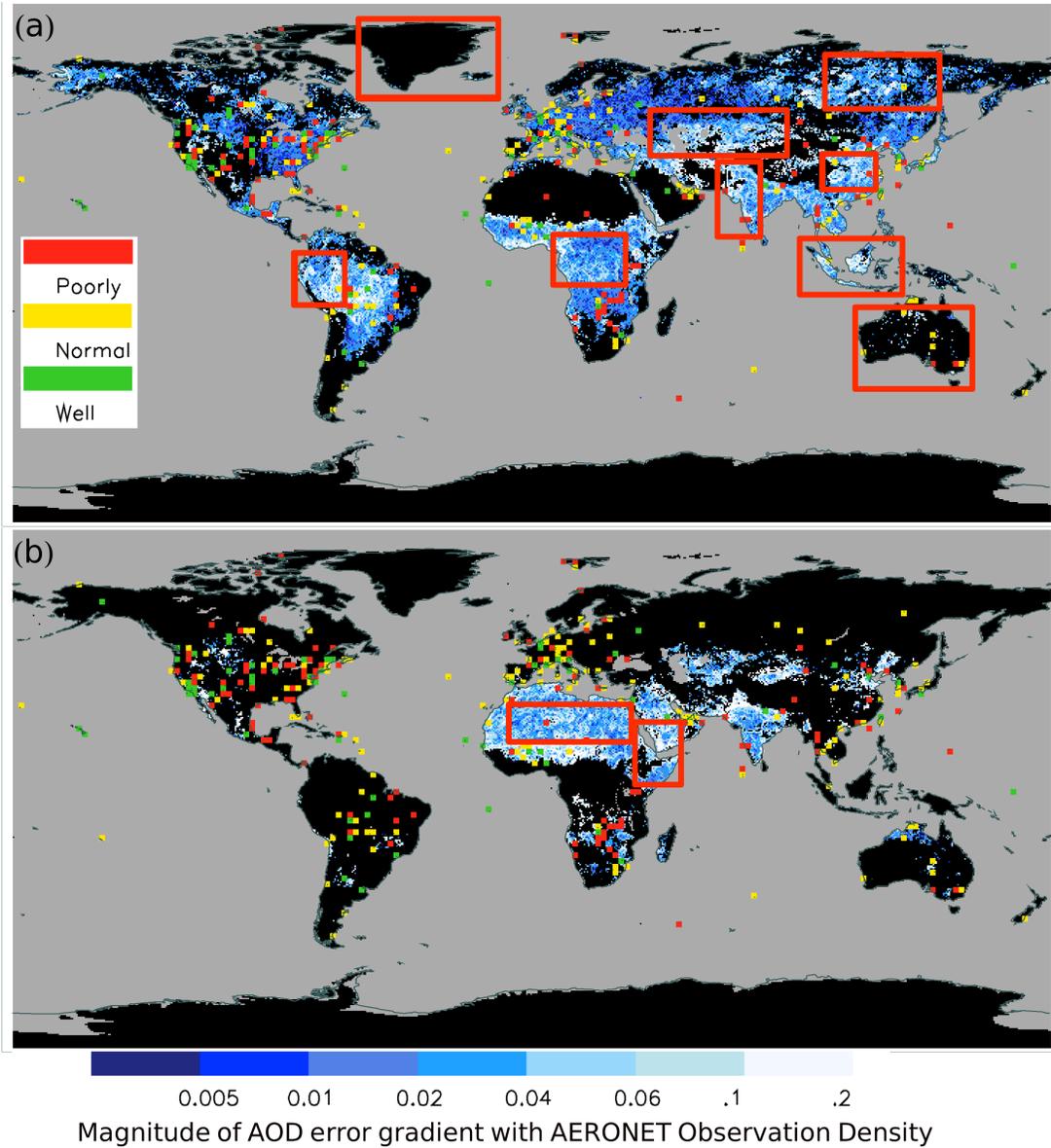
Figure 5. The spatial distribution of the gradient of AOD differences (ΔAOD) between the MODIS and MISR aerosol products. The ΔAOD was computed by subtracting MODIS DT/MODIS DB (0.55 μm) AOD from MISR AOD (0.558 μm). Only land regions that have reported AOD larger than 0.1 from both products were used for computing the gradient. Over-plotted on top of the gradient map is the AERONET density map. For AERONET observation density, for every one by one degree grid, one AERONET site that has observation for a month during the 1993–2009 periods is counted as one. Regions that have index of 0–12, 12–60, and above 60 are considered poorly, normal, well-observed area for red, yellow and green, respectively. Oceans are plotted in grey. (a) for MODIS DT and (b) for MODIS DB.

distributions of AERONET sites are needed for future validation efforts, for example: North India and western South America.

For the AERONET density index, seventeen years of the AERONET level 2.0 data were used (1993-2009). A frequency index of 1 is defined as one AERONET site within a 1° × 1° latitude and longitude region, having at least one measurement during one month of the time series. If there are two AERONET sites, and each has at least one observation during any one month, the index number is set to 2. We increment the index value for a given region even if only a fraction of a month has sun photometer data. For one AERONET site that provides continuous observations for a year, the index for the Lat/Lon grid that the AERONET site locations is set to 12. Regions with indexes of 0–12, 12–60, and above 60 (for the Seventeen year period) are defined as poorly observed (red), normal (yellow), and well-observed (green) regions respectively. Figure 5 includes four by four (4x4) degree averages, which were developed from the one by one (1x1) degree averages, by picking the largest index value of any 1x1 degree box inside the 4x4 degree grid to highlight the signal. Since only regions with AOD values larger than 0.1 from both satellite products were used in creating Figure 5, it is necessary to compare Figure 5 with the AOD ratio/difference plot (Figure 3) that includes all scenarios. Two regions that are not included in Figure 5, but are highlighted in Figure 3, are the Andes Mountains and the West Coast of the US. Again, both regions have complex surface characteristics that could introduce a problem to space-borne satellite aerosol retrievals.

Figure 5 shows that Europe and the West and East Coasts of US are well covered with sun photometer observations. However, it is still useful to identify

regions for future AERONET sites for three scenarios: (1) type A region: regions where it is suspected that aerosol optical property assumptions are poor in satellite retrievals; (2) type B region: regions with moderate to high AOD and lack of AERONET sites; (3) type C region: any sites in large regions of the earth that have no or few sites. Based on Figure 5, type A regions include Central Africa and Northwestern South America. Type B regions include the Middle East, the high latitude Asian part of Russia, Central Asia, Western India, and especially the Malaysia–Indonesia region. The type C regions include Australia and Greenland. All of the previously discussed regions are highlighted with red boxes in Figure 5.

Lastly, based on the discussions from this section, we identified regions that require better surface boundary conditions: 1) Central Asia; 2) Malaysia–Indonesia 3) Central Africa, near Zaire; 4) the Central Sahara; 5) the Eastern Arabian Peninsula; 6) Greenland and Australia, where no long-term monitoring effort is present for a large area. The Malaysia–Indonesia region is also highlighted in this study, yet we expect new sites to be established for the 7-SEAS and SEAC4RS field campaigns; some of these sites will likely remain as long-term sites. The AERONET has data from the UAE that helps address the Eastern Arabian Peninsula. Also, large discrepancies are found over the high-latitude southern ocean that invite further experiments in order to understand the cause of the high AOD band over this area. This question has been at least partially addressed by the ship based sun photometer measurements from the Maritime Aerosol Network (MAN network) (Smirnov et al., 2011). The measured AOD in this region is very low.

For topographically complex regions that introduce high AOD biases, such as the Western US, the Andes Mountains, and the Namibian desert, it would be useful for long-term AERONET sites to be established for satellite validation. Notice that most of the issues with satellite retrievals over these sites relate to surface reflectance characterization and not assumed aerosol optical properties.

3.5. Discussion: Community effort

The purpose of this study is not simply to point to areas of diverging AOD products, but rather to inform the larger scientific community that there are likely regions where local measurements can be made to maximize the benefit for retrieval development. Our regressions show that spatially correlated biases in AOD retrievals are robust. Regional measurements of aerosol or lower boundary condition properties, even over short field studies, are likely to have significant value when measurements are made in poorly observed regions.

3.6. Summary and Conclusions

Using spatially and temporally collocated MODIS and MISR aerosol optical depth retrievals, we examined the spatial difference between the operational MODIS and MISR aerosol products. Differences are indicative of the spatially correlated bias, which are highly detrimental to higher order data analysis methods such as data assimilation and inverse modeling. The spatial comparisons of the two collocated aerosol products reveal regions that need further improvements in future satellite studies. For the first time, our analysis identified the regions that would most benefit

from long-term point measurements and field campaigns for future satellite aerosol studies. The key results from our study are:

1. Comparisons of spatially and temporally collocated MODIS and MISR aerosol optical depth data revealed that the ratio of MODIS to MISR AOD is much larger than 1 for the Western US, South America, East and Central Asia, and Indonesia. Regions where the ratio is significantly less than 1 were found over the East Coast of South Africa, the East Coast of South America, and Western Australia. Note that the ratio in regions of low AOD is not necessarily a good measure of whether errors are significant, as indicated by the AOD difference plot from Figure 8c and d.

2. A closer look of the comparisons between MODIS DT and MISR data shows that over the Western US, the Andes Mountains, and Russia, high AOD "features," which are only visible from the MODIS DT aerosol product, are possibly due to the surface-reflectivity-introduced bias. Also, over South America, China, and the Indonesia regions, MODIS DT tends to overestimate, and MISR tends to underestimate AOD values, due, in part, to differences in the aerosol optical properties used in the MODIS DT and MISR AOD retrievals. Some of these observations support the results of previous studies in which some of the causes are identified (Kahn et al., 2009; Kahn et al., 2010; Levy et al., 2010).

3.   This study also identifies the locations where additional ground based

and *in situ* measurements would have the greatest impact on improving

satellite aerosol retrievals.

CHAPTER IV

CRITICAL EVALUATION OF THE MODIS DEEP BLUE AEROSOL OPTICAL DEPTH PRODUCT FOR DATA ASSIMILATION OVER NORTH AFRICA

4.1 Introduction

Numerical weather prediction of aerosol phenomena has been implemented for air quality and visibility (Lelieveld et al., 2002; Park et al., 2003; Reid et al., 2004; 2009; Al-Saadi, et al., 2005; Hollingsworth et al., 2008). Recent studies have shown that satellite aerosol retrievals can be effectively used, through data assimilation, to improve accuracies of aerosol analysis and forecasts (e.g. Zhang et al., 2008; Benedetti et al., 2009; Sekiyama et al., 2010; Campbell et al., 2010, Zhang et al., 2011). The operational MODIS Dark Target (DT) products in particular are attractive for assimilation, as they provide aerosol retrievals over global oceans and most land areas with near daily coverage. However, due to the high surface reflectance, traditional DT retrievals fail over bright surfaces such as the Saharan and Gobi deserts (Remer et al., 2005). This leaves large spatial gaps in the AOD record in desert regions, some of which host some of the largest aerosol loadings in the world. While other sensors such as the Multi Angle Imaging Spectroradiometer (MISR) and the Cloud-Aerosol Lidar and Infrared Pathfinder Satellite Observation(CALIPSO; Winker et al., 2009) can retrieve over bright surfaces, their limited swath and delayed data processing reduces efficacy in aerosol forecasting applications.

Because arid regions tend to have lower surface reflectance at shorter wavelengths, traditional DT method can often be successfully applied in blue wavelengths. The Deep Blue algorithm takes advantage of this surface phenomenology, performing aerosol retrievals at blue wavelengths (such as the 0.47 μm spectral channel in MODIS) and utilizing the selected aerosol model in the inversion to generate AOD (Hsu et al., 2004; 2006). The DB methodology has been successfully applied to both MODIS instruments and SeaWiFS to allow for large swath coverage for aerosol retrievals over and around desert regions (Hsu et al., 2004, 2006). DB has shown that aerosol optical depth can be retrieved with tolerable uncertainties, even over deserts and semi-arid regions, where traditional DT methods applied to mid-visible and red wavelengths have difficulties (Shi et al., 2011b; Li et al., 2012). This has allowed DB to be applied to such sensitive applications as source function development (e.g., Ginoux et al., 2010).

While filling a significant data gap, the use of DB specifically in data assimilation applications requires the development of a prognostic error model. That is, a realistic and scene dependent uncertainty needs to be assigned to every retrieval. Such errors are not commonly reported by aerosol retrieval developers. Instead, bulk global uncertainties are given, often expressed as an error range and a fraction of retrievals falling within that range (e.g. MODIS Dark Target (DT) over-land AOD has an expected error range of $\pm0.05 \pm 0.15 \times \tau$, and roughly two-thirds of MODIS DT collection 5.1 (c5.1) AOD fall within that error range (Levy et al., 2005). Given that uncertainty is well known to be related to spatially correlated features such as land surface albedo and aerosol microphysical properties, the use of a single

uncertainty value can result in large errors in models during assimilation. The inclusion of data from a region with poorly constrained lower boundary conditions could, for example, result in a fictitious "aerosol plume" in a model forecast. Hence, one necessary and unavoidable step before applying a satellite aerosol product to aerosol data assimilation is an independent evaluation of uncertainties of the product, including an assessment of both random and systematic errors (e.g. Zhang and Reid 2006; Kahn et al., 2009; Hyer et al., 2011; Shi et al., 2011a, Zhang et al., 2010). Data-assimilation (DA) oriented products with reduced bias and more realistic descriptions of uncertainty have been generated from several different aerosol products through detailed analysis of retrieval uncertainties. For example, the data assimilation quality (DA-quality) operational MODIS c5.1 products over both land and ocean are used for operational aerosol forecasting (Zhang and Reid, 2006; Shi, et al., 2011a; Hyer, et al., 2011). NASA GMAO performs their own retrievals based on machine learning as standard products were of insufficient quality for assimilation (Arlindo daSilva, personal communication, 2011). ECMWF similarly has a series of quality control processes. To date, however, arid region retrievals are not operationally assimilated.

As part of the evaluation of satellite aerosol products, the DB aerosol products were evaluated and their uncertainty sources were investigated with a focus over North Africa and the Arabian Peninsula – the world's largest contiguous dust belt. Following Zhang and Reid (2006) and Hyer et al. (2011), this study applied a series of procedures to remove outliers and reduce systematic bias in DB aerosol products. The uncertainties of data were examined as functions of their main sources, such as boundary conditions, observation conditions, and aerosol microphysics. Empirical

studies and quality control procedures were applied to create quality assured DB level 3 aerosol products suitable for data assimilation.

4.2. Methodology

This study is based on the comparisons of MODIS DB c5.1 and AERONET AOD, coupled with a contextual analysis of retrieved aerosol features. The quality assured level 2.0 Aerosol Robotic Network (AERONET) AOD data with a stated uncertainty of 0.015 were used as the "ground truth" (Holben et al., 1998). Eight years of AERONET AOD data were collocated in space and time with Aqua DB (2002-2009) and Terra DB (2000-2007), following the method mentioned in Shi et al. (2011a). To minimize the spatial and temporal difference between these data, pairs of AERONET sun photometer data and MODIS aerosol retrievals were matched if the spatial distance between two observations was within 0.3° (Lat/Lon) and the difference in observation times was within 30 minutes.

AERONET data that are within ±30minutes of satellite overpasses were averaged. However, the satellite observations are not averaged spatially. The averaging process of surface observations reduces the sample biases, but could also filter out real signal peaks. For example, if a small-scale smoke plume passes through a sun-photometer site, the averaged AERONET AOD value could be lower than the AOD value retrieved via a satellite. Also, it is possible that one AERONET observation could be paired with more than one satellite retrievals.

Many studies, different from this study, used averaged satellite and sun photometer data to blur the spatial and temporal differences between the two data sets

(Remer et al., 2005; Kahn et al., in press; Hsu et al., 2006). This approach is understandable considering the spatial and temporal differences between the observations.

Sun photometer provides point observations at a given time whereas a satellite retrieval is a two dimensional spatial observation at a given time. Because of the difference in sampling methods, differences between the two types of observations can exist. However, in this study, in order to study the uncertainties in the satellite retrievals due to observing conditions at the pixel level, satellite data were not averaged. Note that only over-ocean retrievals were used, which implies that only AERONET data from coastal or island sites were selected.

AERONET and satellite data are collocated at three wavelengths: 0.55 μm for MODIS and 0.558 μm for MISR, 0.67 and 0.87 μm. Note that the AERONET data do not include observations at $\lambda = 0.55$ μm and, therefore, the AERONET observations from 0.50 and 0.67 μm were used to interpolate and match MODIS results at λ=0.55 μm. This interpolation is based on the assumption that the Angström Exponent (α— further discussed in the microphysical properties section) derived from two wavelengths is consistent throughout all wavelengths (O'Neill, et al., 2003), with the relationship

$$\tau_{550} = \exp\left\{\ln(\tau_{500}) + \left[\frac{\ln\left(\frac{550}{500}\right)}{\ln\left(\frac{670}{500}\right)}\right] \times \ln\left(\frac{\tau_{670}}{\tau_{500}}\right)\right\} \tag{3}$$

where, τ_{550} and τ_{670} are AOD at 0.55 μm, 0.5 μm and 0.67 μm bands, respectively. Note that 0.44 μm is used when retrievals at 0.5 μm are not available. Due to MODIS

c5.1 DB only retrieves over the bright surfaces, the spatial coverage of the data includes North Africa, the Arabian Peninsula, part of Central Asia, India, Australia, the western US, and Andes Mountains.

4.3 Evaluations

In this section, the general performance of DB is described, along with the sources of uncertainties in the DB products with respect to observing conditions and Quality Assurance (QA) flags provided by the DB products. Details of the evaluation procedures are illustrated in

. Four main steps include (1) evaluating the performance of the DB products with respect to QA flags included in the datasets, (2) studying the uncertainties of the DB products as functions of observation conditions, (3) assessing the uncertainties of the DB products in relation to the spatial variations of AOD and surface albedo, and (4) developing empirical correction procedures. In the second step, the performance of the AOD_{DB} data was analyzed as functions of various parameters including lower boundary conditions, viewing geometry, cloud contamination, aerosol microphysical properties, and other observing conditions. After applying the empirical correction steps, both ¼ degrees and 1 degree (Lat/Lon) DA-quality AOD_{DB} products were generated, and the ¼ degrees products were generated for evaluation purposes only. All analyses were conducted for both Terra and Aqua DB products, however, in most cases, only analyses from Aqua DB data are shown, as similar structures are found for the Terra DB product. The analyses for the Terra DB product are provided in the supplemental materials unless specifically mentioned.

Albedo (α)

Decoupled α with fine mode fraction (η)

Decoupled α with Aerosol type

Angström Exponent

Single scattering albedo (ω)

Viewing Angle

Cloud Fraction (F_{cld})

Step 1 QA filter

Step 2 Analysis

Step 3 Spatial Variation Check

Standard error of AOD (STD_{AOD})

Decoupled Standard error of surface (STD_{sfc}) and STD_{AOD}

Step 4 Empirical Correction

Step 5 Aggregated to Level 3 Data

Figure 6. Flow chart of the production process for the level 3 DB DA quality aerosol product.

4.3.1 Overall nature of the Deep Blue Product

This section starts with the simple global evaluation of the DB product, and then describes the selection of areas with sufficient collocated AERONET and DB data for further evaluation. Figure 7 shows the global comparisons of the collocated Aqua DB and AERONET AOD with respect to different QA flag settings. The fractional data density is shown in Figure 7 for every 0.5 increments of AOD for both AERONET and DB. This figure displays the traditional method of evaluating satellite data against AERONET, which is used to diagnose the uncertainties in the data set. The regression equation $\tau_{DB} = b + a \times \tau_{AERONET}$ is *diagnostic* and describes the quality of the retrieval against a more accurate reference dataset (in our case, $\tau_{AERONET}$). By contrast, the regression equation $\tau_{AERONET} = b + a \times \tau_{DB}$ is *prognostic* and describes the linear transformation that will produce values that are closest to the reference data. In this study, diagnostic regression is used to capture data characteristics, and

prognostic regressions are used to develop correction factors and uncertainty estimation models.
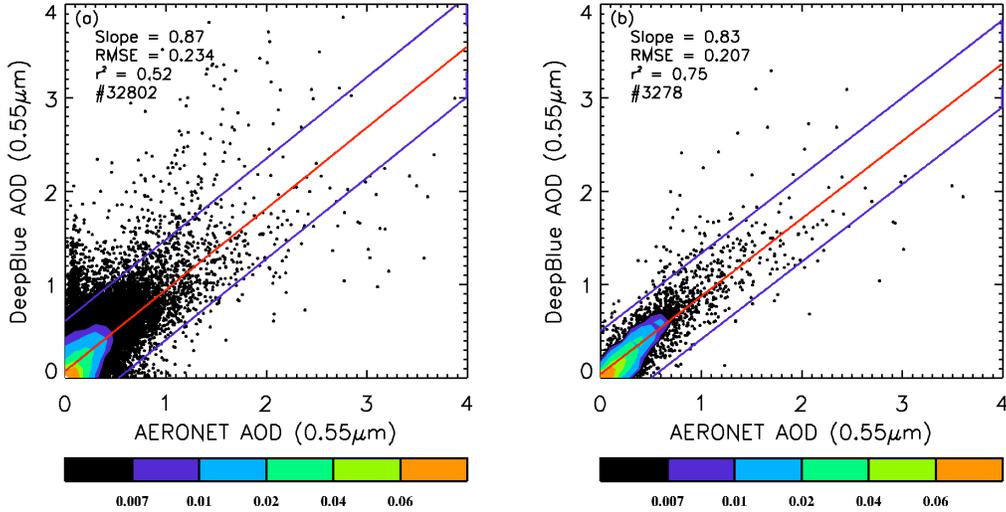
Figure 7. Comparisons between Aqua DB and AERONET AOD 2002-2009 for diagnostic purpose for (a) all data, (b) data with very good QA quality globally. The red line is the linear fit line and the blue lines are the 95% confident interval lines. The color contour shows the fractional data density.

This study makes extensive use of root meet square errors (RMSE), which are calculated using Equation 4

$$RMSE = \sqrt{\frac{1}{n}\sum_{n}\left(\tau_{AERONET} - \tau_{DB}\right)^2} \tag{4}$$

and represent the bias of the evaluated data sets towards the ground truth. The uncertainty estimation model, following Zhang and Reid 2006, is based on a prognostic equation to estimate RMSE as a function of AOD_{DB}. Development of this uncertainty estimate is discussed in Sect. 5.5.

As Figure 7 shows, AOD_{DB} values have a RMSE of 0.234 with respect to $AOD_{AERONET}$ globally, an r^2 value of 0.52, and a slope of 0.87 for all available data. Note that this RMSE is probably a reflection of the data from the highest AOD range.

A total of 42.8% (14023) of AOD_{DB} data points fell outside the reported uncertainty range, defined by $\pm 0.05 \pm 20\% \times \tau_{AERONET}$ (Hsu et al., 2008). When only data with a QA of "Very Good" are used, the RMSE drops to 0.207, r^2 increases to 0.75, the slope changes to 0.83, and the fraction of outliers drops to 31.7% (1038). Although the regression slopes in Figure 7 are not dependent on QA flags, the 11.5% decrement in RMSE and 11.1% decrement in outliers from QA flags equal to "None" to "Very
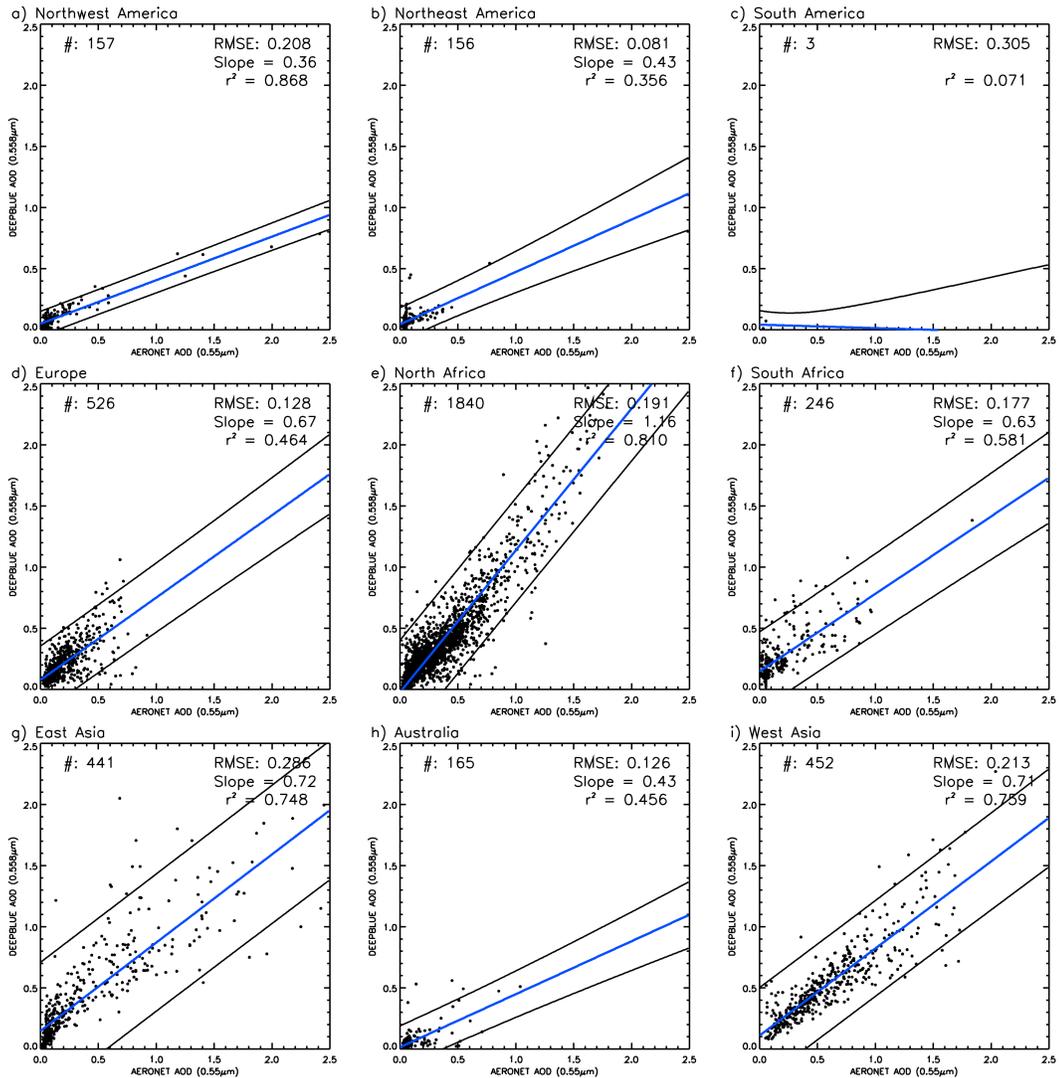
Figure 8. Regional comparisons between AOD_{DB} and $AOD_{AERONET}$ 2002-2009 with only QA equal to "Very Good" for (a) Northwest America, (b) Northeast America, (c) South America, (d) Europe, (e) North Africa, (f) South Africa, (g) East Asia, (h) Australia, and (i) West Asia. The blue line is the linear fit line and the black lines are the 95% confident interval of the linear fit line.
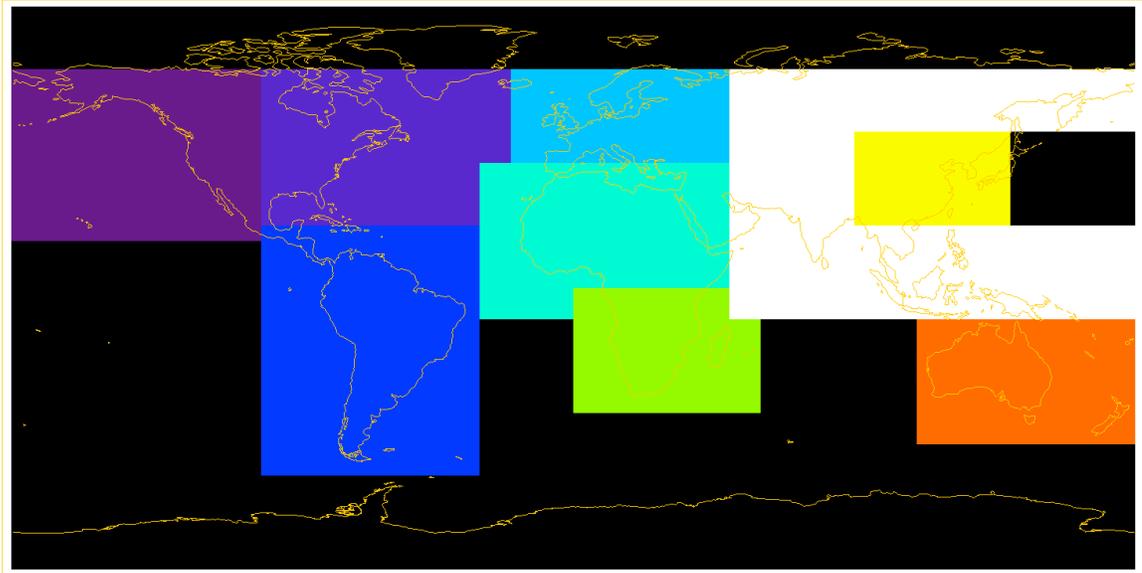
Figure 9. The domains for areas that are shown in Figure 8.Western North America is shown in indigo, Eastern North America is shown in dark slate blue, South America is shown in blue, Europe is shown in sky blue, North Africa is shown in spring green, South Africa is shown in lemon green, Australia is shown in orange, West Asia is shown in white, East Asia is shown in yellow, and other region is shown in black.

Good" show that higher quality data are selected when using the "Very Good" QA flag. However, in addition to an improved performance, an 84.3% data loss is found.

The performance of the AOD_{DB} retrievals, however, shows a regional dependence, particularly in regard to slope. This is suggestive of microphysical bias, but since the DB algorithm utilizes a recalculated surface reflectance database that is based on a minimum reflectivity technique (Hsu et al., 2004), it is possible that the regional dependence of the DB retrieval performance could also be a function of surface albedo as suggested from this study as well. Using all available data with the "Very Good" QA flag, regional comparisons between Aqua DB and AERONET for
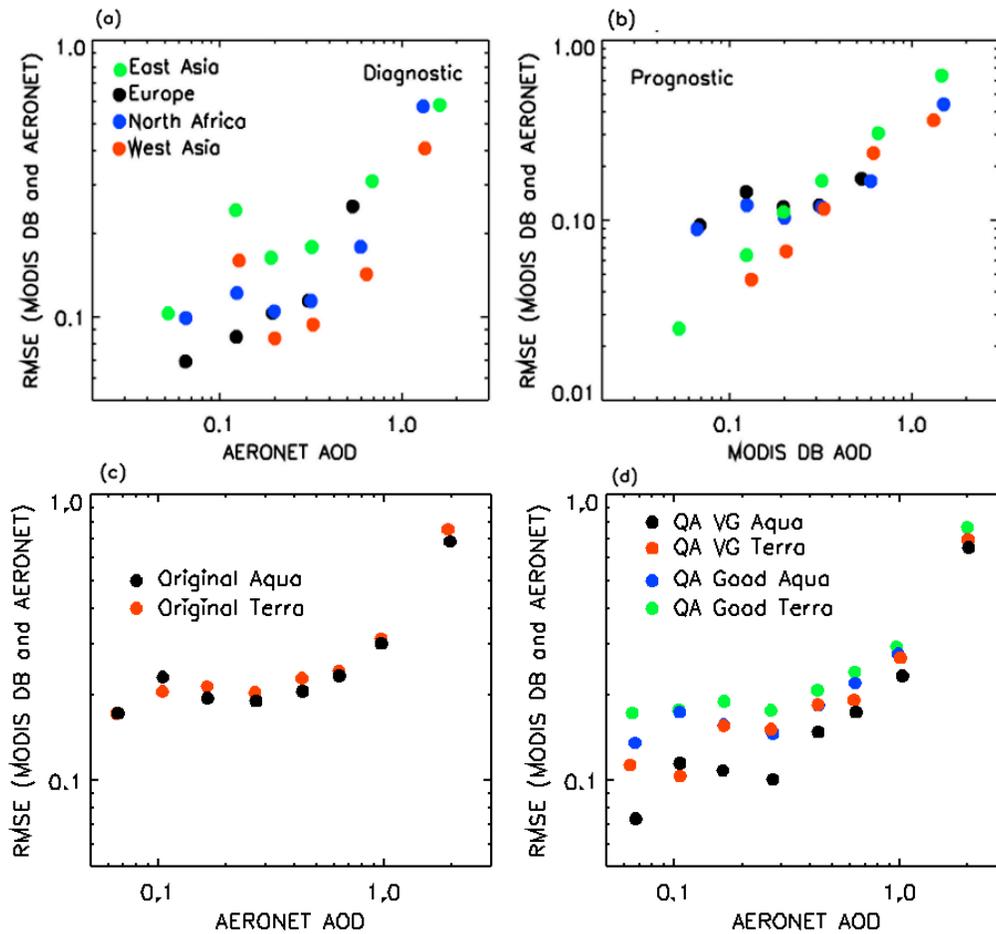
Figure 10. The RMSE of AOD_{DB} against $AOD_{AERONET}$ for a. data with "Very Good" QA flag over Europe (black), North Africa (blue), East Asia (green), and West Asia (red) in Figure 8 as a function of $AOD_{AERONET}$, (b) similar to(a) but as a function of AOD_{DB}, (c) all data over North Africa as a function of $AOD_{AERONET}$ and (d) similar to(c) but with data with QA equals to "Very Good" and "Good."

nine selected regions were conducted as shown in Figure 8, with Figure 9 showing the domain of each area in a different color. As indicated from Figure 8, only four regions, namely North Africa, Europe, East Asia, and West Asia, have more than 400 collocated data points that are sufficient for an evaluation study with respect to various observing conditions. The remaining regions, Western North America, Eastern North America, South America, southern Africa/Sub-Saharan Africa, and

Australasia, either have small number of collocated Aqua MODIS and AERONET data points or have larger scattering of data distribution. Of the nine selected regions, the best performance of DB data is found over North Africa, with a slope of 1.16, an r2 value of 0.81, and an AOD RMSE of 0.19 between DB and AERONET. However, high bias occurs when AOD is greater than one, which could be caused by multiple scattering. Contrary to the overestimation of AOD values over the North Africa region, an underestimation of AOD values is found for DB retrievals over Asia, with a much higher RMSE of 0.21 for West Asia and 0.29 for East Asia. Regions other than North Africa either have very few collocated DB and AERONET data points, or have a much larger scatter between satellite and AERONET AOD values. The diagnostic and prognostic RMSE models were built for regions in Figure 8 with more than 400 data points, namely Europe, North Africa, East Asia and West Asia (Figure 10a and b). The RMSE models were created using the same binning method for all of the components within each panel. The corresponding mean $AOD_{AERONET}$ for all the data points in each bin was plotted as the bin's X-axis value. Europe, shown in black in Figure 10a and b, has low RMSE at low $AOD_{AERONET}$, but higher RMSE at low AOD_{DB}. This can be explained if DB is systematically underestimating AOD in this region, a possibility we will examine later in this section. Because of limited data volume and range of retrieved AOD_{DB} in the matched datasets, only the North Africa and Arabian Peninsula regions (namely "the study region" from now on) were used to construct the DA-quality DB products. These regions will be the main focus of discussion in this study.

Focusing on the study region, the diagnostic RMSE analysis as a function of $AOD_{AERONET}$ was performed for all data and data with QA flag values of "Good" and "Very Good" (Figure 9c and d). For all available data and data with "Good" QA flags, the RMSE values from Aqua and Terra are very similar in both magnitude and pattern. When $AOD_{AERONET}$ values are smaller than 0.8, the RMSE values from both sensors remain relatively constant. Above this value, the RMSE increases as $AOD_{AERONET}$ increases. With a strict QA flag filtering, the RMSE values of AOD_{DB} reduce to approximately 0.1 for $AOD_{AERONET}$ below about 0.4, with a larger reduction of RMSE shown in Aqua data.

Shown in Figure 7 and Figure 8, the QA flag is necessary for highlighting retrievals that are the most "trustworthy" (Hsu et al., 2004). However, there are limitations in using data with only "Very Good" QA flags. For example, using the QA flag also introduces artifacts in AOD spatial distribution. Figure 11 shows the daily spatial distribution of AOD_{DB} over the study region for 1, 2, and 3 May, 2006, with all available data on the left panel, and data with only QA flags of "Very Good" on the right panel. For all three days, two patterns can be observed consistently from the right panel: 1) retrievals in the center of the swaths are removed which are due to the large scattering angles (personal communication with Christina Hsu 2012); 2) the number of retrievals is largely reduced south of 13 °N, and a significant portion of low AOD retrievals are excluded by the "Very Good" QA flags. When averaged over a one-year period (Figure 12), the second pattern shows up as a near-linear feature, indicated by much higher AOD values for "Very Good" data below 13 °N (Figure 12a and b). This pattern is introduced by a significant reduction in the number of

retrievals, especially low AOD retrievals as shown in Figure 11, when applying the "Very Good" QA filters (Figure 12c). This reduction in data samples was caused by artificial thresholds in the DB retrieval algorithm, considering the number of pixels used in the retrieving process. Despite the disadvantage of applying "Very Good" QA flags, only DB data with the "Very Good" QA flags were used hereafter, because of reduced error in these data, and because of systematic bias in AOD values with other QA flags (see Sect. 5.3.2.1).

4.3.2 Detailed analysis for DB over North Africa and Southwest Asia

Series of analyses were performed to investigate the sources of uncertainty in AOD_{DB} product, including angular dependence, aerosol microphysics, surface reflectance, and other observing conditions. Aerosol layer height and surface elevation are possible uncertainty source for retrieving aerosol using shorter wavelengths. For example, Hsu et al., 2004 mentioned that a ±2 km variation in aerosol plume height could introduce a 25% uncertainty in AOD at 412 nm and 5% at 490 nm. "Very Good" quality data were used to conduct most of the analyses except that of angular influences, due to the change of behaviors between all available data and data with "Very Good" quality. Although most discussions are focus on the study region only, global analysis is performed for the aerosol microphysics studies (Sect. 5.3.2.2), as insufficient numbers of fine mode aerosol retrievals are available at the study region.
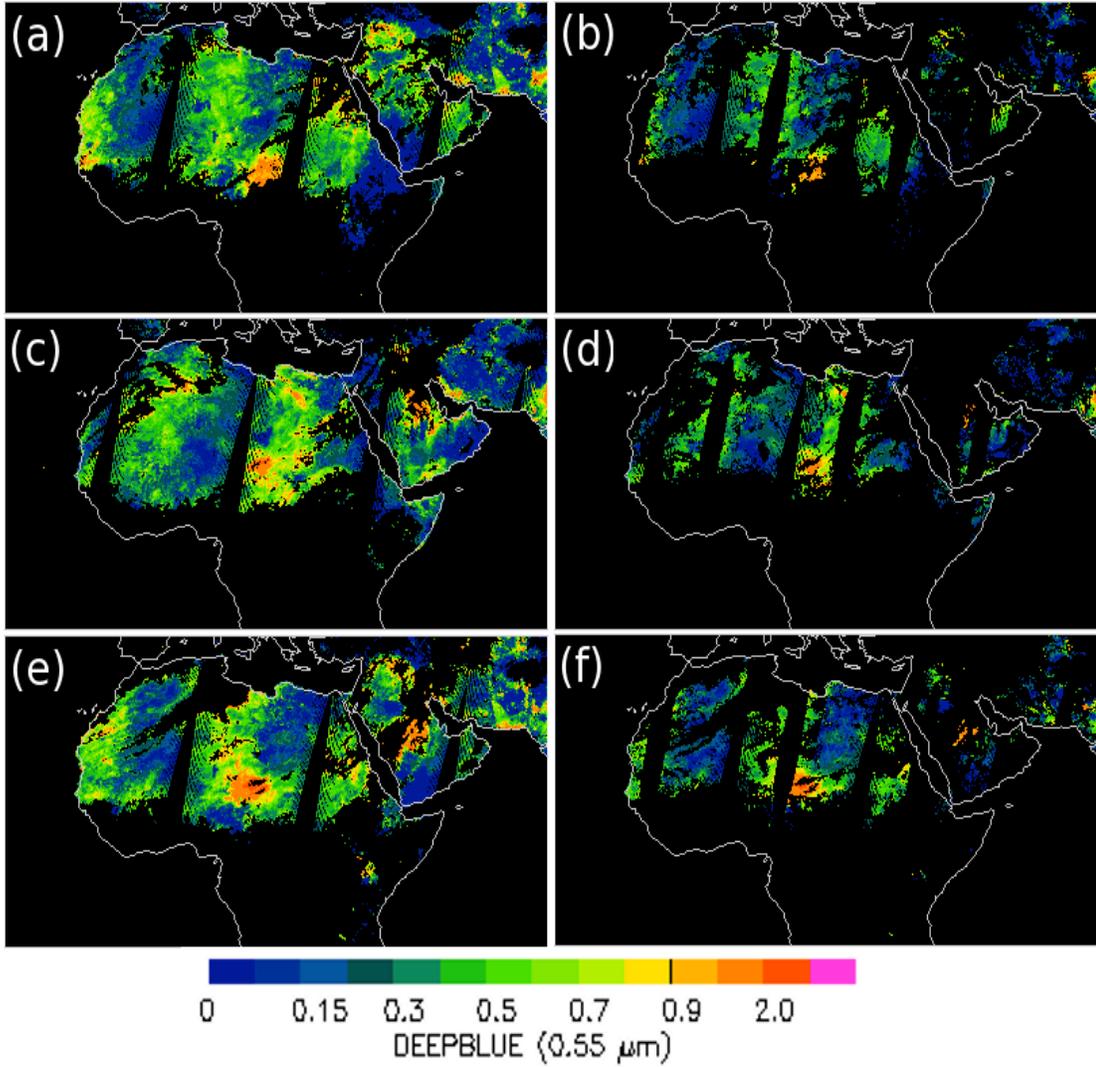
Figure 11. Quarter degrees spatial average of satellite aerosol observation over the study region for AOD_{DB} for three days. The first, second and third rows correspond to DB data at May 1st, 2nd, and 3rd, 2006. The left column is all available DB data and the right column is DB data with QA equal to "Very Good" only.

4.3.2.1 Angular Dependence

An interesting discrepancy between the AOD_{DB} with and without QA flag filtering was discovered for angular dependency in AOD bias. For data with QA flag equals to "Very Good", no systematic bias ($\tau_{AERONET}$ - τ_{DB}, symbol as $\Delta\tau_{A-M}$) is found as functions of viewing zenith angle (θ). However, with all data, there is a strong
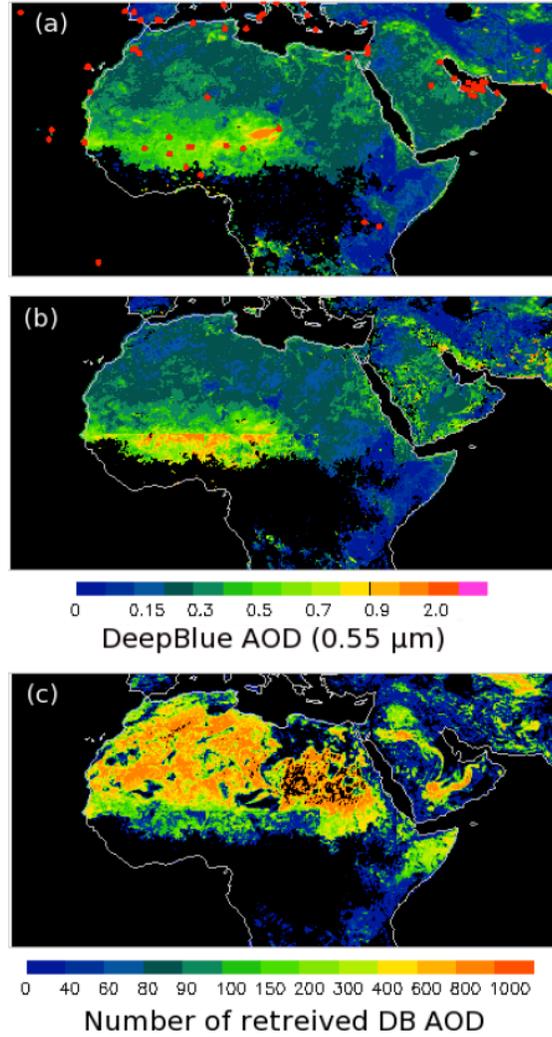
Figure 12. Spatial distributions of DB for 2006 (a) AOD_{DB} before the QA filtering, (b) only AOD_{DB} with "Very Good" QA, and (c).Number of retrievals available after the QA filtering. Red dots in (a) represent the AERONET sites.

relation between increasing viewing zenith angle and increasing $\varDelta\tau_{A\text{-}M}$. Figure 13 shows the average difference between AOD_{DB} and $AOD_{AERONET}$ at 0.55 µm as a function of θ over the study region. As θ values increase the $\Delta\tau_{A\text{-}M}$ changes from -0.07 to about zero, indicating a smaller bias for a larger θ value. However, this relationship between $\varDelta\tau_{A\text{-}M}$ and θ is non-existent when the "Very Good" QA flag
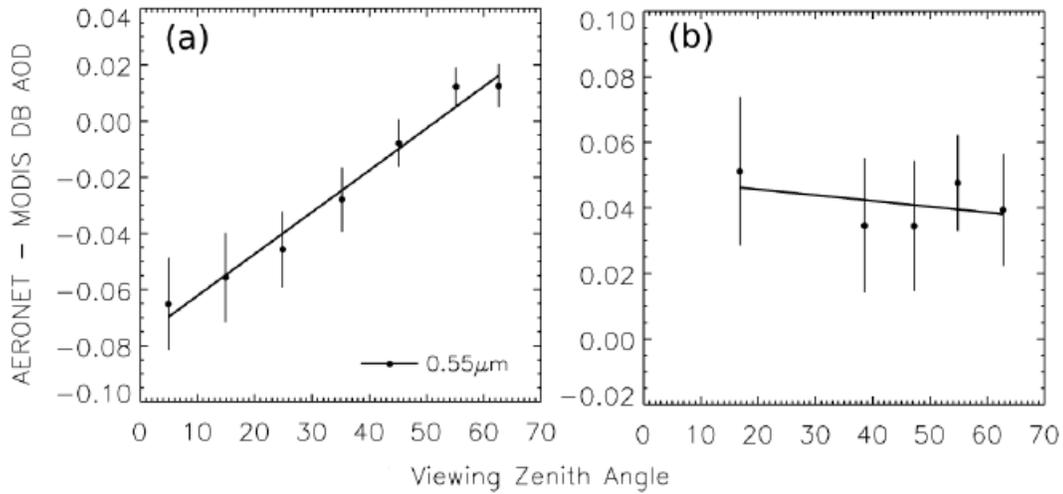
Figure 13. The differences in AOD between Aqua AERONET and DB as a function of viewing angle over North Africa for (a) total AOD_{DB} without QA filter, and (b) AOD_{DB} with "Very Good" QA. Data were averaged for every 10 degrees viewing zenith angle and one standard deviation bars were shown.
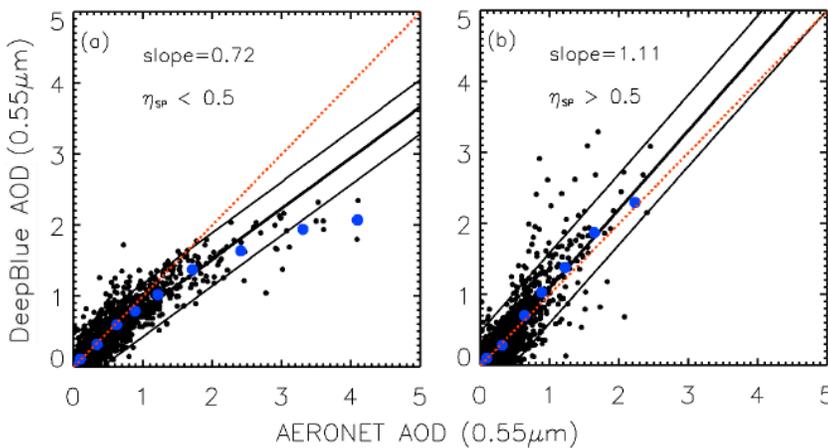
Figure 14. Comparisons between Aqua AOD_{DB} and $AOD_{AERONET}$ globally during 2002-2009 under cloud free conditions for (a) fine mode fraction smaller than 0.5 and (b) fine mode fraction greater than 0.5. The blue dots represent the averaged AOD_{DB} for each $AOD_{AERONET}$ bin. The thicker black line is the linear fit line and the thin black line is the 95% confidence interval. The red dashed line is the 1 to 1 line.

filtering is applied (Figure 13b). Similar patterns were found for scattering angle, but not shown here. The influence of the viewing angle was then decoupled with albedo at 0.412 μm. It is shown that, when the surface is relatively bright (albedo between 5% and 11%), the influence from the viewing angle is minimized. When the surface

62

is dark (albedo smaller than 5%), the bias of AOD varies with viewing angle for all available data.

4.3.2.2 Aerosol Microphysics

Four aerosol microphysical parameters were evaluated for their impacts to the retrieval bias under cloud free conditions. The four parameters were Angström Exponent and Single Scattering Albedo (ω) from the DB product, fine mode fraction (η) calculated from AERONET data using a spectral convoluted method from O'Neil et al. (2003), and the aerosol type flag included in the DB QA flag. Among all the parameters, investigations showed that the AOD_{DB} errors are most sensitive to η. Only one third of the aerosol retrievals over the study region have $\eta > 0.5$ and all data from the matched dataset with $\eta < 0.5$ are from the study region. Figure 14 shows the scatter plot of AOD_{DB} vs. $AOD_{AERONET}$ for two η ranges: $\eta < 0.5$ (Figure 14a) and $\eta > 0.5$ (Figure 14b). Underestimation of AOD_{DB} is found for coarse particles with $\eta < 0.5$, and an overestimation is found for fine particles with $\eta > 0.5$ globally. Consistent relationships are also found over the study region. Since nearly two-thirds of DB aerosol retrievals in the matched dataset over the study region have $\eta < 0.5$, it is likely that AOD_{DB} over the study region as a whole is underestimated.

Although convincing trends are found with respect to η, a parameter that is included in the DB products needs to be selected and used for empirical corrections mentioned in a later section. Thus, other microphysical parameters, including Angström Exponent and ω, were also examined, site by site, and seasonally. However, no significant trends are found for these two parameters. A comparison was made between the retrieved Angström Exponent and AERONET derived η, no relation

between the two parameters was found. Note that the DB Angström Exponent is predefined by the aerosol models contained in the look up table. Therefore, the DB Angström Exponent will not necessarily relate to the AERONET derived η. At last, instead of using external calculated η from AERONET, the aerosol type flag, a parameter that is included in the DB products, was used to represent the aerosol microphysics in the empirical correction step (see Sect. 4.4).

4.3.2.3 Surface Reflectance

The DB algorithm utilize a pre-calculated surface reflectance database that following minimum reflectivity technique (Hsu et al., 2004). Therefore, it is necessary to evaluate the influence of the static albedo on AOD retrievals. Also, as mentioned in Sect. 4.3.2.2, $\Delta\tau_{A\text{-}M}$ can be affected by inaccurate assumptions of aerosol microphysical properties in the retrieval process. To decouple the effects of aerosol microphysics and surface albedo on $\Delta\tau_{A\text{-}M}$, the surface albedo related AOD_{DB} bias was investigated as a function of aerosol type and fine/coarse aerosol modes. Again, global data were used to observe the fine mode aerosol performances and the coarse mode particle analyses are the same for the study region.

For all analyses, the collocated DB and AERONET AOD data were separated into four groups based on DB surface albedo (α) at a wavelength of 0.412 μm. The four albedo ranges are 0–5%, 5%–8%, 8%–11% and above 11%. Figure 15 shows the spatial distribution of the selected albedo ranges over the study area. Illustrated in Figure 15, areas with albedo values higher than 11% are located over the white sand deserts, and regions with albedo values lower than 5% are located over semi-vegetated areas. The influences of surface albedo as well as η to AOD_{DB} data are

shown in Figure 16. Here again, all collocated DB and AERONET data are included as there are insufficient fine mode AOD retrievals over the study area. Left panels of Figure 16 show that for $\eta < 0.5$ (coarse mode), when α is less than 11%, an underestimation in satellite AOD is observed, and a strong non-linear trend is found. The magnitude of the underestimation is reduced when α increases from 5% to 11%. For $\eta > 0.5$ (fine mode), however, an overestimation is found for low albedo ranges, but not for the 8-11% albedo range (Figure 16 right panels). In general, for coarse mode aerosols, a higher albedo results in a smaller underestimation, and for fine mode aerosols, an opposite pattern is observed. Also illustrated in Figure 16, large scatter is found between DB and AERONET AOD when surface albedo (0.412 μm) values are greater than 11% for both $\eta > 0.5$ (fine mode) and $\eta < 0.5$ (coarse mode) cases. Figure 16 highlights the necessity of decoupling the surface and aerosol microphysical factors for empirical corrections.
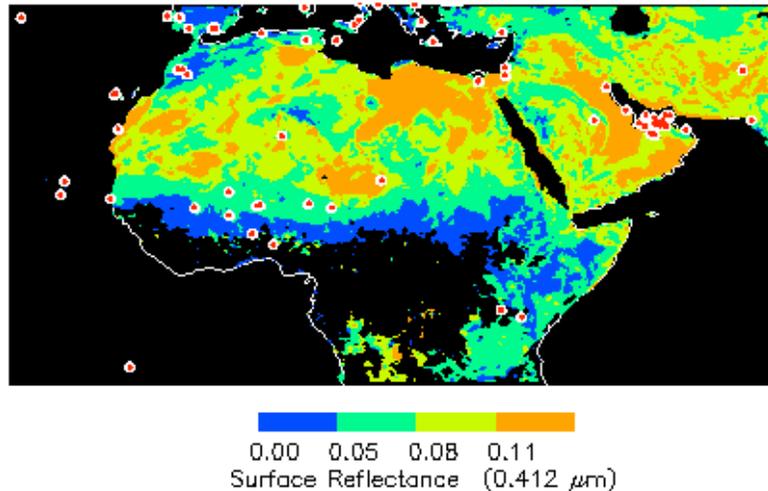
Figure 15. Spatial distribution of surface reflectance at 0.412 μm. The four albedo ranges are 0-5% (blue), 5%-8% (green), 8%-11% (yellow) and above 11% (orange). The highlighted red dots show the locations of AERONET sites used in this analysis.

65

4.3.2.4 Observing Conditions

Cloud contamination is one of the potential sources of uncertainties for satellite aerosol products. However, 93% of retrievals with "Very Good" QA are free of MODIS-detected cloud. The error statistics of the remaining 7% do not show significant differences, and do not demonstrate the systematic offset in AOD shown in the MODIS dark-target over-land product (Hyer et al., 2011).

Surface elevation is another potential source of uncertainties when using the blue wavelength for retrieving. The relationship between $\Delta\tau_{A\text{-}M}$ and the surface elevation of the AERONET stations was studied as a function of AERONET AOD. However, no significant trend was found between surface elevation and $\Delta\tau_{A\text{-}M}$. Yet such a study may be biased, as only a limited number of AERONET sites are located at high elevation.

DB products also contain a parameter that records the number of 1-km level1b MODIS reflectance pixels used in creating the 10 km resolution AOD retrievals. The quality of the DB retrievals was checked with respect to this parameter, and a noticeable high bias in $\Delta\tau_{A\text{-}M}$ of 0.11 was found when all of the 1-km pixels are used in the retrieval process, as shown in Figure 17. The DB data has a low bias over most of the scenarios except when the number of pixels used is around 60–80. The pattern of $\Delta\tau_{A\text{-}M}$ increasing when 100 pixels were used is also found in Terra. However, for the rest of the scenarios, there is no systematic low bias found.
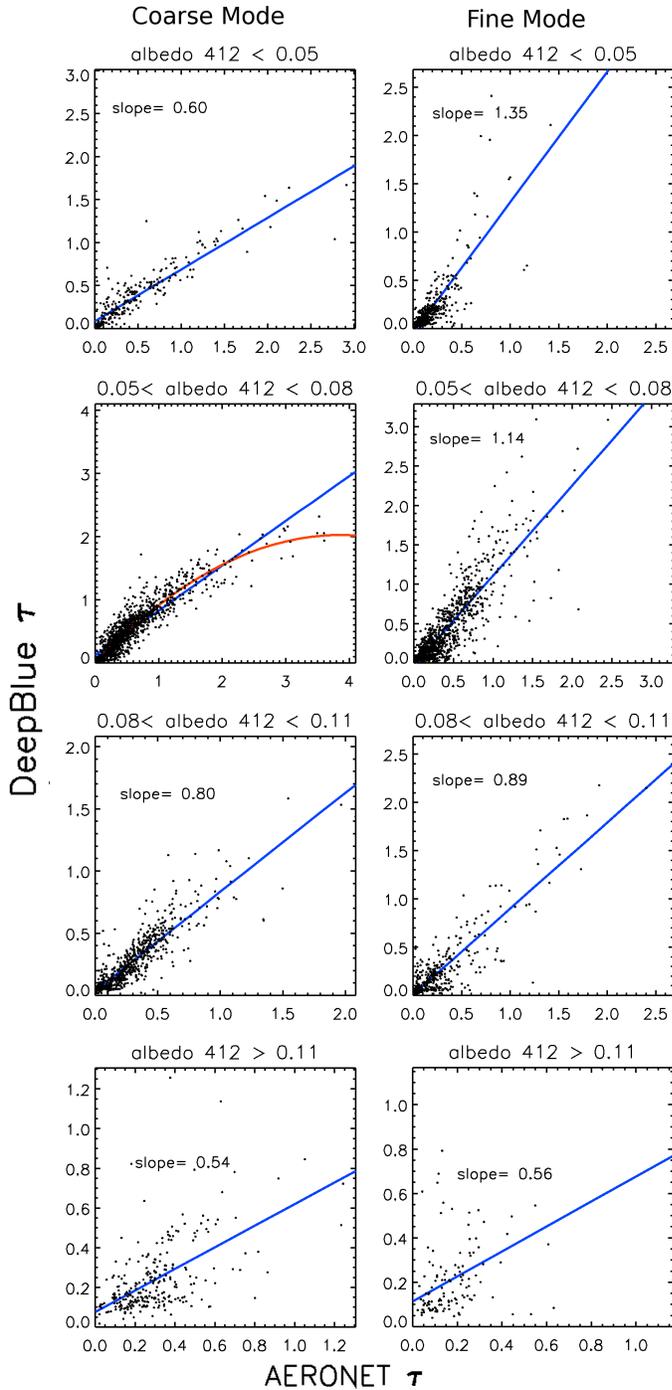
Figure 16. Comparisons between coarse and fine mode Aqua AOD_{DB} and $AOD_{AERONET}$ at 0.55 μm globally 2002-2009 with albedo at 0.412 μm. Each row represents data from a range of albedo: (a) and (b) are for albedo less than 0.05, (c) and (d) albedo ranges between 0.05 and 0.08, (e) and (f) albedo ranges between 0.08 and 0.11, and (g) and (h) are for albedo greater than 0.11. The left panel shows the coarse mode with the fine mode fraction less than 0.5, the right panel shows the fine mode with the fine mode fraction greater than 0.5. The blue line is the linear regression line, and the red line is the polynomial regression line.

67
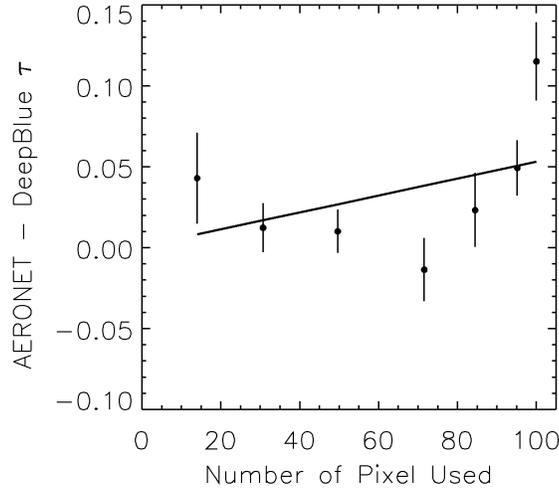
Figure 17. AOD bias ($\Delta\tau_{A-M}$) as a function of the number of pixels used for retrieving Aqua DB over the study region. The error bars indicate one standard deviation above and below the mean.

4.3.3 Statistical Analysis for Spatial Variations

In Sect. 4.3.2, sources of physical-based uncertainties of the AOD_{DB} have been identified. The DB aerosol data are reported at a spatial resolution of 10 km, and, therefore, the regional variations of surface albedo and aerosol optical properties within the 10 km domain could also affect the accuracy of the AOD_{DB} values, as illustrated by Equation 5. Equation 5 shows the relationship between the uncertainties in AOD_{DB} values and three main contributors: 1) regional variations of AOD_{DB} (STE_{AOD}), 2) regional variations of surface albedo (STE_{sfc}), 3) physical based uncertainties as described in Sect. 4.3 (physical parameters, or PP).

$$\Delta\tau = \frac{\partial\tau}{\partial STE_{sfc}} dSTE_{sfc} + \frac{\partial\tau}{\partial STE_{AOD}} dSTE_{AOD} + \frac{\partial\tau}{\partial PP} dPP \qquad (5)$$

Here, STE_x represents the spatial variance of parameter x and is defined as the standard error of component x that is calculated using:

68

$$STE = \frac{\sigma}{\sqrt{N}}$$

(6)

where

$$\sigma = \sqrt{\frac{1}{N} \sum_{i=1}^{N} (x_i - \mu)^2}$$

(7)

N is sample size, x_i is each sample value, μ is the expected value, and σ is standard deviation. The standard error is calculated using a 3 by 3 (approximately 30 km × 30 km) moving window around a given aerosol retrieval.

The goal of this study is to evaluate potential sources of uncertainties in the DB aerosol products, and to develop quality assurance steps and empirical methods to minimize bias and noise. Therefore, the first two terms from the right hand side (RHS) of Equation 5 need to be studied and removed for the further development of empirical correction methods. It is difficult to completely decouple the three terms listed in the RHS of Equation 5. However, it is possible to identify scenarios that minimize the first two terms, as shown in Figure 18. Figure 18 shows the analyses of normalized $\Delta\tau_{A\text{-}M}$ ($\Delta\tau_{A\text{-}M}$ over DB AOD) as a function of STE_{sfc} with respect to surface reflectance, AOD_{DB}, and aerosol type. Figure 18a shows that for darker surfaces (albedo smaller than 8%), the variation of SDE_{sfc} is low. Higher SDE_{sfc} values are found over regions with brighter surfaces (e.g. 8% < albedo < 11%), especially when normalized aerosol bias becomes negative. Figure 18b suggests that larger STE_{sfc} values correspond to regions with low AOD values. When normalized aerosol bias reaches -1.0, the largest mean values of STE_{sfc} correspond to AOD values smaller than 0.25. When separating the STE_{sfc} based on aerosol type, the STE_{sfc} of smoke particles oscillates around 0.0015, while those of "mixed" and "dust" particles fluctuate at

much larger values and reach 0.003. This indicates both "mixed" and "dust" aerosol retrievals contain data that are largely biased by STE_{sfc}. The variations of STE_{AOD} were tested against aerosol type, surface albedo and AOD value as well. Significant trend of STD_{AOD} were found only against AOD.
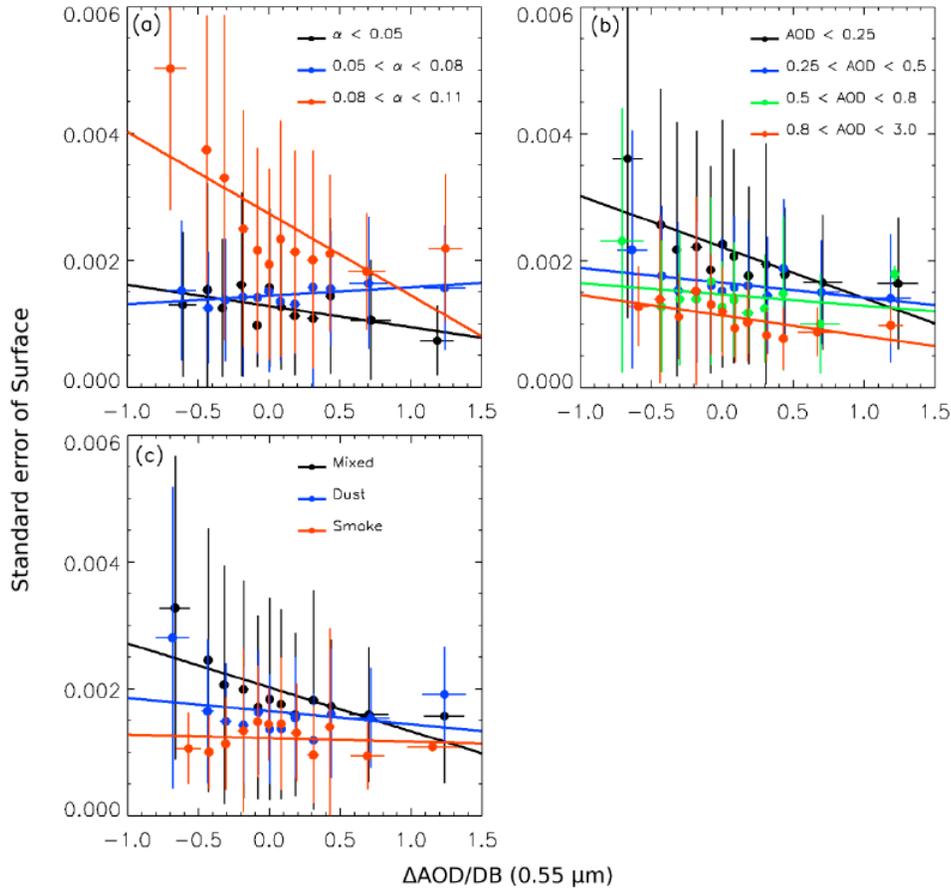
Figure 18. Normalized $\Delta\tau_{A-M}$ ($\Delta\tau_{A-M}$ over Aqua AOD_{DB}) varies with STE_{sfc} as a function of (a) surface reflectance at 0.412 μm, (b) AOD_{DB}, and (c) aerosol type. The error bars indicate one standard deviation above and below the mean.

Similar analyses were conducted for STD_{AOD} as functions of surface reflectance and aerosol type. However, no significant trend was found. Figure 18b was introduced to show the STD_{AOD} as a function of AOD. Although globally an increasing trend is found between STD_{AOD} and AOD (Figure 18a), over the study

region the STD_{AOD} is nearly invariant with respect to AOD other than when AOD is smaller than 0.1 (Figure 18b). STD_{AOD} cutoff has been used as a method to exclude cloud contaminated pixels (e.g., Shi et al., 2010a and Zhang and Reid, 2006). Figure 18b suggests a flat STD_{AOD} cutoff can be applied to the study region, which is applied in the next section. Sect. 4.0 describes how scenarios with significant contributions from STE_{sfc} and/or STE_{AOD} were identified and removed as part of the QC procedures.
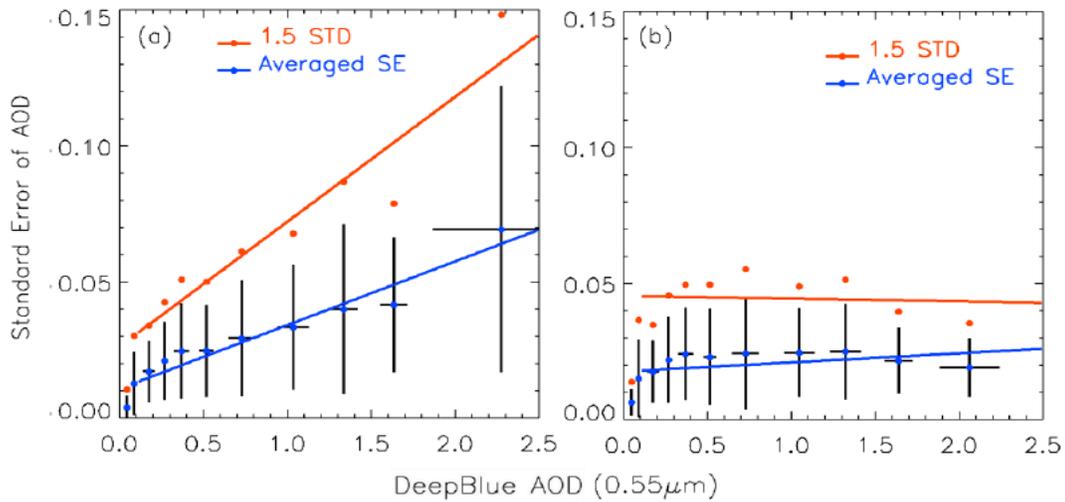
Figure 19. Scatter plot of standard error threshold of Aqua AOD_{DB} versus AOD_{DB} at 0.55 μm. Dots represent the averaged Standard Error (blue) of AOD_{DB} and the 1.5 standard deviation (red) for AOD_{DB} increments of 0.1 for $AOD_{DB} < 0.5$ and increments of 0.3 for $AOD_{DB} > 0.5$. The blue lines and red lines show the linear fit of corresponding dots. (a)for AOD_{DB} globally. (b)for AOD_{DB} over the study region.

4.4 Development of QA/QC Procedures for DA-quality DB over North Africa and Southwest Asia

Based on discussions from section 3, Level 3 DA-quality DB data over the study region were constructed in two steps. Initially, noisy data were removed using various filters, including QA flags, standard error check, and buddy checks over the study region. Table 2 shows all the filtering standards with corresponding data loss.

Next, empirical corrections were applied based on each of the aerosol microphysical properties and surface conditions.

Table 2. Filters and thresholds that are used in QA procedures with corresponding data loss for generating DA-quality Aqua AOD_{DB}, with data concerning Terra DB were presented in prentices. The percentage of data loss for all procedures after the QA filtering were calculated based on the number of retrievals that had QA equal to "Very Good."

	QA Flag	Decoupled STD_{sfc} and STD_{AOD}	Cloud Fraction (F_{cld})
Thresholds	"Very Good"	$STE_{sfc} < 0.004$ and $STE_{AOD} < 0.03$	$F_{cld} < 60\%$
Data Loss	84.3% (82.6%)	20.8% (33.1%)	0.7% (0.5%)

During the standard error check, scenarios with significant contributions from STE_{sfc} and STE_{AOD} were identified. Among nine cases for three STE_{sfc} ranges (0.00-0.001, 0.001-0.002, and 0.002-0.004) and three STE_{AOD} ranges (0.0-0.01, 0.01-0.03 and 0.03-0.05), large scatter is found for STE_{AOD} ranging from 0.03-0.05. Therefore, to filter out data with large spatial variations in either AOD or surface albedo, only data with STE_{sfc} less than 0.004 and STE_{AOD} less than 0.03 were used to construct DA-quality AOD_{DB} data.

Following the STE_{AOD} filtering, buddy check was performed, which is a test that searches for the adjacent retrievals, where retrievals without any adjacent retrieved AOD_{DB} are rejected. It is designed to detect isolated retrievals and is aimed at removing retrievals that occur in between clouds and are subject to cloud contamination. Also, retrievals within the geographical range of 10° S to 13° N and 12° W to 25° E were excluded due to the spatial AOD bias related to the QA flag as discussed in Sect. 3.1.

As mentioned in Sect. 5.3.2.2, aerosol type was decoupled with the surface albedo for empirical correction purpose. Four aerosol species, defined by the aerosol type flag, are: "mixed," "dust," "smoke," and "sulfur." Over the study region, no retrieval labeled as "sulfur" was found for the collocated dataset. Therefore, only retrievals with the aerosol type reported as "mixed," "dust," or "smoke" were discussed. Figure 20 to Figure 22 show the comparisons between DB and AERONET AOD with decoupled aerosol type and albedo range (similar setting as Figure 16). Empirical correction steps were established, based on Figure 20 to Figure 22 but use AOD_{DB} as the independent variable, for a total of nine scenarios. Three types of aerosols (mixed, dust and smoke) for three ranges of albedo (low: 0-5%, median: 5-8%, and high: 8-11%) were considered. Coefficients (slopes and offsets) for the linear empirical correction equations are listed in Table 3 and Table 4 for Aqua and Terra respectively. Figure 20 to Figure 22 show that both linear and nonlinear patterns exist between DB and AERONET AOD values. Linear corrections were, therefore, applied to the identified scenarios that showed linear relationships between satellite and $AOD_{AERONET}$. For low albedo regions with mixed aerosol types (Figure 20a), a non-linear relationship is found between DB and AERONET AOD. Therefore, two linear corrections were made for the AOD ranges of 0.0 to 0.25 and 0.25 and above. Similarly, for dusty regions (as identified by the DB product) with surface albedo (412 nm) range of 5-8% (Figure 21b), linear corrections were made for AOD ranges of 0.0 to 1.0 and 1.0 and above for Aqua (ranges of 0.0 to 0.9 and above 0.9 for Terra). These corrections were based on linear regressions in prognostic analyses, which used AOD_{DB} as the x-axis. When slopes from prognostic analyses are

inversely proportional to slopes from diagnostic analyses, slope corrections were applied. In three cases, prognostic and diagnostic slopes are inconsistent, and no corrections were made for those scenarios: Aqua data over mixed aerosol and dust regions with albedo between 8% and 11% and Terra data over mixed aerosol regions with the same albedo range. As mentioned before, the coarse mode aerosol is the dominant aerosol mode over the study region, and there are an insufficient number of collocated pairs of Aqua DB and AERONET data for smoke aerosol types. Therefore, one linear correction was applied to retrievals with DB smoke aerosol type. We also excluded smoke aerosol retrievals for regions with DB retrieved surface albedo values greater than 0.08.

Table 3. Coefficients used in the empirical corrections for Aqua DB data.

Aerosol Type	Parameters	Range of surface albedo (α) at 0.412 μm		
		0.0-0.05	0.05-0.08	0.08-0.11
Mixed	offset	0.00697 (0.0; AOD < 0.25)	-0.0134	0.0
	slope	1.201 (0.887; AOD < 0.25)	1.149	1.0
Dust	offset	0.0	0.0 (0.0; AOD < 1.0)	-0.0285
	slope	1.3	1.3 (1.0; AOD < 1.0)	1.038
Smoke	offset	0.0		No data were taken in this range
	slope	1.3		

Finally, slope corrections are restrained to 1.3 for both Aqua and Terra DB data, respectively. These slope thresholds are rather arbitrary and were applied to avoid significant corrections to the AOD_{DB}. Details of the steps and parameters for

the corrections mentioned above are included in Table 3 and Table 4. Table 5 shows

the sensitivity study concerning the arbitrary limitation of the slope corrections. For

Table 4. Coefficients used in the empirical corrections for Terra DB data

Aerosol Type	Parameters	Range of surface albedo (α) at 0.412 μm		
		0.0-0.05	0.05-0.08	0.08-0.11
Mixed	offset	-0.0107	0.0261	No change
	slope	1.264	1.056	
Dust	offset	0.0	0.0 (0.0869; AOD < 0.9)	-0.0502
	slope	1.3	1.3 (0.705 AOD < 0.9)	1.145
Smoke	offset	0.0		No data were taken in this range
	slope	1.3		
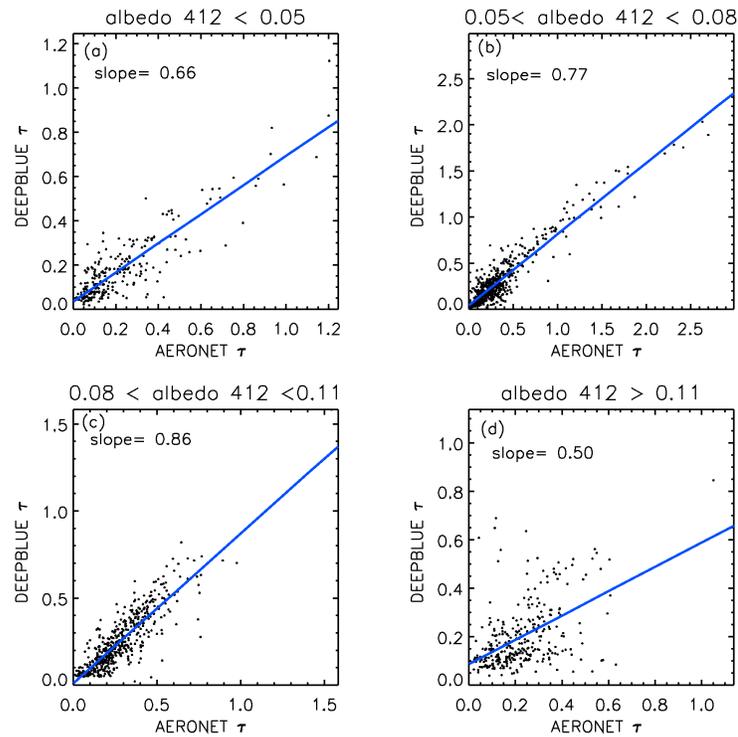
Figure 20. Comparisons between Aqua AOD$_{DB}$ and AOD$_{AERONET}$ over the study region from 2002-2009, grouped by albedo (0.412 μm) ranges for the mixed aerosol type, (a) albedo less than 0.05, (b) albedo ranging between 0.05 and 0.08, (c) albedo ranging between 0.08 and 0.11, and (d) albedo greater than 0.11. The blue line is the linear fit line.

the selected slope limits of 1.1, 1.2, and 1.3, the smallest RMSE occurs when the slope correction limit is restrained at 1.3. Again, the main concern for restraining the slope correction is to avoid potential discontinuities in the data that are created by the application of large corrections.

4.5 Estimation of Prognostic Uncertainty for DA-Quality DB AOD

Using the data screening steps and empirical correction procedures mentioned in the previous section, the DA-quality AOD_{DB} data were generated. In this section, the accuracy of the newly generated data was evaluated through inter-comparison with ground observations and through the prognostic and diagnostic models of the RMSE.
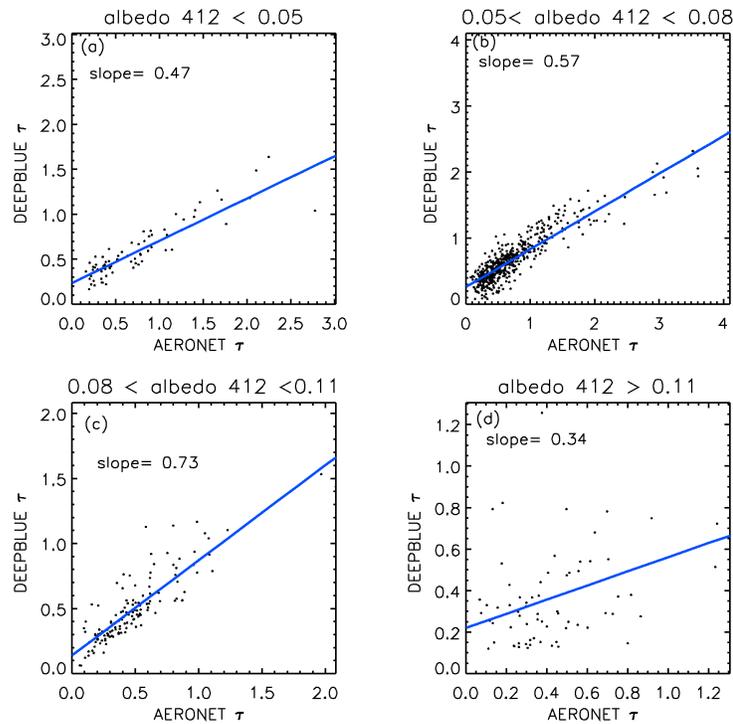
Figure 21. Similar to Figure 20 but for dust type aerosol.
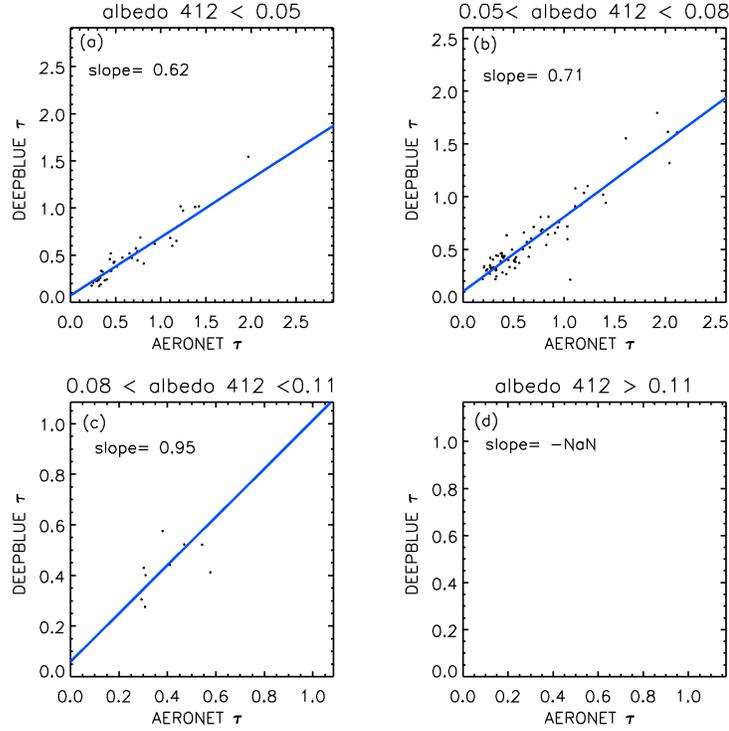
Figure 22. Similar to Figure 20 but for smoke type aerosol.

Table 5. Statistical analyses of different slope limitations for the empirical correction procedures for Aqua DB data when validating against $AOD_{AERONET}$.

Slope limitation	1.2	1.3	1.4	No limit
RMSE (all data)	0.160	0.157	0.159	0.149
RMSE (data > 0.5)	0.252	0.242	0.244	0.224
RMSE (data > 1.0)	0.391	0.367	0.367	0.332
r^2	0.87	0.87	0.87	0.89
slope	1.05	0.99	0.95	0.98

The comparison of DB and AERONET AOD before and after the quality assurance and empirical corrections steps are shown in Figure 23 for Aqua and Terra over the study region in order to estimate the prognostic uncertainty. Reductions in both bias and noise are clearly visible for both DA-quality Terra and Aqua AOD_{DB} data. The slopes of AERONET and the newly generated AOD_{DB} are 0.88 and 0.87 for

Aqua and Terra respectively. The non-linear features for both Aqua and Terra are weakened, but not eliminated, due to the restriction in empirical corrections that the multipliers cannot exceed 1.3. The RMSE values were checked for three AOD ranges: total AOD, AOD greater than 0.5 and AOD greater than 1.0. The corresponding RMSE are from 0.19 to 0.16 with 18.1% error reduction, from 0.33 to 0.24 with 26.3% reduction, and from 0.54 to 0.37 with 32.3% reduction for Aqua after applying the QA steps and empirical corrections. Similarly, for Terra, the corresponding RMSE are from 0.24 to 0.17 with 18.2% error reduction, from 0.35 to 0.27 with 22.9% reduction, and from 0.55 to 0.35 with 36.4% error reduction. The total data losses, calculated against the total number of retrievals with "Very Good" QA flags, are 28.5% for Aqua and 44.5% for Terra.

Figure 24 shows the RMSE of the new product as a function of DB AOD before and after all processes. The upper panels are for total AOD, while the lower panels are separate dust and mixed aerosol types. Smoke aerosol particles were not included due to insufficient data samples. In Figure 24 the same binning methods were used for the original data and the corresponding DA-quality data. However, the methods of binning vary for different data sets (e.g. dust vs. mixed aerosol) due to their respective data distributions. Figure 24a shows two lines of noise floors. The noise floor is defined as the RMSE value when RMSE is invariant to AOD variations. The noise floor represents the basic RMSE introduced by the system. As Figure 24a show, RMSE values are reduced for all AOD ranges after the correction processes. For total AOD less than 0.4, the noise floors of RMSE of original and newly generated data are 0.113 and 0.104, respectively. Different trends are found for

different aerosol types. For example, the RMSE values show an increasing pattern as AOD_{DB} increases for mixed-type aerosol particles. However, for dust particles, the minimum RMSE appears around AOD_{DB} value of 0.3. This V-shaped RMSE distribution indicates a larger retrieval uncertainty for dust AOD values smaller than 0.3. Figure 24b and d show a similar analysis to Figure 24a and c, but use Terra DB data. One distinct difference from Aqua to Terra is that no noise floor of RMSE is found for Terra data. In the prognostic analyses, a sudden increase of RMSE values is found at AOD value around 0.5 (black dots in Figure 24d). This sudden increase in RMSE values is due to outliers from the mixed type of aerosol particles in the high surface albedo case. Generally, the RMSE analyses show that the newly generated DA-quality data has smaller RMSE values when compared to the original data for both Aqua and Terra. The level 3 quality-assured data were generated over the study region by spatially averaging the AOD data in a one-degree or a quarter-degree latitude and longitude resolution.

Figure 25 shows the spatial plots of the original DB data, the "Very Good" QA quality DB data, and the newly generated data for Terra and Aqua separately for 2007. The main features are similar before and after the empirical corrections and QA procedures. When compared with DB data that has the "Very Good" QA flag, high AOD noise was reduced, and general AOD values were increased due to the correction of the non-linear features. All data with surface albedo values exceeding 11% were removed. Also, data for regions below 13° N were not included due to the
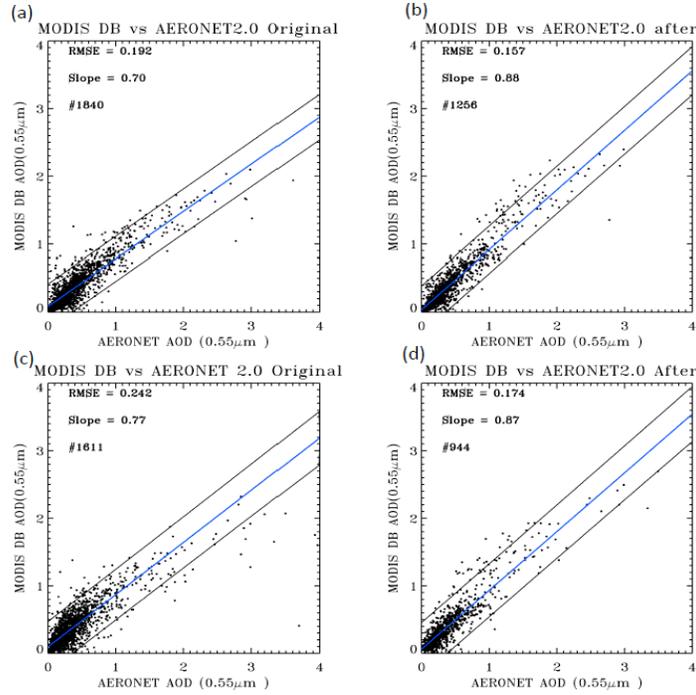
Figure 23. Scatter plot of AOD_{DB} and $AOD_{AERONET}$ level 2.0 AOD at 0.55 μm over the study region. The blue line is the linear regression line for all data (except in 18c, is for data smaller than 1.5) and the black lines are the 1.0 standard deviation lines of the data. (a)for the original Aqua DB aerosol products, (b) for the DA-quality Aqua DB aerosol products, (c) and (d) are similar to (a) and (b) but for Terra DB.
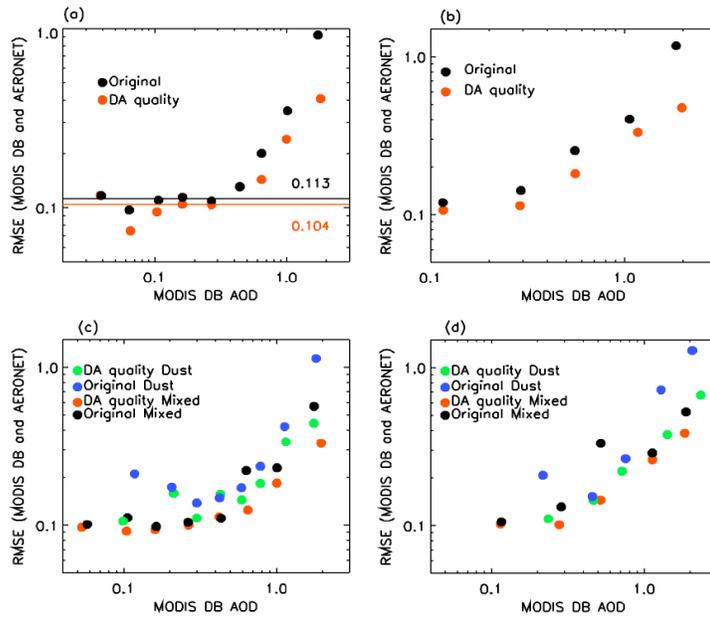
Figure 24. RMSE of AOD_{DB} compared to $AOD_{AERONET}$ as a function of AOD_{DB} for all data and for mixed and dust aerosol types over the study region – (a) and (c) for Aqua, and (b) and (d) for Terra. The RMSE of original and DA-quality mixed and dust aerosols are indicated by the different colors of dots.

80

QA-filtering issue mentioned in Sect. 4.3.1. It is shown in Figure 25 that Terra AOD have higher values, approximately 0.1, than Aqua AOD. Knowing that dust aerosols have a diurnal feature, the difference in local passing time for the two satellites may cause this problem. Also Terra AOD have a larger bias, as shown in Figure 10d and Figure 24b, which can also contribute to this problem.
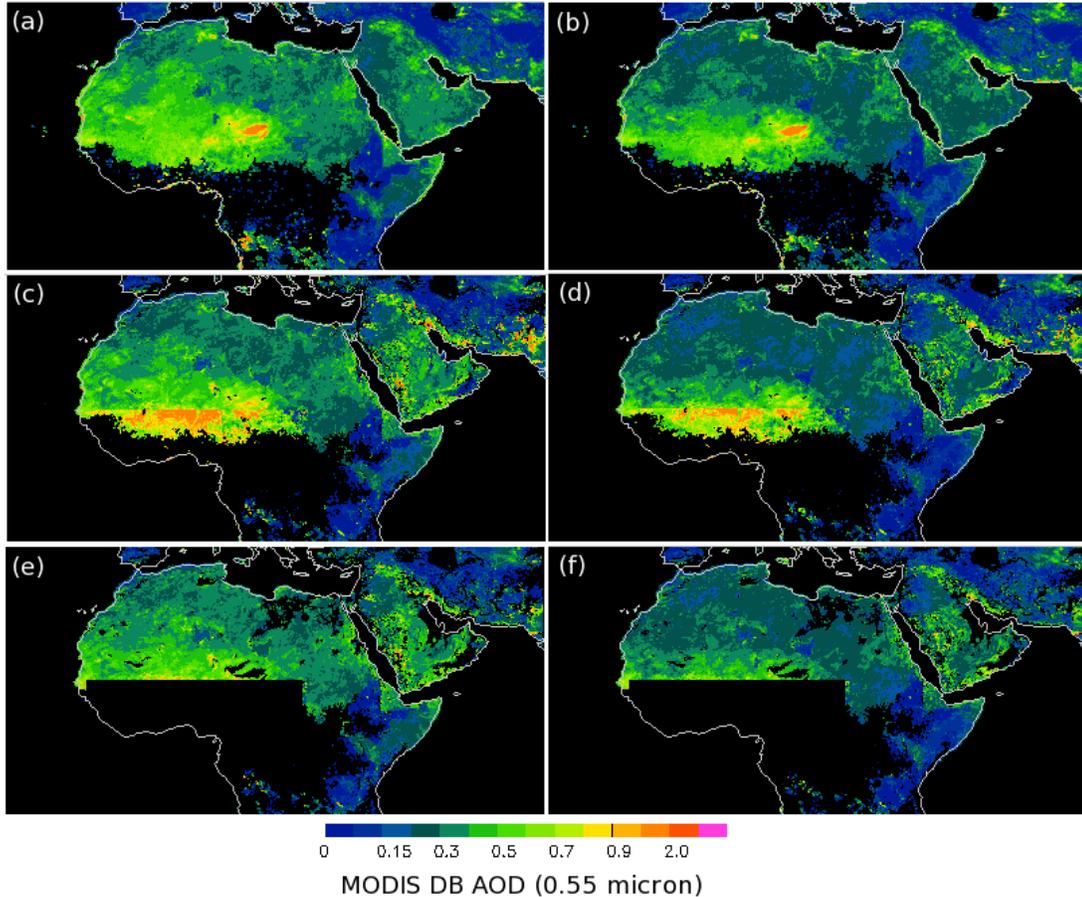
Figure 25. Spatial distribution of c5.1 AOD$_{DB}$ at 0.55 μm from the DB aerosol products for 2007.The black color represents regions with no data, the blue color represents areas with low AOD loadings, and the pink color indicates locations with extremely high AOD values. Rows 1, 2, and 3 represent the original data, data with "Very Good" QA flags, and the DA-quality data respectively. The left column is Terra DB data and the right column is Aqua DB data.

As an independent study, we have also evaluated the newly generated level 3 Aqua DB AOD data for 2010 and 2011 that are not included in the analyses as mentioned in Sect. 4.2 to 4.4. AERONET level 1.5 data were used instead of

AERONET level 2.0 data, since level 2.0 AERONET data were not available from all sites over the study region for 2010 and 2011 when the study was conducted. Again, with the empirical correction and quality assurance steps, both bias and noise are reduced. The RMSE for newly generated data is reduced 11% from 0.227 to 0.202, and the r^2 changes from 0.74 to 0.77 for prognostic purpose (Figure 26). Noted that there were four outliers that showed in blue dots from Figure 26, which were manually removed from the analyses for both original and DA-quality DB data.

4.6 Conclusions

A thorough analysis with an emphasis on North Africa and Southwest Asia was conducted to evaluate the DB c5.1 aerosol products through the use of ground-based AERONET data. Retrieval biases and uncertainties were analyzed as functions
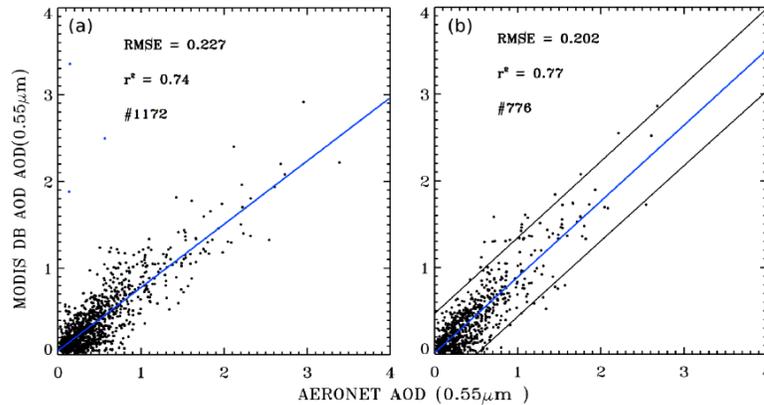
Figure 26. Scatter plot of Aqua DB versus AERONET level 2.0 AOD at 0.55 μm from 2010 to 2011 for an independent study. The blue line is the polynomial / linear regression line for all of the data. (a) for the original Aqua DB aerosol products, (b) for the DA-quality Aqua DB aerosol products

of sampling and observation-related factors such as surface conditions, observation geometry, aerosol microphysics, cloud contamination, and other parameters that are used in the retrieval process. Updated quality assurance procedures, filtering processes, and empirical correction steps were developed for constructing new

quality-assured DB products. Prognostic models were built for evaluating the newly developed data product against AERONET observations. Our findings include:

1. QA flags can be used to improve the quality of the AOD_{DB} data. An important systematic bias in AOD_{DB} as a function of viewing angle is eliminated by the use of the "Very Good" QA flag. However, both the data density and the geographic distribution of DB data are affected by the QA flag, and users of the product should be aware of this.

2. Particle size and surface albedo were identified to be significant to retrieval accuracies, and were highlighted and decoupled from the remaining parameters. For coarse mode aerosols, the higher the surface albedo is, the lower the underestimation of AOD_{DB}. For fine mode aerosols, however, the higher the albedo is, the lower the overestimation of AOD_{DB}.

3. The new QA and empirical correction procedures were constructed, and new level 3 DB c5.1 product was created for future implication in data assimilation. Reductions in RMSE, which were calculated using ground-based AOD from AERONET as truth, of 18.1% and 18.2%, were found for the quality-assured products when compared to the original DB products for Aqua and Terra DB products, respectively.

4. An independent validation of DB c5.1 data over 2010 and 2011 was also conducted and improvements to the new data set were found as well. The newly developed level 3 products will be used in aerosol data assimilation and aerosol climate studies.

CHAPTER V

CRITICAL EVALUATION OF CLOUD CONTAMINATION IN THE MISR AEROSOL PRODUCTS USING MODIS CLOUD MASK PRODUCTS

5.1 Introduction

The MISR instrument has been successfully applied to observe and study atmospheric aerosols for over a decade (e.g., Kahn et al., 2005). Featuring nine unique camera angles, MISR observations have been used to retrieve aerosol optical properties over most surface types, including bright surfaces, which thwart many other passive sensors (Diner et al., 1998; Kahn et al., 2010). One of the known issues for satellite aerosol products, including the MISR aerosol products, is cloud contamination (e.g., Zhang et al., 2005; Kahn et al., 2010). Extensive research efforts been attempted to study but the impacts of cloud artifacts and cloud contamination to aerosol retrievals from other sensors, such as MODIS (Zhang et al., 2005; Hyer et al., 2011; Shi et al., 2011b; Toth et al., 2013) and Advanced Very High Resolution Radiometer (AVHRR) (Zhao et al., 2013), the impacts of cloud contamination on MISR aerosol products have not been fully explored or quantified. We do know that over-ocean AOD from standard operational MODIS and MISR products have positive biases as large as 0.025–0.04, or roughly one-third of mean background AOD values (Zhang and Reid, 2010; Kahn et al., 2010). This is in stark contrast to the

accuracy requirement commonly professed by climate scientists of 0.01 (CCSP, 2009) and may impact estimates of long-term aerosol trends (Zhao et al., 2013).

As suggested from previous studies, effective cloud screening for aerosol retrieval requires sophisticated algorithms and multispectral visible and infrared radiance data (e.g., Remer et al., 2005). However, MISR lacks channels in the near- and far-infrared region where cirrus clouds are most easily detected. The operational cloud-screening algorithm for AOD_{MISR} products is based on cloud-induced perturbations in either spectral radiance or angular-dependent radiance values with the assistance of a reflected layer height technique (e.g., Kahn et al., 2007). Note that the operational MISR cloud screening method does not fully exploit the MISR data for aerosol-related applications. For example, Pierce et al. (2010) show, with their research algorithm, that MISR can retrieve thin cirrus with optical depth below ~ 0.3 under favorable conditions. A recent study by Witek et al. (2013) has extended the cloud screening effort by requiring 60% clear pixels for every AOD_{MISR} retrieval using a 1.1 km resolution clear flag that is included in the MISR aerosol products. Using the Witek et al. (2013) method, AOD_{MISR} are reduced by 0.04 with an 85% data loss rate, and the averaged AOD_{MISR} are in line with the Navy MODIS data assimilation grade product. However, cloud detection may be incomplete with the use of only visible and near-IR channels, especially for thin clouds over bright surfaces. On board the same satellite platform as MISR, MODIS has a total of 36 spectral channels, including cirrus cloud- sensitive channels as well as infrared channels, which provide an enhanced capability of detecting the presence of clouds in an observed scene (e.g., Ackerman et al., 1998). Previously published study of cloud

contamination in the MISR retrieved AOD have not yet taken advantage of collocated Terra-MODIS cloud masking data. In this study, level 2 cloud mask products from Terra MODIS were used to evaluate the cloud contamination in the Terra MISR aerosol products and evaluate different methods for eliminating cloud contamination from MISR aerosol products.

5.2 Methodology

Three data sets are used in this study. They are MISR AOD product, MODIS cloud mask product, and AERONET AOD. During this study, the baseline quality assessment steps (referred as "self-QAed" hereafter) for AOD_{MISR} are based on data included in the MISR aerosol products (Kahn et al., 2009; Bull et al., 2010). The following filters are used for the "Self-QAed" data sets:

– The Retrieval Applicability Mask flag (= 0) is used to identify pixels free of cloud, glint, and other factors.

– The Regional Classification Indicator (= 0) is used for selecting retrievals above clear background region.

– The Aerosol Retrieval Success Flag (=7) is used to identify successful retrievals.

– The Regional Surface Type Indicator is used to separate over-land from over-water retrievals; and also to exclude potential problematic regions such as shallow/coastal waters and Polar regions.

Note that within the MISR aerosol product, a retrieval applicability mask is available at a 1.1 km resolution, for nine camera angles and four spectral bands. Only

the red and near-IR bands are used for over-water aerosol retrievals (Martonchik et al., 1998). This mask is in a much finer resolution than the 17.6 km AOD retrievals and includes environmental conditions such as "clear," "glitter-contaminated," "cloudy" and "topographically obscured." Using the clear indicator in the retrieval applicability mask, a clear flag fraction (CFF) can be calculated for each of the MISR AOD retrievals by taking the ratio of clear versus total flags for a total of 16×16×9 flags (9 angles, 16×16 MISR pixels at 1.1 km). Witek et al. (2013) discussed the possibility of using the MISR CFF (use CFF > 60%) as a means of removing cloud-contaminated MISR AOD retrievals. The MODIS-based MISR cloud screening method developed from this study was compared to the method included in Witek et al. (2013). The results are shown in Sect. 3.0.

The impacts of cloud contamination on the MISR aerosol product were evaluated using 7years (2001–2007) of collocated AERONET, MODIS and MISR data sets. One year of collocated MODIS and MISR products (2007) were also used for evaluating various cloud masking methods spatially. MISR aerosol scenes were collocated with AERONET data following the method presented in Zhang and Reid (2006). Pairs of observations were recorded when the spatial distance between the MISR and AERONET data is within 0.3° (Lat/Lon), and the temporal difference is within ±30min. The collocated MISR and AERONET data were further collocated with MODIS cloud mask data for the cloud-clearing analysis for the MISR aerosol products (see Sect. 2.4).

The spatial resolution of the MODIS cloud masking data is 1 km. However, the geo-location data in the Terra MODIS cloud mask products have a spatial

resolution of 5 km. Therefore, to speed up the processing time, the cloud mask data were first averaged to a 5 km × 5 km resolution, providing occurrence ratio for each cloud status. The 5 km × 5 km Terra MODIS cloud masking data were then collocated with the Terra MISR aerosol products, with the spatial and temporal differences between the two products set to 6km and 30min, respectively. The spatial resolution for the Terra MISR aerosol retrievals is ~ 17.6 km, thus one MISR aerosol retrieval can be collocated with multiple MODIS cloud masking values. The occurrence ratios from the 5 km averages were further averaged to compute a total of four parameters for one MISR AOD retrieval: cloudy fraction (F_{cd}), uncertain clear fraction (F_{uc}), probably clear fraction (F_{pc}), and confidently clear fraction (F_{cc}). The collocated thin cirrus cloud flag was processed the same way to construct an additional parameter that represents the fraction of the thin cirrus cloud-free regions at the MISR AOD resolution (F_{cirrus_free}).

Lastly, 7 years (2001–2007) of collocated MISR and AERONET aerosol, as well as MODIS cloud mask products, were used to evaluate the impacts of various cloud screening methods on the AOD_{MISR}. One year of collocated Terra MISR aerosol and MODIS cloud mask products were used to investigate the impacts spatially.

5.3 Results: a case study

An example of potential cloud contamination in the MISR aerosol products is shown in Figure 27, over remote southern oceans (~44° to 52 °S and 124° to 136 °W,
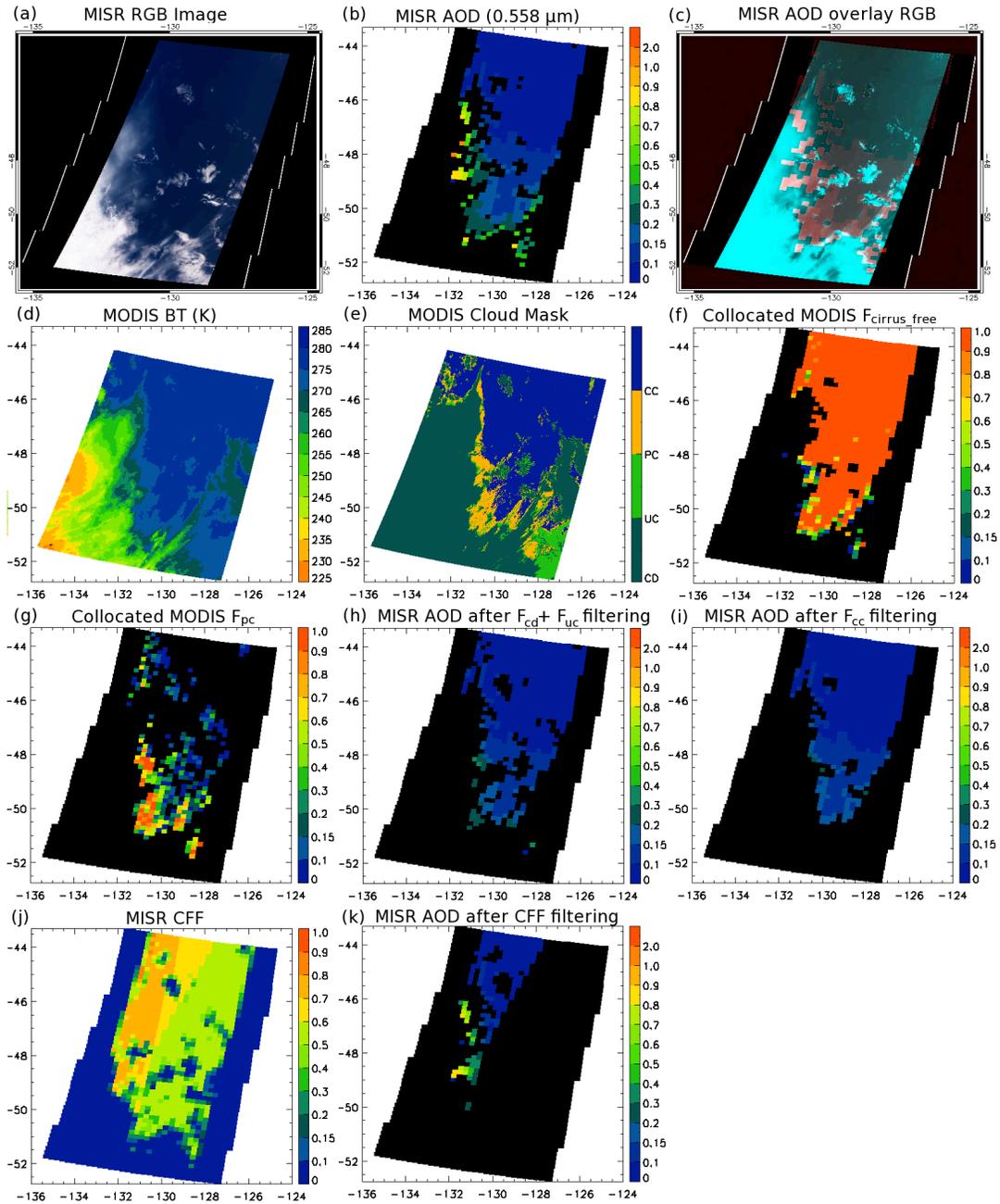
Figure 27. A case study on January 3rd 2007, over the remote oceans (44° to 52° S and 124° to 136° W), (a) RGB image created using the MISR Near IR, green and blue bands, (b) MISR AOD over the case study region, (c) Overlay of (a) on (b) where the intensity of red is correlated with the magnitude of the aerosol, (d) MODIS brightness temperature (BT), (e) MODIS cloud mask, (f) collocated MODIS thin cirrus free cloud fraction (F_{cirrus_free}) in MISR AOD domain, (g) similar to (f) but for the collocated MODIS probably clear fraction (F_{pc}), (h) AOD_{MISR} after passing the MODIS cloudy fraction (F_{cd}) < 10% and the MODIS uncertainty clear fraction (F_{uc}) < 20% cloud filters, (i) AOD_{MISR} after passing the MODIS confident clear fraction (F_{cc}) > 20% cloud filter, (j) MISR clear flag fraction (CFF), and (k) AOD_{MISR} after passing the MISR CFF > 60% filtering.

on 3 January 2007), where a pristine marine environment is expected. Figure 27a shows the RGB image constructed using nadir- viewing MISR near-IR, green and blue bands. Cloudy and clear regions are observed in the bottom and upper parts of Figure 27a, respectively. Figure 27b is the corresponding MISR self-QAed AOD_{MISR} plot with AOD_{MISR} values ranging from near zero to over one. The nearly homogeneous low AOD_{MISR} of less than 0.1 are found from cloud-free oceans. Near cloud edges and within cloudy regions, AOD_{MISR} of 0.2–0.3 are more typically found. To better illustrate the relative location between cloud edges and the retrieved AOD_{MISR}, Figure 27c was created by overlaying Figure 27a (in aqua color) and Figure 27b (in red color) in a false-color composite. Bright red colors indicate high AOD_{MISR}. Most of the highest AOD_{MISR} ($\tau_{MISR}>0.3$) are located within cloudy regions and higher AOD_{MISR} of around 0.2 to 0.3 are found near the edge of clouds. Figure 27d shows the MODIS brightness temperature (BT) at a 5 km resolution. Retrievals that have AOD_{MISR} values above 0.8 are found within regions that have BT values lower than 255 K, a clear indication of cloud contamination. Figure 27e shows the MODIS cloud mask data at a 1 km resolution with each pixel flagged as one of the four cloudy conditions: CD, UC, PC, and CC. Regions with high AOD_{MISR} values are mostly associated with pixels that have PC, UC, or CD cloud flags. This concept is further demonstrated in Figure 27f–i. Figure 27f shows the fraction of MODIS cloud mask data that are free from thin cirrus cloud contamination ($F_{cirrus\_free} = 100\%$), averaged in the AOD_{MISR} resolution. Most thin cirrus cloud-free regions ($F_{cirrus\_free} = 100\%$) are associated with low AOD_{MISR} of ~ 0.15 or less. Figure 27g is similar to Figure 27f, but was created using the PC flag. High AOD_{MISR} of 0.2–0.3 are still

observed when F_{pc} is set to above 0.8, suggesting that the PC flag may not be a good cloud-free sky indicator. Using stringent threshold values of F_{cd} and F_{uc} ($F_{cd} < 10\%$ and $F_{uc} < 20\%$), Figure 27h shows that most of the AOD_{MISR} larger than 0.3 are removed, although there are still some AOD_{MISR} around 0.3 located between clouds in the bottom right of the image. Figure 27i shows the cloud clearing with the use of the F_{cc} filter ($F_{cc}> 20\%$), most high AOD_{MISR} are removed, showing that the F_{cc} filter can be effectively used for cloud screening of MISR data. Attempts were also made to filter out cloud contamination in the AOD_{MISR} using the MISR CFF data (Figure 27j and k). The fraction of the clear flag within the scene is shown in Figure 27j. Figure 27k shows the MISR AOD retrievals after applying the MISR CFF filter (CFF $> 60\%$) as used in Witek et al. (2013). Shown in Figure 27k, high AOD_{MISR} at the bottom right of the image are removed, including a significant portion of cloud-free AOD_{MISR} as identified by MODIS, causing a 75% data loss. More importantly, some of the high AOD_{MISR}, located within the totally cloudy regions as seen from Figure 27c, passed the MISR CFF filter. This case study suggests that the MISR CFF method can be used to remove cloud-contaminated AOD_{MISR}, but may not be as effective as the MODIS-based method, and incurs a cost of significant data loss. Thus, MODIS F_{cc} is the primary parameter used in the remainder of this study for cloud-clearing of the AOD_{MISR} retrievals. Shown from this case study, cloud contamination exists in MISR aerosol products, and MODIS cloud mask data can be used, effectively, to exclude most of the cloud contaminated AOD_{MISR}, especially with the use of the MODIS F_{cc} filter. Still readers should be aware that there are uncertainties in cloud

masking itself and such issues are discussed later in the Recommendations and Conclusions section.

5.3.1 Cloud screening using the MODIS cloud mask products

A statistical analysis was conducted to explore the relationships between the four fractional parameters derived from the MODIS cloud mask products (F_{cd}, F_{uc}, F_{pc}, and F_{cc}) and AOD_{MISR}. Shown in Figure 28 are the means, medians, and data distributions of AOD_{MISR} as functions of F_{cd}, F_{uc}, F_{pc}, and F_{cc} for both the over-water (Figure 28a to d) and over-land (Figure 28e to h) cases using collocated AOD_{MISR} and MODIS cloud mask data for 2007, with the fractional data density illustrated in color contours for every 10% of a given fraction. The fractional data density is the contour of the number of pixels for every 0.02 AOD_{MISR} and every 10% cloud fraction over the total number of pixels within the corresponding 10% cloud fraction. Notice that fractional values of F_{cd}, F_{uc}, F_{pc}, and F_{cc} indicate the probability of occurrence. For example, an increase of F_{cd} from 0 to 100% indicates a change from an unknown cloudy or clear scene to a 100% high confident cloudy scene (or low confident cloudy in case of F_{uc}), while an increase of F_{cc} from 0 to 100% means a change from an unknown scene to a 100% high confident clear scene (or low confident clear in case of F_{pc}). In Figure 28a, the mean and median MISR AOD show a decreasing trend as F_{cc} (e.g., percentage of clear regions) increases. In comparison, Figure 28d shows an increasing trend in AOD_{MISR} as F_{cd} (confident cloudy fraction) increases. Both Figure 28a and d show a similar feature as that found in the MODIS AOD_{DB}, a feature identified by Zhang et al. (2005) as cloud contamination in the MODIS DT aerosol products. Mixed information is shown in Figure 28b (F_{pc}) and Figure 28c (F_{uc}) when

the detection of cloud and clear scenes is less certain, indicating that PC and UC flags are not good for use in cloud masking of MISR data. Figure 28e–h show a similar analysis as Figure 28a–d but for the over-land case. Again, decreasing/increasing trends are found for the F_{cc}/F_{cd} cases. Comparing the over-land mean AOD_{MISR} at a confident clear sky (F_{cc} = 100%, Figure 28e) with the similar scenario for the over-water case (Figure 28a), a higher mean AOD value of 0.18 is found for the over-land case. In comparison, increasing F_{uc} and F_{cd} percentages to 100% raises the over-land AOD_{MISR} to values over 0.3 and 0.4, a clear indication of cloud contamination in the AOD_{MISR}. Suggested from Figure 28, it is feasible to use F_{cc} for cloud filtering of the MISR aerosol products.
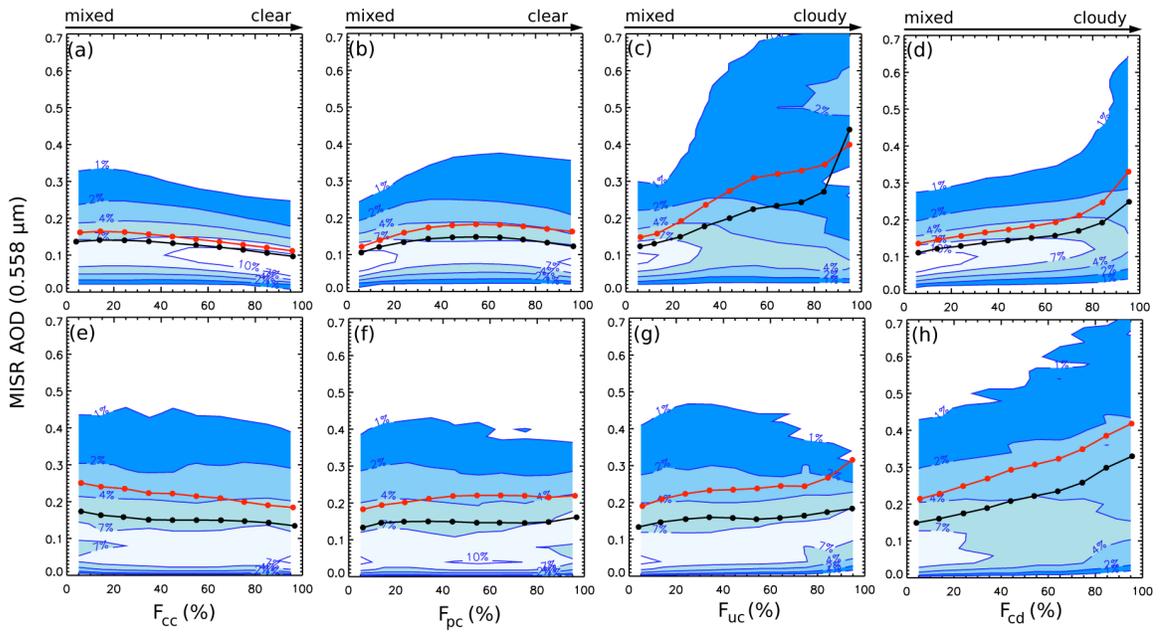
Figure 28. AOD_{MISR} as functions of the percentage of occurrences of the cloud flags from the MODIS cloud mask products: (a), (e) confident clear fraction (F_{cc}), (b), (f) probably clear fraction (F_{pc}), uncertainty clear fraction (F_{uc}) and (d), (h) cloudy fraction (F_{cd}). Figure 28a–d are for the over-water data and Figure 28e–h are for the over-land data. The color contour represents the fractional data density for every 10% cloud fraction. The red and black dots represent the mean and median AOD_{MISR} values within a 10% cloud fraction bin, respectively.

Using 7 years of collocated MODIS, MISR and AERONET data (2001–2007),

a sensitivity study was conducted to investigate different cloud filtering methods

using F_{cd}, F_{uc}, F_{pc}, and F_{cc}. Table 6 and Table 7 show the root mean square errors

(RMSEs), the mean absolute error (MAE) of AOD_{MISR} (validated against AERONET

data), and the fraction of data within the expected uncertainty range (0.05 or 0.2 ×

$\tau_{AERONET}$) (e.g., Kahn et al., 2010) for 12 cloud-filtering steps for over-ocean and

over-land cases, respectively.

Table 6 The RMSE, the fraction of data within the expected error (0.05 or 20% of $AOD_{AERONET}$), and the data loss rates (both for the MISR AOD data that are collocated with AERONET data and for all MISR AOD data) under nine conditions over oceans. F_{cd} is the cloudy fraction, F_{uc} is the uncertainty clear fraction, and F_{cc} is the confident clear fraction. The thin cirrus cloud filter refers to thin cirrus cloud free (set $F_{cirrus\_free} = 100\%$) as detected by MODIS.

	RMSE	MAE	% within the expected error	Data loss and number of cases (collocated with AERONET)	Data Loss (All MISR AOD data)
Self-QAed	0.082	0.059	59%	0% (2091)	
$F_{cd} < 50\%$	0.080	0.056	60%	7% (155)	
$F_{cd} > 50\%$	0.137	0.107	40%	93% (1936)	
$F_{uc} < 50\%$,	0.084	0.059	60%	1% (2070)	
$F_{uc} > 50\%$,	0.096	0.081	43%	99% (21)	
$F_{cc} > 20\%$	0.073	0.053	61%	27% (1527)	35%
$F_{cc} > 50\%$	0.068	0.050	63%	37% (1312)	46%
$F_{cc} > 80\%$	0.063	0.047	65%	51% (1019)	65%
$F_{cc} > 20\%$+ thin cirrus cloud filter	0.070	0.050	63%	36% (1328)	45%
$F_{cc} > 50\%$ + thin cirrus cloud filter	0.065	0.048	65%	44% (1177)	53%
$F_{cc} > 80\%$ + thin cirrus cloud filter	0.060	0.046	66%	54% (952)	67%
Thin cirrus cloud filter	0.076	0.054	62%	22% (1636)	21%

The 12 scenarios are self-QAed, Fcd< 50%, Fcd> 50%, Fuc<50%, Fuc>50%,

Fcc>20%, Fcc>50%, Fcc> 80%, three Fcc cloud-filtering steps combined with the

cirrus cloud filter (F_{cirrus_free}= 100%), and cirrus cloud free (F_{cirrus_free} = 100%). There

are two types of data loss rates presented. One is calculated based on the collocated MISR and AERONET data and another is recorded using all available AOD_{MISR} data in 2007. The data loss rates are not reported for F_{uc} and F_{cd} cases simply because F_{uc} and F_{cd} are not used for cloud clearing of the MISR aerosol products.

Table 7 Similar to Table 6 but for the over-land case.

	RMSE	MAE	% within the expected error	Data loss and number of cases (collocated with AERONET)	Data Loss (All MISR AOD data)
Self-QAed	0.143	0.072	61%	0% (9326)	
$F_{cd} < 50\%$	0.136	0.136	62%	3% (9016)	
$F_{cd} > 50\%$	0.262	0.144	42%	97% (310)	
$F_{uc} < 50\%$,	0.136	0.069	62%	1% (9219)	
$F_{uc} > 50\%$,	0.400	0.189	47%	99% (107)	
$F_{cc} > 20\%$	0.123	0.067	62%	13% (8160)	6.5%
$F_{cc} > 50\%$	0.121	0.065	63%	18% (7639)	11%
$F_{cc} > 80\%$	0.113	0.061	65%	32% (6352)	21%
$F_{cc} > 20\%$ + thin cirrus cloud filter	0.120	0.066	63%	25% (7039)	15%
$F_{cc} > 50\%$ + thin cirrus cloud filter	0.118	0.064	64%	28% (6706)	18%
$F_{cc} > 80\%$ + thin cirrus cloud filter	0.109	0.060	65%	38% (5765)	27%
Thin cirrus cloud filter	0.143	0.070	62%	20% (7432)	10%

Using the $F_{cd} > 50\%$ filter, an increase of more than 60% in RMSE is found for AOD_{MISR} retrievals over both land and ocean with 20% less data that fall within the expected error range. Even for the $F_{uc} > 50\%$ filter, a 20% increase in RMSE is shown globally, indicating that cloud contamination is physically identifiable in the AOD_{MISR} data, causing a high bias to the AOD retrievals (also discussed later in the text). Note that AERONET data may also be impacted by the thin cirrus contamination (Chew et al., 2011).

For the over-ocean case, when increasing the F_{cc} filtering values from 20% to 80% with the cirrus-free filter, a reduction in RMSE (compared to the self-QAed case) from 15% to 27% is found along with an increase in the fraction of data that falls within the expected error range. An approximately 0.006 decrease in bias (validated against AERONET) is observed with a 30% data loss. A larger bias reduction is expected in cloudy regions, which is critical to aerosol modeling studies. For aerosol forcing studies, a 0.006 decrease in bias is welcomed, as the required accuracy of AOD for aerosol forcing studies is 0.01 (CCSP, 2009). Over global land, increasing the F_{cc} filtering values from 20% to 80% with the cirrus-free filter introduces an increase in RMSE reduction from 16% to 24%, but with an increasing data loss rate from 15 to 27% for all AOD_{MISR}. Negligible effects are found over land for increasing F_{cc} from 20 to 50%. This may be caused by less data available within this F_{cc} range. Also, the RMSE and MAE values have insignificant changes after using the thin cirrus filter for the over land case. It may be possible that the MODIS cirrus cloud mask is not sensitive to cirrus clouds under certain circumstances (for example, COD < 0.3) (Sassen and Cho, 1992).

Figure 29 shows the spatial distributions of AOD_{MISR} for year 2007 at a half-degree Lat/Lon resolution, using the self-QAed MISR data (Figure 29a) and the AOD_{MISR} after applying the 20% and 80% F_{cc} cloud filters combined with the thin cirrus cloud filter (F_{cirrus_free} = 100%) (Figure 29b and c). Although the overall patterns are similar, differences are also visible (Figure 29e and f). For example, the aerosol belt over the high-latitude southern oceans from Figure 29b and c is much reduced. Indeed, a similar aerosol belt is also observed from the original MODIS

aerosol data and can be reduced with stringent cloud screening and quality assurance steps (Shi et al., 2011a). Although other factors could also contribute (Toth et al., 2013), cloud contamination is one of the sources for causing the elevated AOD over southern oceans (Shi et al., 2011a). The decrease in mean AOD_{MISR} is more pronounced with the F_{cc} cloud filter at $F_{cc} > 80\%$ compared with $F_{cc} > 20\%$. Similar suppression in AOD is also found in high latitude northern oceans, which could be partially related to the broad regions of winter storm tracks. Over the west coast of North Africa, the AOD values are reduced in Figure 29b and c compared with Figure 29a (also seen from Figure 29e and f, which were created to represent the differences between the self-QAed and the cloud-filtered AOD_{MISR}). Thick aerosol plumes could be labeled as cloudy pixels and excluded from the cloud-filtered data sets. To further investigate if the reduction in AOD values over the regions mentioned above is caused by the thin cirrus cloud screening, the analysis was repeated using only the self-QAed MISR data that passed the cirrus cloud filter ($F_{cirrus\_free} = 100\%$) for 2007. Figure 29d shows that after the thin cirrus filter, the aerosol loadings over the focus area (west coast of North Africa) remain at a similar magnitude as Figure 29a. Thus, the weakened aerosol features over the west coast of North Africa could be caused by applying the confident clear cloud filtering. Over the North African region, positive biases are found. The positive biases are introduced for two reasons: (1) the averaged AOD_{MISR} values are high over the region, and (2) some of the retrievals with AOD_{MISR} values less than 0.2 are removed by the MODIS cloud mask filtering, thus increasing the averaged AOD_{MISR} values. Also, a discontinuity is found between the over-ocean and over-land aerosol features along the west coast of North Africa (e.g.,

97

Figure 29c). This discontinuity may be caused by the differences in the over-ocean

versus over-land cloud screening algorithms from the MODIS cloud mask products.
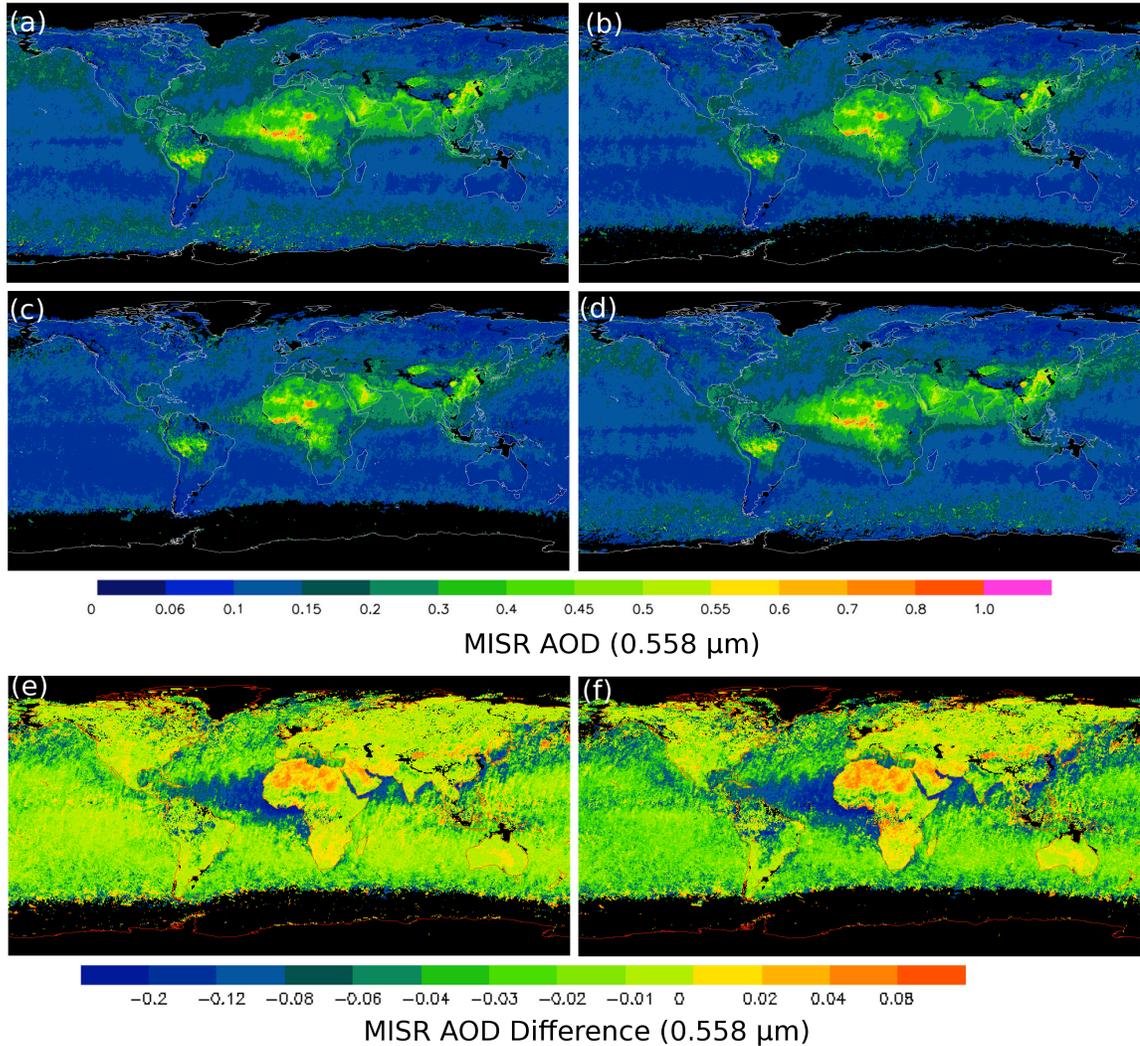
Figure 29 Spatial distribution of AOD$_{MISR}$ for the 2007 dataset using the half degree (Lat/Lon) gridded level 3 AOD$_{MISR}$. (a) for self-QAed MISR data, (b) for MISR data after applying the F$_{cc}$ > 20% and F$_{cirrus\_free}$ = 100% cloud filters, (c) for MISR data after applying the F$_{cc}$ > 80% and F$_{cirrus\_free}$ = 100% cloud filters, (d) for MISR data that passed the thin cirrus cloud filter (F$_{cirrus\_free}$ = 100%), (e) AOD$_{MISR}$ plot of (b) minus (a), and (f) AOD$_{MISR}$ plot of (c) minus (a). Color contours progressing from cold to warm represent increasing AOD$_{MISR}$ values with the black color representing regions with no data.

5.3.2 A longer-term study of cloud contamination in the AOD$_{MISR}$ using F$_{cc}$ data

The monthly and zonal differences were evaluated between the MISR self-QAed AOD_{MISR} data and AOD_{MISR} sets with three different cloud screening methods for 2007. Figure 30 shows the monthly and zonal mean deviations from the self-QAed MISR AOD_{MISR} data for three data sets: (1–2) AOD_{MISR} after applying the $F_{cc}>$ 20% and 80% filters combined with the thin cirrus cloud filter and (3) AOD_{MISR} after applying the thin cirrus cloud filter($F_{cirrus\_free} = 100\%$). Figure 30a shows the monthly mean of AOD_{MISR} minus the self-QAed AOD_{MISR} over global oceans. When compared to the self-QAed AOD_{MISR}, the cirrus-free ($F_{cirrus\_free} = 100\%$) data have mean AOD_{MISR} values that are consistently 0.01 to 0.015 lower throughout the year. Although uncertainties exist in the MODIS 1.375 μm cirrus detection method (Gao et al., 2002; Pierce et al., 2010), it is possible that thin cirrus cloud contamination is present in the AOD_{MISR} that could introduce a high bias of ∼0.01 over global oceans. The thin cirrus related bias could reach 0.015–0.02 over oceans at mid to high latitudes. Although not shown here, a higher bias of ∼0.02 was also found over Southeast Asia (15° S to 25° N, 90° E to 160° E). The F_{cc} cloud screening method combined with the thin cirrus cloud filter introduces a year-round reduction in AOD_{MISR} of 0.02 to 0.06 depending on the thresholds, especially during May, June and July. Figure 30b is similar to Figure 30a but for the over-land case. When compared with self-QAed AOD_{MISR}, the thin cirrus cloud filter introduces a ∼0.005 reduction in the averaged AOD_{MISR} from February to August. The reduction is found to be around 0.005 to 0.015 when the F_{cc} filters are applied. Figure 30c and d show similar plots as Figure 30a and b but for the differences in zonal mean AOD_{MISR} averaged every 5° latitude bin. Over global oceans, the F_{cc} filters introduce larger
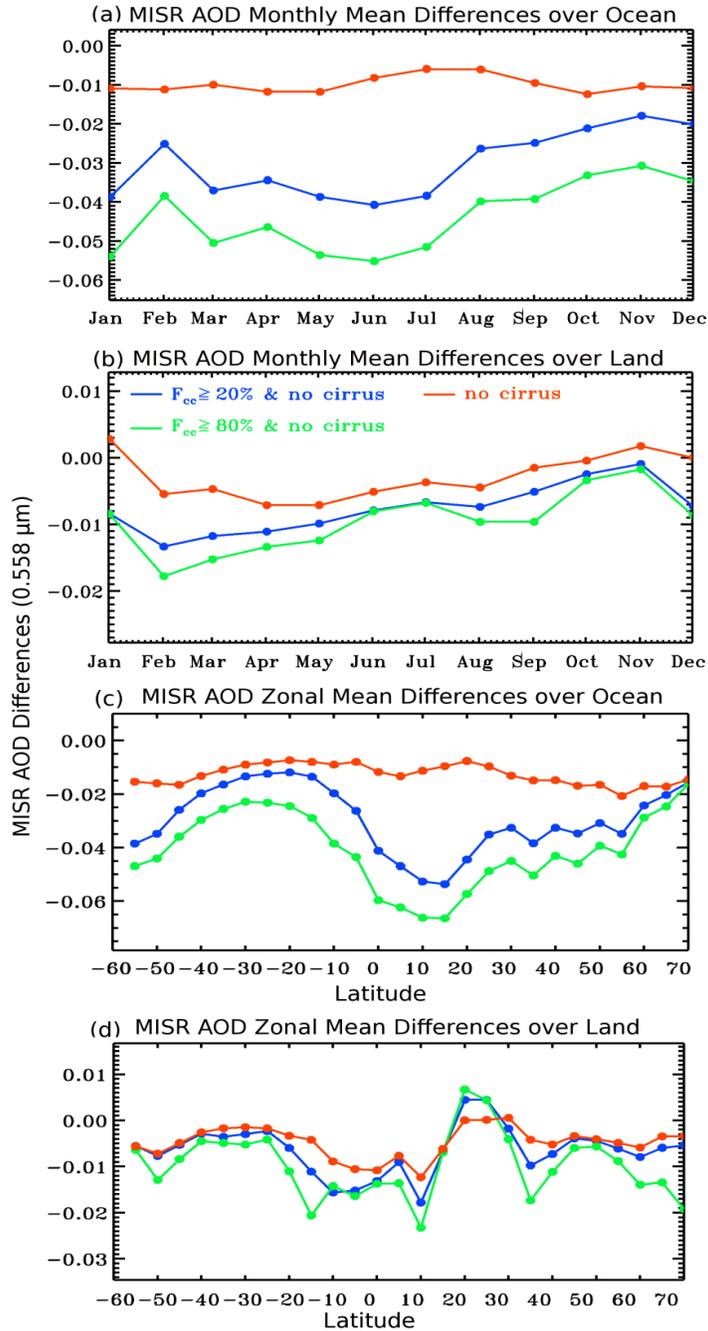
Figure 30. AOD$_{MISR}$ monthly and zonal mean deviations from the self-QAed AOD$_{MISR}$ for 2007 (minus self-QAed). (a) the over-water monthly mean, (b) the over-land monthly mean, (c) the over-water zonal mean, and (d) the over-land zonal mean. Four data sets are plotted representing the data that passed the thin cirrus cloud filter (F$_{cirrus\_free}$ = 100%) in red, data that passed F$_{cc}$> 20% and F$_{cirrus\_free}$ = 100% filters in blue, and data that passed F$_{cc}$> 80% and F$_{cirrus\_free}$ = 100% filters in green.

reductions in AOD_{MISR} occurring from 0° to 20° N and beyond 50° S with the largest reductions reaching 0.05 and 0.07 for 20% and 80%F_{cc} cut off, respectively. After applying the F_{cc} filtering method, there is almost no MISR data available beyond 55 °S. Over-land, while compared with the self-QAed MISR zonal mean AOD_{MISR} values, reductions in AOD_{MISR} are also found globally after applying the F_{cc} screening method.

5.4 Recommendations and conclusions

This study used collocated MODIS cloud mask products to evaluate potential cloud contamination in the MISR aerosol products. Major findings include:

1. Cloud contamination exists in the AOD_{MISR} data. Especially, thin cirrus cloud contamination introduces a possible mean AOD_{MISR} high bias of ~0.01 over global oceans and 0.015–0.02 over the mid to high latitudes and Southeast Asia. This study suggests that additional cloud screening methods may be needed for using MISR aerosol products for future studies.

2. New MISR cloud screening methods such as the MISR CFF method (Witek et al., 2013) have been developed to reduce cloud contamination in the MISR aerosol retrievals. However, with the use of only visible and near- IR channels from MISR, such methods may still have difficulty in identifying thin cirrus clouds, even while excluding a substantial fraction of the observations. The MODIS cloud masking data can be effectively used for reducing cloud contamination

in the MISR aerosol retrievals, and is more effective in removing thin cirrus-cloud-contaminated cloudy MISR aerosol retrievals in comparison with cloud screening methods using only MISR observations.

3. Cloud masking using MODIS data introduces some potential problems. For example, it is possible that some of the high AOD are misidentified as cloudy pixels and are removed by the MODIS-based cloud filtering methods when stringent thresholds are used. The misidentification of thick dust and smoke scenes as cloud scenes by the MODIS cloud mask products, however, has a lesser effect on operational MODIS aerosol retrievals. For example, Levy et al. (2013) discussed an approach to restore thick dust and smoke scenes that are misidentified as clouds by the MODIS cloud screening method. A regional-based cloud screening method, such as a spatial variability test, may be needed for rescuing these misidentified heavy aerosol polluted scenes, through the combined used of MODIS and MISR data at the radiance level.

4. A closer look into the distance between the aerosol retrievals and cloud edge (Levy et al., 2013) may help users to choose the thresholds of the F_{cc} cloud filter for their applications. For example, MODIS c6 DT aerosol products include a parameter called "Average Cloud Distance Land Ocean" that is helpful in solving this problem. It may also facilitate further investigation over the cloud contamination due to

cloud 3D effects, aerosol hydration over the high humidity environment, and the twilight zone issue.

5.   This project demonstrated that data from one sensor (MODIS) can be applied to another (MISR) for the development of an improved product. Sensors that lack near-IR bands should consider this procedure when developing an aerosol product, for example Ocean and Land Colour Instrument (OLCI) on Sentinel-3. The far-sighted developers of systems such as on Terra and within the A-train were correct in that the sensor combinations can result in improvements over any single sensor algorithm. This will pave the way for future algorithms, or even systems (such as NPP, Korean COMS, and EarthCARE), which require multiple sensors feeding single algorithms.

CHAPTER VI

**REVISE C5-BASED ANALYSES USING THE NEWLY RELEASED C6
MODIS DATA, A PRELIMINARY STUDY**

6.1 Introduction

A new version of Aqua MODIS DB and DT aerosol products, the collection 6 products, were released in 2014. Early in 2015, the c6 Terra MODIS DT and DB products have also become available to the public. New changes and updates, as described in details below, have been implemented to both c6 MODIS DT and DB aerosol products. It is anticipated that the c5 MODIS aerosol product will be fully replaced by the c6 MODIS aerosol products which provide nearly real time data stream. Thus, DA-quality c6 MODIS aerosol products need to be constructed for data assimilation applications that require near real time MODIS aerosol products (e.g. Zhang et al., 2008a).

In this chapter, new changes to MODIS c6 DT and DB products are investigated and the paired comparisons between MISR and MODIS c6 data are studied. Updates are also made to c5-based analysis to construct DA-quality c6 Aqua DT over-ocean and DB aerosol products. No DA-quality Terra DT and DB data are constructed as the dataset has only been recently released (April of 2015).

6.2. Paired-comparisons of Terra c6 MODIS DT/DB and MISR AOD products

Following CHAPTER I, a paired comparison in between MODIS and MISR AOD data has been conducted using c6 MODIS DT and DB products. Figure 31a and b are the reconstructions of Figure 3a and b from CHAPTER I, but using c6 MODIS DT and DB data. Compared Figure 31a with Figure 3a, a major difference can be observed over global oceans. While the ratios of the c5 DT versus MISR AOD are near one. For the c6 MODIS DT and MISR comparison, these ratios are much reduced, especially over high latitude southern oceans. The differences are not unexpected for c5 over water DT algorithm because a fixed near ocean wind speed was used. For c6 over water DT algorithm, ocean surface characteristics are modified, which is dependent upon near surface wind speeds (Levy et al., 2013). Another noticeable difference is that over regions with complicated land surface features no c6 DT data are available, such as the Andes Mountains, southwest US, central Asia, where ratios of c5 DT to MISR AODs are greater than 1.6 (Figure 3a),. This is partially due to the change in aerosol models in the algorithm and partially due to a bug fix in the operational codes (Levy et al., 2013). Increased ratios are found over South America, central Africa, East Asia, East US and Europe, indicating an increase in AODs from c6 Terra MODIS DT data over these regions.

Compared with Figure 3b (c5 DB/MISR), Figure 31b (c6 DB/MISR) shows a much-improved spatial coverage for c6 DB products. As shown in Figure 31b, most of the ratios are around unity. Yet ratios of above 1.4 are found over South America, East Canada, Central Africa, and South East Asia and ratios of less than 0.6 are found over the western US, the Andes Mountains, the southern part of South Africa, the

Middle East, Central Asia, and Australia. Clearly, these regions need to have further investigations performed.
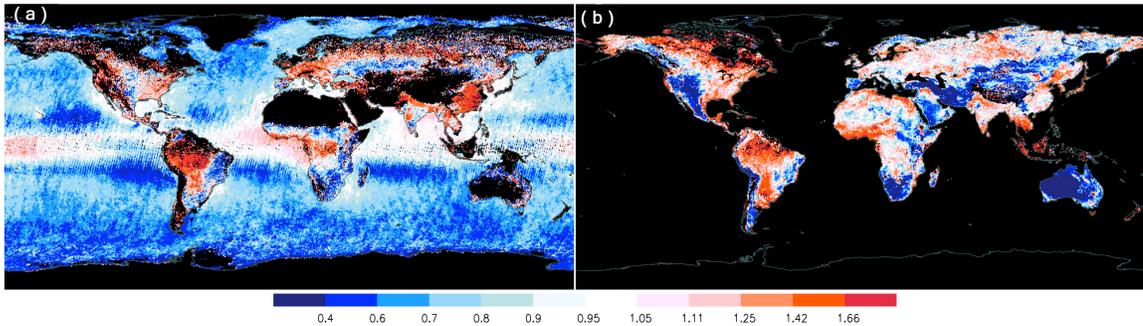
Figure 31. (a) The ratios of operational MODIS c6 DT (0.55μm) over MISR AOD (0.558μm) during the period 2005–2007. b) Similar to (a) except for MODIS DB to MISR AOD.

6.3. Extending c5 based analysis into c6 Aqua MODIS DT over ocean

Three major sources of uncertainties were identified in c5 DT over-ocean products from Shi et al. (2011a): (a) lower boundary conditions, such as near surface wind-related white cap contamination; (b) cloud contamination and artifacts, and (c) uncertainties related to aerosol microphysical property retrievals. Following Zhang and Reid (2006) and Shi et al. (2011a), similar analyses were performed for MODIS c6 DT over-ocean aerosol products.

Compared with c5 DT products, improvements in c6 DT products are obvious. For example, in c5 analysis, the differences (AOD at 0.55 μm) between c5 DT and AERONET AOD can be quantified as a function of NOGAPS near-surface-wind-spend. A 0.04 change in ΔAOD is found for wind speed increasing from 0 to 14m/s. In comparison, a much smaller increase in ΔAOD of 0.015 is found for c6 DT AOD

data. Clearly, with the newly implemented changes in c6 DT MODIS AOD data, the near-surface-wind-speed related bias is reduced.

Similarly, in c5 analysis, Shi et al. (2011a) found an overestimation in DT AOD for fine aerosols ($\eta < 0.45$) and an underestimation for coarse aerosols ($\eta > 0.7$). For c6 DT data, similar overestimation is found for fine mode aerosols, yet an insignificant underestimation is found for coarse aerosols.

Cloud contamination still exists in MODIS c6 aerosol products and introduces an overestimation in c6 DT AOD. However, the magnitude of the cloud-contamination-induced overestimation is reduced compared to c5-based analysis. Also, in addition to the evaluation procedures mentioned in Shi et al. (2011a), a few new parameters are included in c6 DT data, such as the "Average_Cloud_Pixel_Distance_Land_Ocean" parameter, which can be used for further evaluating cloud contamination related bias. This parameter records the averaged distance in term of number of pixels between the retrieved aerosol pixel to the closest cloud pixel (short as "averaged distance to clouds", ADC). Figure 32 shows the differences between Aqua DT and AERONET AOD (ΔAOD) as a function of ADC where ΔAOD decrease with increasing ADC. For example, the ΔAOD is around 0.4 with ADC = 1, when the retrieved aerosol pixel is very close to clouds while the ΔAOD is much reduced to 0.01 with ADC = 12. It is obviously that ADC can be used as a new data filter to screening potential cloud contaminated data for aerosol retrievals.
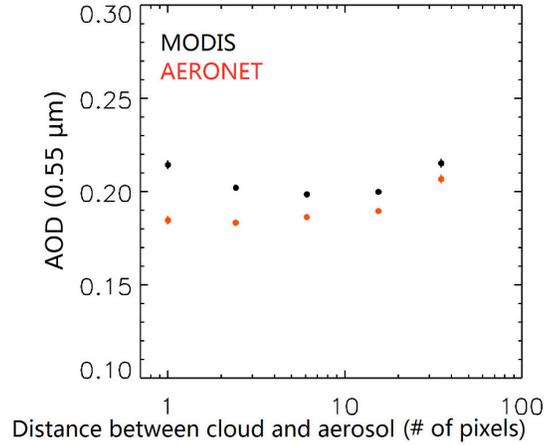
Figure 32. MODIS c6 Aqua DT and AERONET AOD as a function of the averaged distance between an aerosol retrieval and the closest nearby cloudy pixel (measured by number of pixels in distance). Red filled circles represent AERONET AOD and black filled circles represent over-ocean c6 Aqua MODIS AOD$_{DT}$.

As mentioned in Shi et al. (2011a), biases and uncertainties in satellite reported AOD values are dependent of observing conditions, and can be corrected using empirically methods. For low aerosol loading cases (AOD < 0.2), the empirical correction step is described as Equation 8,

$$\tau_{new} = \tau_{old} + A - B \times u - C \times F_{cld} \tag{8}$$

where u is near surface ocean wind speed, F_{cld} is cloud fraction, and τ_{old} and τ_{new} are c6 DT AODs before and after empirically adjusted. As mentioned in Shi et al. (2011a), Equation 8 should also be stratified as a function of glint angle (ψ). In this study, we adopted the same empirical correction steps, but updated the coefficients (A, B and C) based on c6 DT AOD data as shown in Table 8. No empirical correction steps are applied to retrievals with AOD > 0.2, due to a reduced uncertainty/bias in both cloud contamination and aerosol microphysical property related bias.

Table 8 Coefficients for parameters A, B and C that are included in Equation 8 as a function of Glint Angle (ψ). All coefficients are estimated for c6 Aqua DT AOD data.

Ψ range	A	B	C
$30° < \psi < 60°$	0.00186	0.0025	0.00025
$60° < \psi < 80°$	0.00328	0.0015	0.00025
$80° < \psi$	-0.00250	0.00078	0.00023

Also, a further data filter step is applied to remove data samples that have cloud fractions larger than 80% or ADC $\leq$ 2. Both requirements are aimed for removing potential cloud contaminated data.

Lastly, the empirical corrections and data filter steps are validated with the use of AERONET data. Figure 33 shows the AOD comparisons between MODIS c6 DT and AERONET for operational and the DA-quality c6 Aqua DT products (dataset after applying the empirical corrections and filtering steps). Compared with the
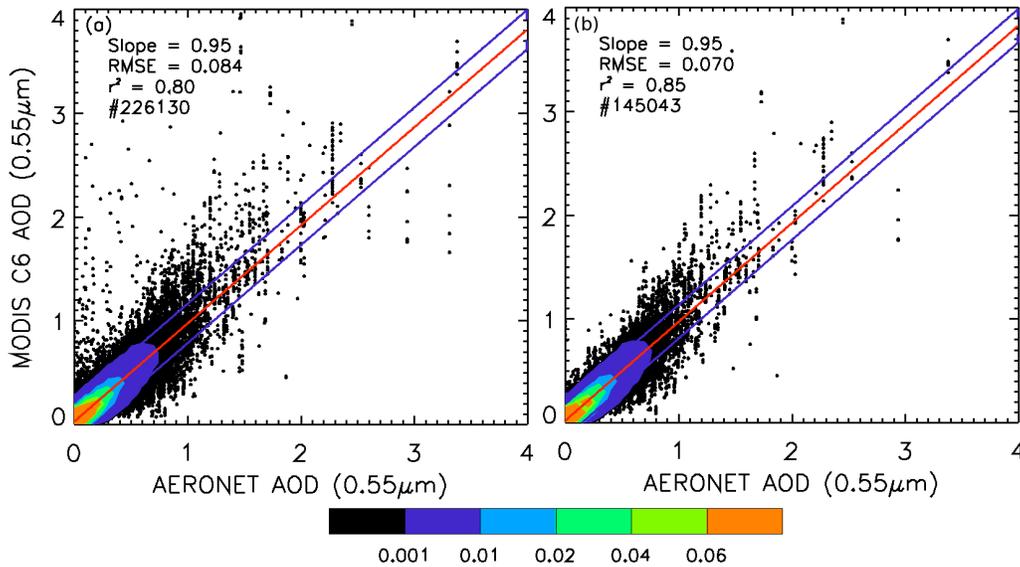
Figure 33. Scatterplot of c6 Aqua MODIS DT AOD versus Level 2.0 AERONET AOD (0.55 μm) for 2002–2009. (a) Operational over-ocean DT AOD data and (b) DA-quality AOD data. The red line is the linear regression line for all data and the blue lines are the 1.0 standard deviation lines of the data.

operational c6 DT AOD, RMSE of the DA-quality c6 DT AOD is reduced about 17% from 0.084 to 0.070. The r^2 value is increased from 0.8 to 0.85 with a data loss of 36%.

Figure 34 shows the seasonal distribution of over-water AOD for c5 operational product, c6 operational and c6 DA-quality products during year 2006. One noticeable feature is that the elevated AOD features over high latitudes of both
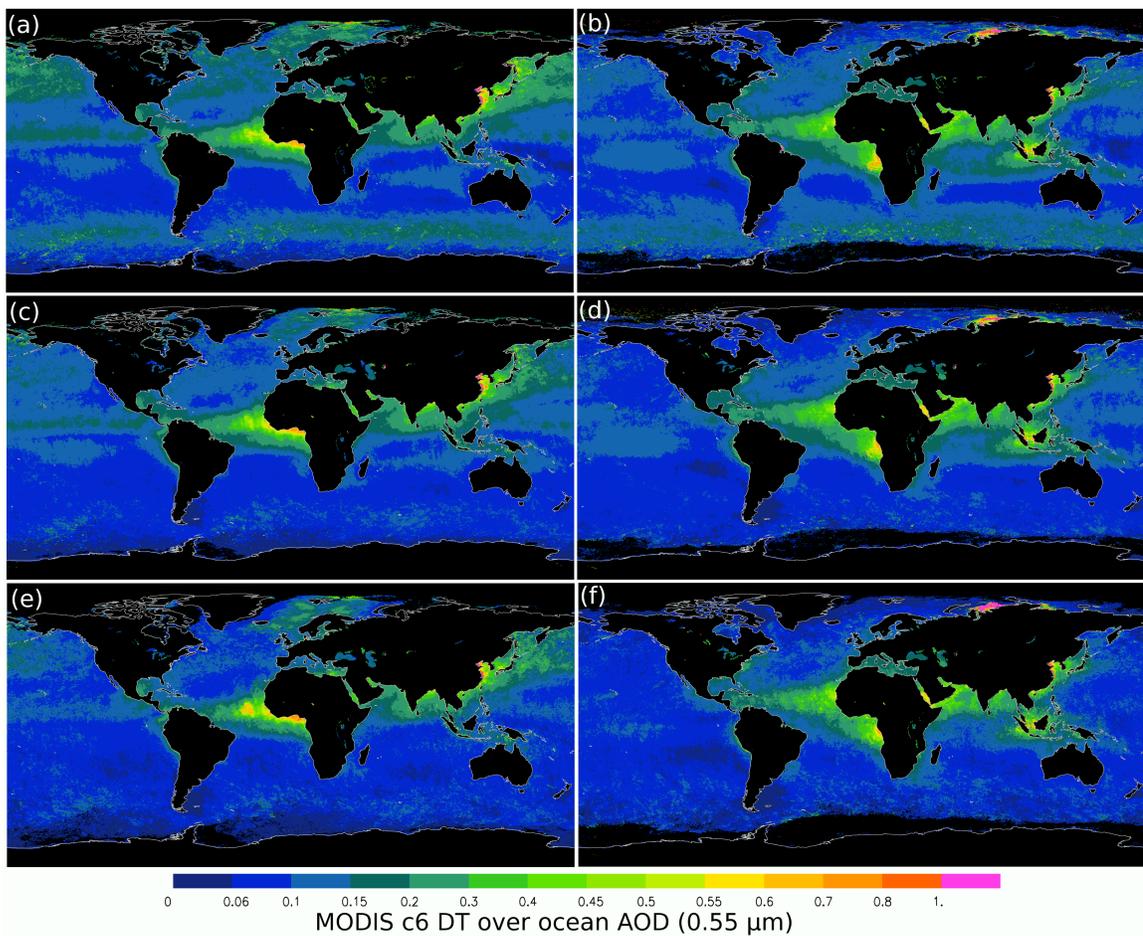
Figure 34. Spatial distributions of Aqua MODIS AOD_{DT} (0.55 μm) for 2006. The black color represents regions with no data. The left column shows the data from December to May, and the right column shows the data from June to November. The top row is for the operational c5 Aqua MODIS AOD_{DT}. The middle row is for the operational c6 Aqua MODIS AOD_{DT}, and the bottom row is for the newly developed DA-quality c6 Aqua MODIS AOD.

northern and southern hemispheres are much reduced from c5 to c6 AOD products. As a result of a more stringent cloud-screening step, the averaged operational and DA-quality c6 DT AOD values are reduced compared to those from c5.

6.4. Extending the c5 based analysis into c6 Aqua MODIS DB aerosol product

6.4.1 Collocation Method

Methods shown in CHAPTER IV are adopted here to construct DA-quality c6 Aqua DB data. To assist the analysis, 11 years (2002–2013) of AERONET AOD data were collocated in space and time with c6 Aqua DB data, following the method mentioned in Shi et al. (2011a). The collocation thresholds for the spatial and temporal differences of the two observations are set to 0.3° (Lat/Lon) and 30 minutes respectively. Mentioned in CHAPTER IV, a one-to-one matched dataset (only the closest DB retrieval is paired with a given AERONET data point) was constructed and used. In this study, besides constructing a one-to-one dataset, a one-to-many dataset was also constructed to increase data samples, including all DB retrievals that satisfy the collocation criteria for a given AERONET data point. The one-to-one dataset is used to evaluate c6 MODIS DB retrievals, and the one-to-many dataset is used to study uncertainties in DB retrievals as functions of observing conditions.

6.4.2 Evaluation

In this section, similar evaluation steps as mentioned in CHAPTER IV are adopted as well. For brevity, only results that derivate from what have been shown in CHAPTER IV are discussed in this section. Similar to the evaluation steps applied to c5 DB data, the general performances of c6 DB products are studied with respect to

QA flags, the uncertainties of DB products are evaluated as functions of observation conditions, the empirical correction procedures are developed along with several data filters, and as the final step, the ¼ degree (Lat/Lon) DA-quality level 3 product is generated.

6.4.2.1 Overall nature of the Deep Blue Product

Figure 35 shows the comparisons of collocated c5 and c6 Aqua DB and AERONET AOD with respect to MODIS retrievals. The one-to-one datasets from 2002–2009 are used and only DB retrievals with "very good" QA flag settings are selected. The fractional data density is shown in Figure 35 for every 0.5 increments of AOD for both AERONET and DB AOD values. As illustrated in Figure 35, the number of collocated AERONET and MODIS DB data pairs has increased 78 times from c5 to c6. Also shown in Figure 35, a consistent underestimation in c6 AOD_{DB} can be found when compared to AERONET data. For retrievals with $\tau_{DB} < 0.5$, a near one to one relationship is observed between AERONET and DB AOD values, with a slight underestimation in AOD_{DB} can be found. For retrievals with $\tau_{DB} > 2.0$, stripped feature of AOD_{DB} are presented, suggesting that there are some issues and uncertainties in the c6 DB AOD retrievals over this AOD regime. Similar to c5, uncertainties in c6 AOD_{DB} retrievals are regional dependent. Using the one-to-one dataset and selecting the c6 DB data having the QA flag of "Very Good" during the period 2002–2013, regional comparisons between Aqua DB and AERONET AOD values for nine selected regions were conducted as shown in Figure 36 (similar as Figure 8 for c5 MODIS DB data).
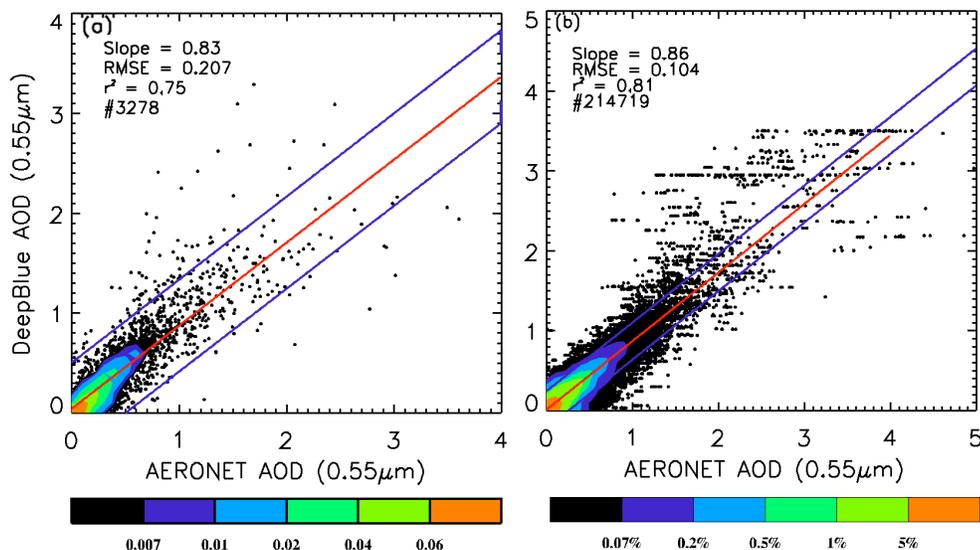
Figure 35. Comparisons between Aqua DB and AERONET AOD from 2002–2009 for (a) c5.1 DB AOD. Only "very good" retrievals as indicated by the QA flag are used, (b) similar to (a) but for c6 DB AOD data. The red line is the linear fit line and the blue lines are the 95% confident interval lines. The color contour shows the fractional data density.

The definitions of the nine selected regions are the same as illustrated from Figure 9. Figure 36 shows that a consistent underestimation in c6 AOD_{DB} values is found for all other eight regions except for Northwest America. The magnitudes of the underestimation vary from region to region. Of all nine regions, lower uncertainties in c6 AOD_{DB} are found over North Africa, Southern Africa/sub-Saharan Africa, East and West Asia. For example, slopes of 0.8–0.9 are found in between c6 DB and AERONET AOD with a RMSE of around ~0.15 for the regions with the presence of heavy aerosol loading cases. Comparing with c5 MODIS DB products (e.g. Figure 8), improvements in c6 Aqua DB products are clearly visible, especially for regions such as North and South Africa, East and West Asia where reduced RMSE values are observed. For example, the RMSE value for AOD_{DB} has reduced from ~0.2 (c5) to

113

~0.1 (c6) over East and West Asia. Still, outliers and low bias are clearly visible in Figure 36b, c, and d, possibly due to the lack of ability of retrieving highly absorbing fine mode aerosols by the DB aerosol retrieval algorithm (personal communication with Dr. Jeffrey Reid, 2015).

6.4.2.2 Uncertainty analysis

Similar to the analyses applied to c5 MODIS DB products, series of analyses were performed to investigate the sources of uncertainty in c6 AOD_{DB} product, including angular dependence, aerosol microphysics, surface reflectance, and other observing conditions. In addition, a new snow contamination test, which utilizes the MODIS 16-day albedo products, has also been implemented.

Figure 37 shows the scatter plots of AOD_{DB} vs. $AOD_{AERONET}$ for three fine mode fraction (η) ranges: $\eta \leq 0.4, 0.4 < \eta < 0.8$, and $\eta \geq 0.8$. Here η is computed from the collocated AERONET data using a method as described in O'Neil et al. (2003). As indicated from Figure 37, an increase in η from 0.4 to 0.8 only introduces a minor change in the slopes between AOD_{DB} and $AOD_{AERONET}$ (from 0.82 to 0.88). Clearly, compared with the c5 DB data-based analysis, the effect of η to c6 AOD_{DB} is much reduced. As mentioned above, one of the major updates in c6 Aqua MODIS DB products is the use of a pre-calculated the surface reflectance database that is built as a function of NDVI. Thus, as the next step, the effect of surface characteristics on c6 AOD_{DB} is studied. Table 9 shows the error statistics of c6 AOD_{DB}, including Absolute Error (AE), RMSE, RMSE at $\tau_{DB} > 1.5$, r^2, slope, and offset as approximated
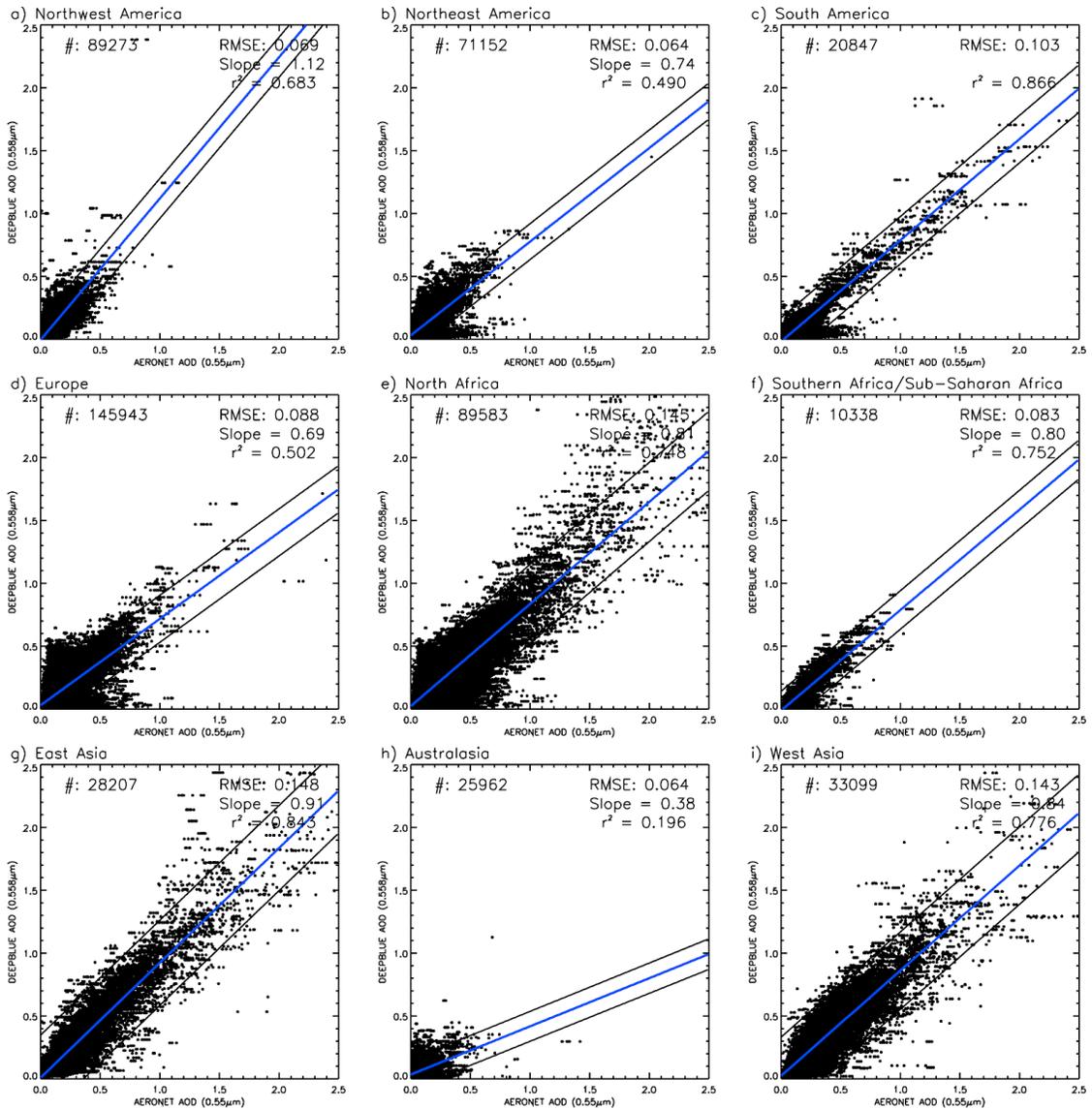
Figure 36. Regional comparisons between Aqua c6 DB and AERONET AOD for 2002–2009. Again, only "very good "retrievals, as indicated by the QA flag are used. (a) Northwest America, (b) Northeast America, (c) South America, (d) Europe, (e) North Africa, (f) South Africa, (g) East Asia, (h) Australia, and (i) West Asia. The blue line is the linear fit line and the black lines are the 95% confident interval of the linear fit lines.

using $AOD_{AERONET}$, as a function of surface reflectance at the 0.412 μm (R_{412}) spectral channel. Shown in Table 9, an increase in R_{412} from 5 to 10% introduces an observable increase in AE and RMSE values and a decrease in r^2 and slope values. This indicates that uncertainties related to surface albedo still exist in c6 AOD_{DB} data.
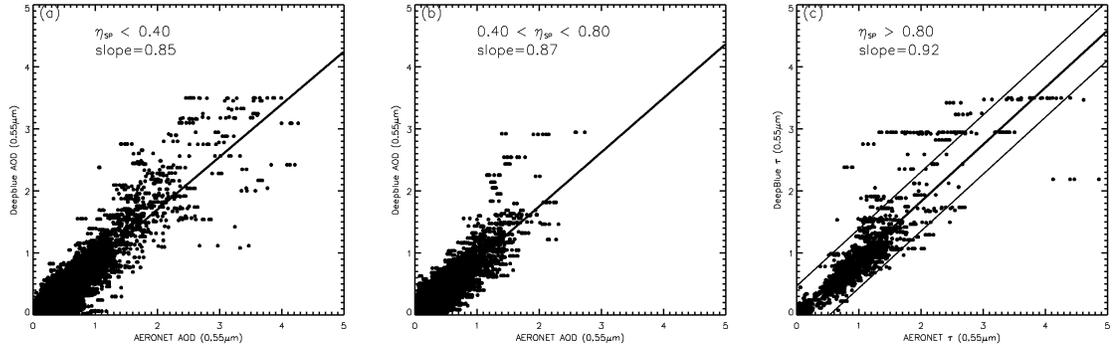
Figure 37.Comparisons between Aqua AOD_{DB} and $AOD_{AERONET}$ (0.55 µm) for 2002–2013. (a) for AERONET derived η < 0.4, (b) for 0.4 < η < 0.8, (c) for η > 0.8. The thick black line is the linear regression line

Table 9 Error statistics as a function of surface reflectance (at 0.412 µm) for c6 DB AOD data.

R_{412} Range	Absolute Error	RMSE	RMSE (τ_{DB}>1.5)	R2	Slope	Offset
< 0.05	0.048	0.080	0.72	0.84	0.90	0.006
0.05–0.065	0.069	0.112	0.55	0.83	0.86	0.005
0.065–0.09	0.088	0.143	0.59	0.74	0.80	0.000
0.09–0.1	0.081	0.12	0.52	0.70	0.73	0.073
0.1–0.12	0.140	0.186	0.72	0.42	0.50	0.176
> 0.12	0.148	0.197	0.20	0.21	0.51	0.130

In addition, snow contamination is studied and the snow fraction percentage from MODIS 16-day albedo product is used to represent snow coverage within each 10 by 10 kilometer scene. Figure 38 shows the c6 AOD_{DB} bias as a function of snow coverage. While a less than 0.01 difference is found between $AOD_{AERONET}$ and c6 AOD_{DB} ($\Delta AOD_{AERONET-DB}$) over snow free region, the magnitude of the $\Delta AOD_{AERONET-DB}$ increases as a function of the increasing snow coverage and reach -0.07 for the average snow cover of 70%. Clearly, snow contamination is present in c6 Aqua DB products and needs to be accounted for when constructing DA-quality products.
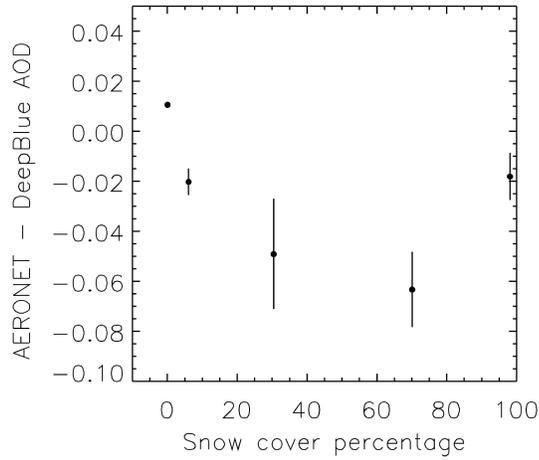
Figure 38. AOD bias ($\Delta\tau_{A-M}$) as a function of the snow coverage percentage (from MODIS 16day albedo product). The error bars indicate one standard deviation above and below the mean.

The DB products contain a parameter that records the number of 1-km MODIS level1b reflectance pixels used in creating the 10 km resolution AOD_{DB} retrievals (refer to Number of Pixel Used or NPU). As shown in CHAPTER IV, a noticeable high bias in ΔAOD of 0.11 was found for the c5 AOD_{DB} values when all of the 1-km pixels are used in the retrieval process. This high bias is reduced to 0.02 for the c6 AOD_{DB} retrievals. To further investigate the relations of NPU and the data uncertainties, the percentage of DB c6 data that fall outside of the reported uncertainty envelope, which is *±0.03 ± 20% × τ_{DB}* (defined as percentage of outliers) is analyzed. Figure 39 suggests that AOD retrieval with smaller NPU values normally has a higher chance to fall outside of the reported uncertainty envelope, or a higher chance to be a noisy retrieval. Thus, based on Figure 39 and Table 9, the criteria to filter out noisy retrievals was developed and parameterized as functions of R_{412} and NPU values.
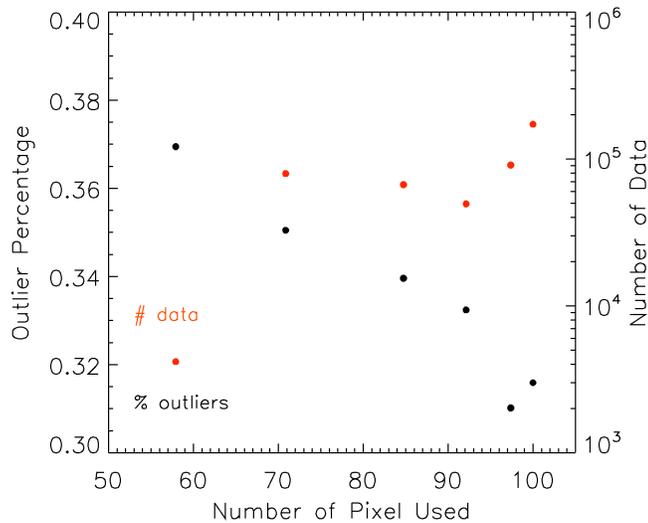
Figure 39. Percentage of DB data that are outside the uncertainty envelope (*0.03 ± 20% × τ*) (% outliers) as functions of number of pixels used (black) and the number of data within each bin of number of pixels used (red).

6.4.3 Development of QA/QC Procedures for DA-qualityc6 DB level 3 data

Updates to the QA/QC procedures as implemented for c5 DB data are made. In particular, based on Sect. 6.4, no significant systematic bias is found in c6 DB AOD as a function of aerosol microphysical properties, and thus, no empirical correction is applied. Still, as suggested in Sect. 6.4.2, it is necessary to set up the criteria to filter out noisy retrievals, which excludes snow and cloud contaminated pixels. Thus, AOD retrievals with cloud fraction greater than 40% and snow coverage above 0% are excluded from the study. Also, for AOD retrievals within regions that have surface reflectance less than 10% (at $\lambda = 412$nm), only retrievals with NPU greater than 60 are selected.
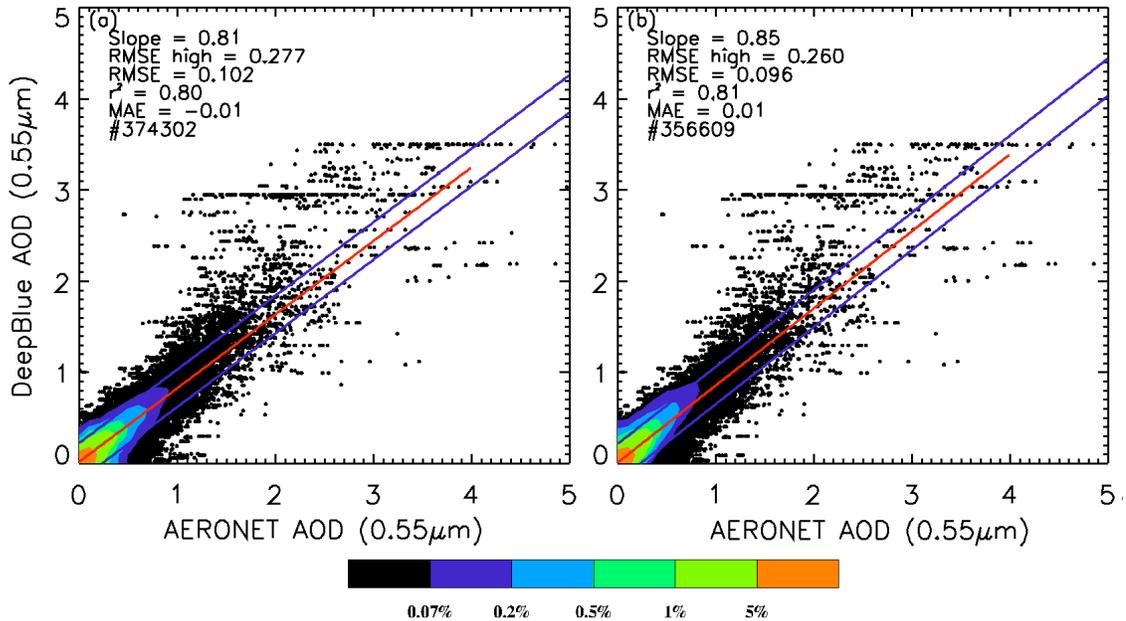
Figure 40. Scatter plots of AOD_{DB} versus $AOD_{AERONET}$ (0.55 μm) for Aqua c6 DB AOD data for 2002–2013. (a) is for operational MODIS Aqua DB AOD data and (b) is for DA-quality data. The red line is the linear regression line and the blue lines are the 1.0 standard deviation lines.
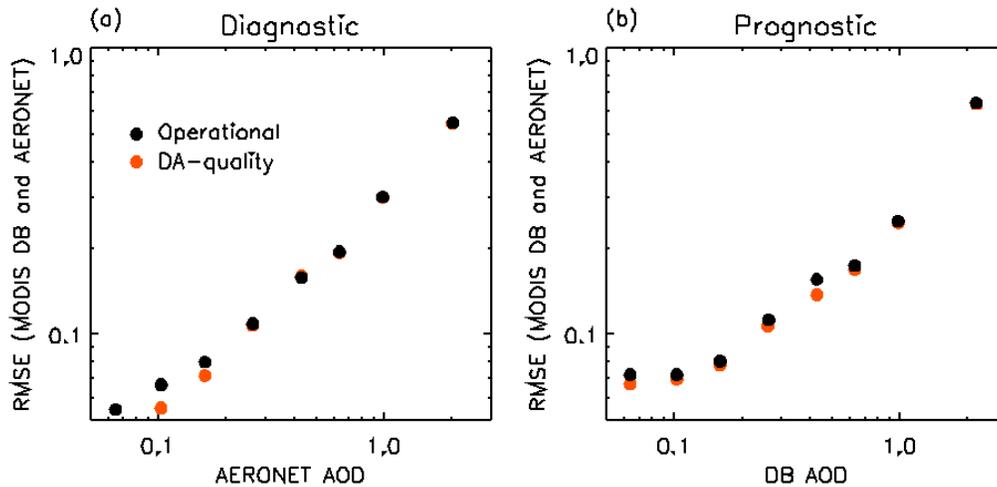
Figure 41. The RMSE of AOD_{DB} against $AOD_{AERONET}$ for (a) diagnostic error analysis and (b) prognostic error analysis. Black filled circles are for operational c6 DB retrievals and red filled circles are for DA-quality DB AOD data.

Figure 40 shows the comparisons between operational c6 AOD_{DB} and $AOD_{AERONET}$ during the period 2002–2013 with the c6 DB AOD data went through

the filtering steps. Figure 40 demonstrates that the underestimation in AOD_{DB} is reduced and RMSE is reduced about 10% after filtering out noisy data. Marginal improvements in RMSE are also observed, both for prognostic and diagnostic estimates, throughout the entire AOD regime (Figure 41).

6.5 Conclusions

MODIS c6 DT and DB aerosol products were recently released. As a preliminary study, significant efforts are conducted on evaluating MODIS c6 DT (over water) and DB AOD products for aerosol modeling-related applications. Paired-comparisons of MODIS c6 Terra DT and DB with MISR v22 aerosol products were conducted for highlighting new changes in c6 DT and DB aerosol products. A preliminary analysis was conducted to evaluate c6 Aqua DT over-ocean and c6 Aqua DB aerosol products through the use of ground-based AERONET data. Retrieval biases and uncertainties were analyzed as functions of sampling and observation-related factors Updated quality assurance procedures, filtering processes, and empirical correction steps were developed for constructing new quality-assured DT and DB products. Our findings include:

1. When compared with c5 Terra MODIS DT and MISR data, a reduction in over-ocean AOD retrievals is observable for c6 DT AOD data. Also, problematic regions such as the Andes Mountains, west US, and central Asia, where large difference in c5 Terra DT and MISR AOD are found in CHAPTER I, are excluded from c6 DT retrievals.

2.   Evaluated with the use of AERONET data, systematic biases that related to the near surface wind speed and aerosol microphysical properties are much reduced in c6 Aqua DT over-ocean products. Also, the impact of cloud contaminations on AOD retrievals is minimized. In particular, elevated aerosol features over high latitude ocean are much reduced in c6 DT product when compared with that of c5 AOD_{DT}.

3.   Empirical correction steps and extra data filtering are applied to generate the DA-quality c6 Aqua DT over-ocean product. A 17% reduction in RMSE is found for the newly developed DA-quality Aqua AOD_{DT}. In general, the overall performance of c6 Aqua AOD_{DB} is improved compared with c5 Aqua MODIS DB products, especially over regions of North Africa, East and West Asia. A much larger spatial coverage is also observed.

4.   While uncertainties related to aerosol microphysical bias are much reduced, uncertainties related to snow and cloud contamination, as well as other surface characteristics still exist in c6 Aqua AOD_{DB}. Preliminary attempts are applied to construct QA/QC steps for c6 DB AOD data. A 10% reduction in RMSE ($\tau_{DB} > 0.5$) is found for the quality-assured Aqua c6 DB products when compared to the operational c6 DB products.

CHAPTER VII

AN INVESTIGATION OF THE POTENTIAL LOW BIAS IN THE MODIS AEROSOL PRODUCTS OVER ASIA

7.1 Introduction

One of the least explored biases in satellite aerosol products is the low aerosol optical thickness bias due to the misclassification of aerosol plumes as clouds. For example, MODIS DT aerosol retrievals are performed over cloud free regions (Remer et al., 2005; Levy et al., 2013; Hsu et al., 2013). To identify and exclude cloudy pixels, multiple cloud screening steps, including a visible reflectance threshold test, are implemented (Ackerman et al., 1998; Ackerman et al., 2008). Very thick aerosol plumes could be misclassified as clouds due to their high reflectivity. Clearly, by excluding optically thick aerosol events, this misclassification may introduce a low bias in aerosol optical thickness climatology, especially over regions such as east Asia, where a higher frequency of heavy aerosol plumes is expected (Sun et al., 2004; Chan et al., 2008; Logan et al., 2010). This low bias in satellite aerosol products is of a particular interest to aerosol data assimilation and modeling efforts because significant aerosol events are important for air quality and visibility forecasts and could be miss-predicted due to the exclusion of such events in the assimilated satellite aerosol data. Knowing the limitations, data producers have attempted to mediate this

misclassification-related low bias. For example, an adjustment is included in the c6 DT retrieval algorithm to "recover" some heavy aerosol retrievals (Levy et al., 2013). Still, this low bias remains as an issue in both c6 DT and DB products, and is not well quantified.

In this study, with the synergistic use of satellite observations from MODIS, OMI, and CALIOP, the under-sampling of the heavy aerosol plumes in DT and DB aerosol products is studied globally with a focus over Asia. A new Heavy Aerosol Identification System (HAIS) was developed for detecting very optically thick aerosol plumes in CALIOP observations by coupling OMI AI values with CALIOP level 1B as well as cloud and aerosol profile data. Collocated CALIOP, MODIS, and OMI data were then used to further investigate the potential low bias in the DT and DB aerosol products, in an attempt to quantify the magnitude of this under-sampling in regional DT and DB retrievals. This study attempts to answer the following questions:

1. Does this misclassification-induced low bias also exist in CALIOP aerosol products? Can CALIOP observations be applied to study this low bias in c6 DT and DB products?

2. Can this low bias from c6 DT and DB products be quantified over Asia using the combined OMI, CALIOP, and MODIS data?

3. Under what conditions do c6 DT and DB algorithms misclassify thick aerosol plumes as clouds?

This chapter is organized in such that in Sect. 7.2, a heavy smoke aerosol case is presented. In Sect. 7.3, a heavy aerosol identifying system (HAIS), designed for

discriminating heavy smoke aerosol plumes from clouds using CALIOP observations, is described. In Sect. 7.4, with the assist of HAIS, the potential low biases in CALIOP aerosol and cloud products and c6 DT and DB products are estimated over Asia.
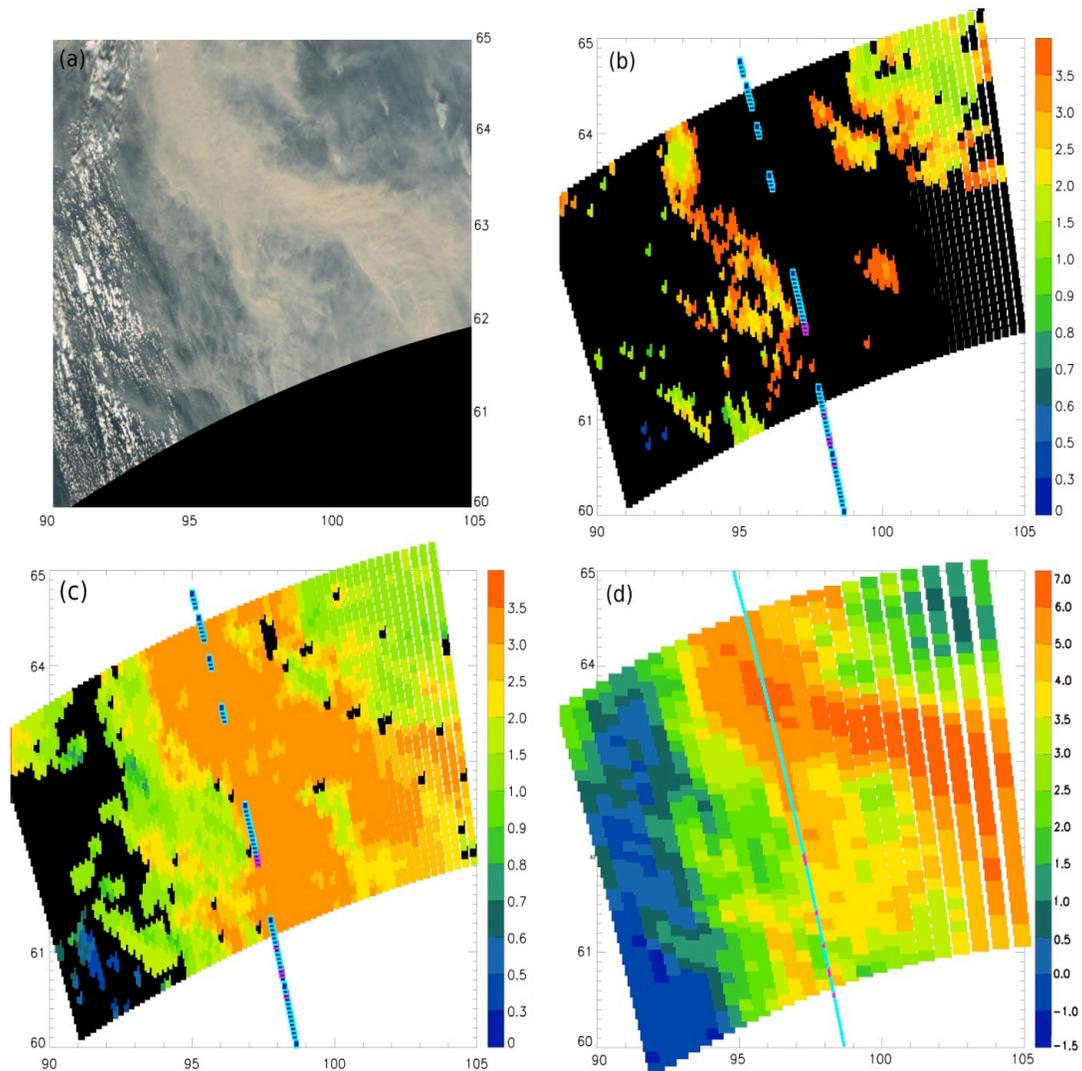
Figure 42. A case study of a wild forest fire over Siberia that occurred on 24 July, 2006. (a) MODIS RGB image, (b) MODIS c6 DT AOD retrieval, (c) MODIS c6 DB AOD retrieval, (d) OMI AI. CALIOP tracks are shown on both Figure 42b and d. The aqua color boxes/dots indicate CALIOP detected cloud scenes (from atmospheric composition flags). The pink color boxes/dots indicate CALIOP cloud-free aerosol scenes. The calculated CALIOP AODs are also color coded within the boxes in Figure 42b.

7.2 Case study: An extreme wild fire heavy smoke case over Siberia

The potential low bias in satellite aerosol retrievals can be illustrated by a Siberia smoke aerosol event that occurred on 24 July, 2006. Figure 42a shows the Aqua MODIS RGB image over 59° to 65° N and 90° to 105° E. Significant smoke aerosol plumes, in dark grey color, can be observed across the image and are clearly distinguishable with the white clouds observed at the far left side of the image. Figure 42b and c show the corresponding AOD retrievals from c6 Aqua MODIS DT and DB aerosol products and Figure 42d shows the OMI AI values. Over aerosol-polluted regions where OMI AI values exceed 3.0, however, aerosol retrievals are partially or mostly missing from the MODIS DT aerosol products. The collocated CALIOP observations are mapped on Figure 42b, c, and d are. The aqua color boxes/dots are cloudy CALIOP overpasses, as identified with CALIOP cloud and aerosol products. The pink color boxes/dots are cloud-free CALIOP overpasses. In Figure 42b, filled colors within the boxes represent the column integrated CALIOP AODs. Figure 42 suggests that the misclassification of aerosol features as clouds does exist in both DT aerosol products (97 °E and 64 °N). Also, CALIOP reported AODs are mostly less than 0.2, indicating that the similar low bias may also influence CALIOP retrievals.

This case study demonstrates that both passive- and active-based observations may have difficulty in separating heavy aerosol plumes from clouds. In comparison, OMI AI can be effectively used to detect optically thick UV-absorbing aerosol plumes that may be misclassified as clouds by CALIOP and MODIS aerosol products.

Thus, it is feasible to study the low bias over Asia with the use of collocated OMI AI, CALIOP, and Aqua MODIS data.

7.3 Methodology

7.3.1 Theoretical background for HAIS

Ideally, active-based observations (such as CALIOP data) have a better cloud-clearing capability relative to passive-based aerosol and cloud measurements, especially for optically thin clouds and over mixed cloud and aerosol scenes (Winker et al., 2009). Thus, measurements from active-sensors such as CALIOP can be used to study the misclassification-induced low bias in passive-based aerosol retrievals. However, as suggested from the previous section, this misclassification may also exist in CALOP data and needs to be further explored.

The misclassification of aerosol plumes as clouds is not unexpected for CALIOP retrievals. To distinguish clouds from aerosol plumes, a machine learning technique (Winker et al., 2013) is applied to three measured quantities, the total attenuation at 532 nm (TAB_{532}), the depolarization ratio (DPR, ratio of cross-polarization component and the total attenuated backscattering at 532 nm), and the color ratio (CR, ratio of attenuated backscattering at 1064 nm and 532 nm). Optically thick clouds can be easily identified because of their larger TAB_{532} values. Optically thick aerosol plumes, however, may have the comparable TAB_{532} values as clouds and thus can be misclassified as clouds.

Still, correction steps can be applied to the CALIOP cloud detection method to "rescue" heavy aerosol plumes as illustrated in Figure 43, which shows the curtain

126
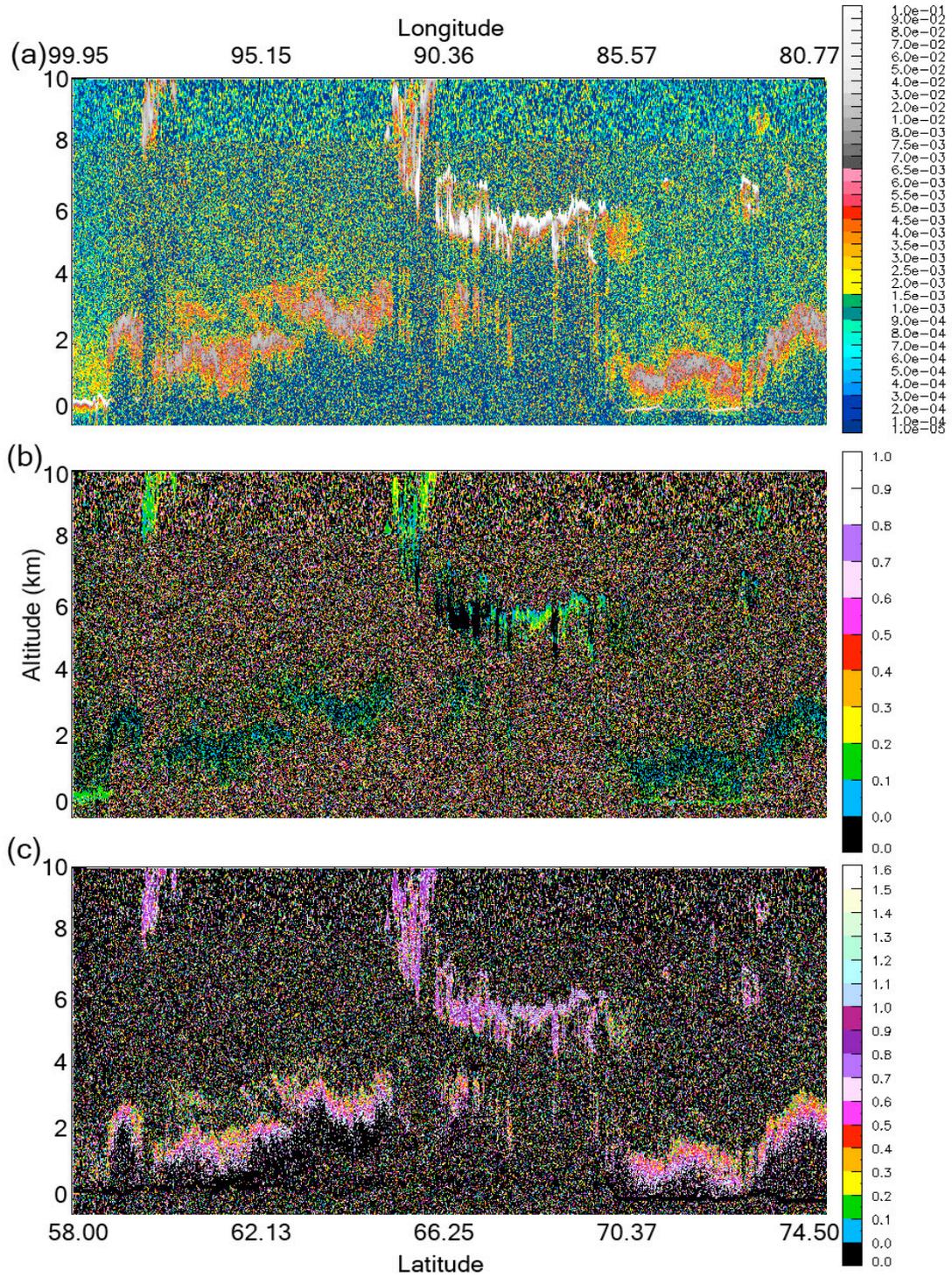
Figure 43. CALIOP curtain plots for the case study shown in Figure 42. (a) Total attenuation at 532 nm, (b) Depolarization ratio, and (c) Color ratio.

plots of CALIOP TAB_{532}, DPR, and CR for the case study. As shown in Figure 43a, cloud layers with TAB_{532} values of near 0.3 are found at or above 6 km altitude around 65º–70º N and 86º–92º E. Smoke plumes with TAB_{532} values of 0.002–0.02 are visible at altitudes of 2–4 km. Aerosol particles such as smoke and polluted aerosol particles are generally smaller than liquid-phase cloud particles. Thus, lower DPR values of less than 0.2 are expected for a smoke/polluted aerosol plume, while larger DPR values are expected for water clouds (Figure 43b, personal communication with David Winker, 2014). Also, optically thick smoke plumes generally have slightly lower TAB_{532} values of around 0.01–0.02 (Figure 43a, personal communication with David Winker, 2014) than clouds. Lastly, shown in Figure 43c, a significant vertical gradient in CR values is present in the smoke plume. The sharp vertical change in the vertical gradient of CR values from the top to the bottom of the smoke layer (from 0.2 to 1.0) is understandable, as larger attenuations in radiation are expected at the 532 nm spectral channel relative to the 1064 nm spectral channel for aerosol particles. Clearly, with the combined use of OMI AI and CALIOP TAB_{532}, DPR, and CR data, it is possible to develop a scheme to better detect heavy smoke aerosol plumes in CALIOP data.

7.3.2 The HAIS algorithm

HAIS that is developed in this study, is designed to detect thick UV-absorbing aerosol plumes that are within 0–6 km altitude, because it is assumed that typical smoke aerosol plume heights are lower than 6 km (Johnson et al., 1991; Tosca et al., 2011; Vadrevu et al., 2012; Personal communication with Dr. Winker, 2014). Also,

CALIOP level 1B data are rather noisy (e.g. Figure 43), especially during day time, and thus various averaging schemes are applied as discussed later.

As the first step, over regions with OMI AI values larger than 2 (or with the presence of heavy UV-absorbing aerosol particles), every two vertical columns of CALIOP profiles are averaged, and a recursive feature detection scheme is applied to detect the top and the bottom layers of resolvable features such as cloud and aerosol layers. It is assumed that the horizontally averaged TAB_{532} values of a feature should be greater than 0.0025 for cloud or heavy aerosol features. Once the vertical boundaries of a feature are identified, as the second step, the feature type is estimated with a series of threshold tests based on the averaged TAB_{532}, DPR, and CR values as illustrated in Figure 44.
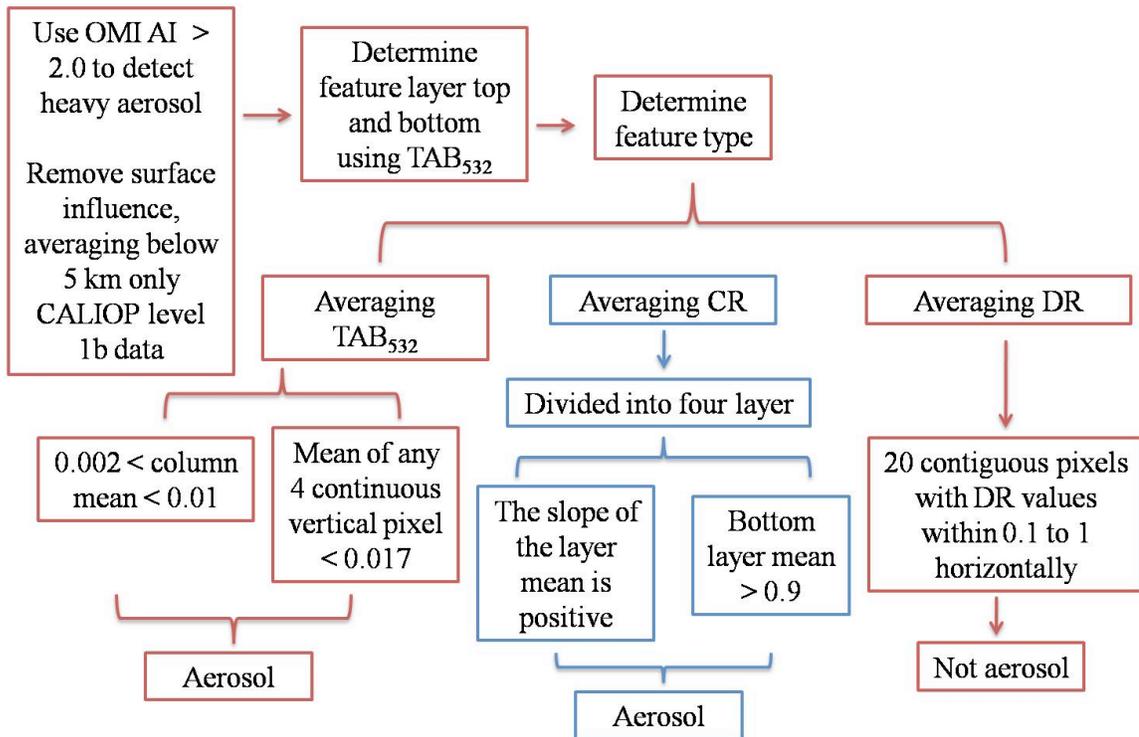
Figure 44. The flowchart of HAIS. The section colored in blue is for confirmation tests.

129

Optically thick clouds typically have large TAB_{532} values, which can be used to distinguish from aerosol plumes. The average layer TAB_{532} value is required to be in the range 0.002–0.01 for a layer to be considered as an aerosol plume. Although individual TAB_{532} values from heavy smoke plumes can reach as high as 0.02 on an individual basis, the layer average is usually lower. Other than the layer mean threshold, a vertical-continuity-test is also conducted to further separate clouds from aerosol plumes. Smoke aerosol TAB_{532} signals are typically smaller and nosier than those of clouds. Thus, to exclude potential clouds that are embedded in an aerosol layer, the averaged TAB_{532} values for four continuous pixels (or a vertical distance of 120 m) are required to be smaller than 0.017. However, optically thin clouds may have the similar TAB_{532} values as thick aerosol plumes. Thus, DPR values are also used to separate optically thin clouds from aerosol plumes. Initially, a layer averaged DPR value of 0.2 is used as the threshold to distinguish aerosol plumes from optically thin clouds. However, due to significant noises in DPR fields, the layer mean and median values of a feature may easily exceed this number. Therefore, instead of using DPR values to identify aerosol layers, DPR values are used to exclude potential clouds that are within an aerosol layer. Again, the collocated AI and the TAB_{532} tests should have already confirmed the existence of an aerosol layer. Clouds usually have a much smoother DPR field with continuous horizontal signals in DPR values. Such a characteristic is not found for an aerosol layer. Thus, a continuous-horizontal-DPR test is used to identify clouds within an aerosol plume. If a feature with 20 contiguous horizontal pixels (or 6.6 km in distance horizontally) has DPR values within the range 0.1–1.0, then the feature is identified as a cloud layer. In

comparison, the mean DPR value for an identified smoke layer is typically less than 0.1. The DPR test is designed to remove relatively uniform clouds that are within or underneath an aerosol plume. Still, the 20-pixel threshold is rather arbitrary. Sensitivity tests show that lowering the 20-pixel threshold results in unwanted misidentifications when an aerosol plume is close to the ground.

Although theoretically all three parameters (TAB_{532}, DPR, and CR) can be used to distinguish heavy aerosol features from clouds, CR is the noisiest parameter among all three parameters. Attempts have been made to horizontally and/or vertically average the CR signals. However, regardless of these attempts, it is found that CR values are too noisy to be implemented for distinguishing aerosol plumes from clouds. Thus, CR values are used to aid in validation of HAIS through visual inspection only.

7.3.3 Collocation of MODIS, OMI and CALIOP data

To implement HAIS developed in this study, MODIS, CALIOP, and OMI data need to be spatially and temporally collocated. In this study, one year (2007) of CALIOP level 1B data and level 3 cloud and aerosol profile products, OMI AI product, and c6 DT and DB products were collocated. To collocate CALIOP and MODIS data, a spatial difference equal to or less than 0.2° Lat/Lon is required between a CALIOP data point and the center of a MODIS data point. The temporal threshold between CALIOP and MODIS overpass times is set to 30 minutes.

The outputs of the collocated data include atmospheric composition flags (ACF) from the CALIOP level 3 clouds and aerosol profile products, which categorize a pixel into aerosol, cloud, or a mixed type. In order to use ACF

efficiently, layer-mean feature types were estimated for three selected vertical layers (above 10 km, between 5–10 km, and between the surface and 5 km). Above 10 km in altitude, where thin cirrus clouds are frequently present, a cloud flag was assigned to a layer when two vertically adjacent pixels are identified as clouds. For the remaining layers, a cloud or a mixed flag was assigned to the whole layer if an ACF flag reports a cloud pixel. Also included in the collocated CALIOP and MODIS dataset are the aerosol optical depth values that are computed through integration of total extinction from CALIOP (Campbell et al., 2012), aerosol top and bottom layer heights, as well as aerosol sub-types reported from the CALIOP level 3 cloud and aerosol profile products. The collocated CALIOP and MODIS data pairs were then collocated with OMI AI data with a spatial difference requirement of 0.3° Lat/Lon and a temporal difference requirement of 50 minutes. The thresholds used for collocating OMI and the paired CALIOP and MODIS data are larger than those that are used to construct the paired data, as OMI has a large footprint. Also, it is found that one collocated CALIOP–MODIS pair may correspond to more than one OMI AI values over the tropics and, thus, both the mean and the closest OMI AI values were used.

7.3.4 Evaluation of the HAIS system through case studies

7.3.4.1 Two selected case studies

The performance of HAIS was hand-checked with two case studies. The first case is over 58°–66° N, 80°–90° E from 24 July 2006. The second case is over 75°–77° N and 13°– 48° E from the same day. In both cases, as shown in Figure 45, heavy UV-absorbing aerosol plumes are identified with OMI AI data, yet are

misclassified as clouds by CALIOP aerosol and cloud profile products. Figure 45 shows the averaged TAB$_{532}$ for both cases over-plotted with HAIS detected aerosol plumes. Figure 45a shows that HAIS is able to detect the top and bottom of aerosol layers and is able to detect the presence of heavy aerosol plumes. Also, as suggested in Figure 45a, HAIS could identify clouds that are lower than 6 km (around 66° N). Figure 45b also shows that HAIS could successfully identify clouds embedded within an aerosol plume. Note that to identify cloud features above 6 km in altitude, CALIOP cloud and aerosol profiles products are used. The two case studies show
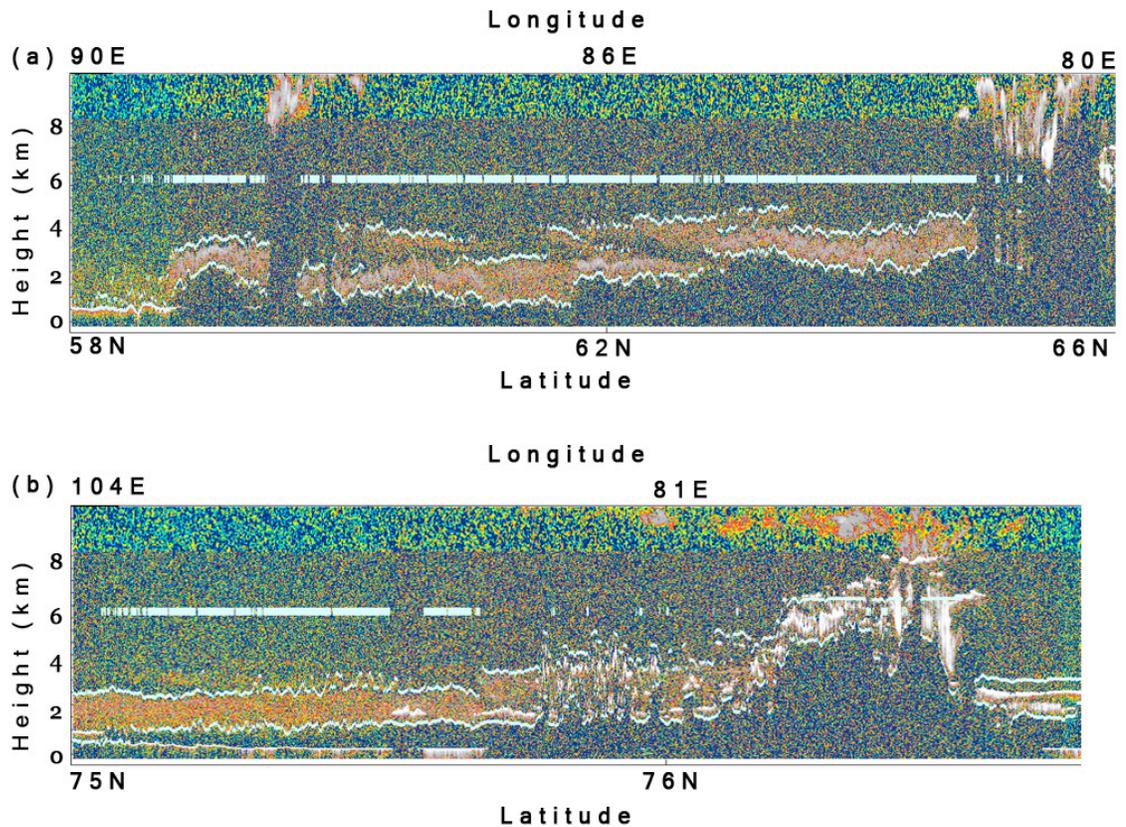
Figure 45. Implementation of HAIS for two selected case studies. (a) a section from the study case as shown in Figure 42 and (b) a weaker aerosol loading case with clouds embedded in the aerosol plume. The thick white line at an altitude of 6 km indicates regions that are detected by HAIS as cloud-free heavy aerosol scenes. The thin white lines are the top and the bottom of the detected features.

that the HAIS system could be used to identify heavy aerosol plumes with or without the presence of clouds.

7.3.4.2 Case studies over an extended study domain

Encouraged by the success from the two case studies, similar hand checks were performed within the extended spatial and temporal domains. To be specific, using collocated MODIS AOD, OMI AI, and CALIOP data from 2007, potential heavy aerosol scenes were generated over 70°–180° E and -15° S–80° N, for regions with OMI AI values larger than 3.0 that have no CALIOP detected clouds above 6 km altitude. A higher OMI AI threshold of 3.0 was used to reduce the number of selected cases. All selected scenes in January and June were checked along with some cases randomly picked from May and July. Table 10 listed the dates, times, and the geolocations of all hand-checked cases.

Table 10 Locations as well as satellite overpass times for the 81 selected cases.

# cases	MM/DD/YYYY	Time HH-MM-SS	Latitude start (°E)	Latitude end (°E)	Longitude start (°N)	Longitude end (°N)
1	1/2/2007	T06-49-08	27.8266	27.8266	89.4129	89.4129
2	1/3/2007	T09-11-17	18.9555	20.0327	56.0107	55.762
3	1/6/2007	T06-24-31	37.9261	38.7264	92.8235	92.5797
4	1/9/2007	T08-34-25	28.1979	28.3775	63.0711	63.0253
5	1/14/2007	T07-14-16	29.3786	29.4235	82.8724	82.8608
6	1/18/2007	T08-28-43	29.8831	32.0287	64.1969	63.6275
7	1/19/2007	T09-12-01	18.7942	20.142	56.0778	55.7667
8	1/20/2007	T06-37-39	28.6823	29.3535	92.3132	92.1405
9	1/22/2007	T06-25-25	36.35	38.9331	93.3041	92.5285
10	1/23/2007	T05-29-53	36.7548	36.8882	107.087	107.048
11	1/24/2007	T06-13-16	26.4209	26.5109	99.0534	99.031
12	1/26/2007	T04-22-12	37.6455	39.5594	123.809	123.222
13	1/26/2007	T06-01-02	36.2909	36.9139	99.4901	99.3072
14	1/26/2007	T09-18-53	18.4316	19.2389	54.595	54.4096
15	1/29/2007	T06-32-17	40.4204	40.5535	90.4969	90.4543

16	1/30/2007	T03-57-49	48.6921	49.3523	126.157	125.887
17	1/30/2007	T08-54-30	25.5651	25.9246	59.0744	58.9858
18	1/31/2007	T06-20-03	35.7099	36.0212	95.0097	94.9198
19	2/1/2007	T08-42-21	24.9487	25.1724	62.3107	62.2561
20	2/3/2007	T03-33-32	46.9556	46.9556	133.009	133.009
21	2/3/2007	T08-30-13	25.5531	28.6421	65.2486	64.4728
22	2/4/2007	T09-13-31	19.2759	24.6566	55.9243	54.6506
23	2/6/2007	T07-22-32	27.4356	27.5692	81.7715	81.7376
24	2/6/2007	T09-01-22	25.8887	25.9783	57.4351	57.4128
25	5/5/2007	T03-25-11	39.1522	39.3301	140.335	140.28
26	5/7/2007	T03-13-00	54.7477	54.8787	137.322	137.255
27	5/7/2007	T04-51-54	39.3628	39.452	118.641	118.613
28	5/8/2007	T03-56-20	37.9047	39.4177	132.992	132.528
29	5/9/2007	T03-00-45	35.8649	37.3805	147.5	147.055
30	5/16/2007	T04-46-21	33.4413	37.0985	121.936	120.892
31	5/25/2007	T04-40-44	33.4502	38.2207	123.461	122.083
32	5/26/2007	T03-45-07	36.6478	36.6478	136.455	136.455
33	6/1/2007	T06-26-05	41.4216	42.5759	94.804	94.4216
34	6/1/2007	T09-43-51	22.2213	24.6872	50.5959	50.005
35	6/2/2007	T05-30-28	45.4093	46.2056	107.336	107.043
36	6/2/2007	T07-09-19	37.5736	41.445	85.1883	83.9799
37	6/2/2007	T08-48-14	25.4905	25.803	63.7139	63.637
38	6/3/2007	T02-56-00	51.9016	52.1204	143.331	143.232
39	6/3/2007	T09-31-30	28.0684	28.7395	52.2547	52.0837
40	6/5/2007	T07-40-19	25.8742	26.5465	80.6142	80.4479
41	6/5/2007	T09-19-14	25.5877	30.3767	55.9627	54.7483
42	6/6/2007	T06-44-40	40.6559	42.3431	90.4141	89.8618
43	6/6/2007	T08-23-35	23.9775	24.1569	70.2604	70.2171
44	6/7/2007	T05-49-04	41.8127	41.8569	103.943	103.928
45	6/7/2007	T07-27-59	25.3709	25.8625	83.828	83.707
46	6/8/2007	T03-14-39	50.7176	53.9679	139.22	137.719
47	6/8/2007	T08-11-16	30.0578	32.0247	71.8281	71.3065
48	6/9/2007	T07-15-39	40.4998	41.7438	82.738	82.335
49	6/9/2007	T08-54-35	25.4791	30.4923	62.1692	60.8981
50	6/10/2007	T04-41-12	37.4521	37.5858	122.303	122.263
51	6/10/2007	T07-58-58	28.13	30.6355	75.4146	74.7671
52	6/10/2007	T09-37-48	22.5137	30.7977	52.0689	50.0023
53	6/11/2007	T07-03-21	37.3411	41.5233	86.8016	85.4987
54	6/11/2007	T08-42-11	25.3909	32.459	65.2819	63.4643
55	6/12/2007	T09-25-29	24.0831	24.5315	54.7838	54.6751
56	6/13/2007	T05-12-06	35.6664	36.646	115.102	114.817

57	6/13/2007	T08-29-52	28.0807	29.6919	67.7022	67.2888
58	6/14/2007	T09-13-05	25.9703	36.027	57.4142	54.739
59	6/15/2007	T08-17-28	34.0341	37.1998	69.2125	68.3024
60	6/16/2007	T07-21-51	38.9941	39.617	81.6667	81.4734
61	6/16/2007	T09-00-46	37.8649	37.8649	57.2879	57.2879
62	6/17/2007	T08-05-09	31.4103	31.4103	73.0191	73.0191
63	6/17/2007	T09-43-59	16.1122	24.6805	52.0008	50.0068
64	6/18/2007	T08-48-22	25.4566	30.1122	63.7239	62.5465
65	6/19/2007	T09-31-40	24.0239	29.3081	53.2573	51.9403
66	6/20/2007	T08-35-58	29.3709	32.8125	65.8311	64.9176
67	6/21/2007	T07-40-21	37.6495	39.9639	77.4439	76.7331
68	6/21/2007	T09-19-17	26.7322	30.0882	55.6852	54.8292
69	6/22/2007	T08-23-35	36.8505	36.8505	66.8662	66.8662
70	6/23/2007	T07-27-58	38.3854	40.4773	80.315	79.6636
71	6/23/2007	T09-06-53	25.5014	34.7589	59.0822	56.655
72	6/25/2007	T07-15-34	40.3275	40.6386	82.8043	82.705
73	6/25/2007	T08-54-29	30.0961	30.1408	61.0128	61.0011
74	6/26/2007	T09-37-42	20.7415	25.8981	52.4974	51.2629
75	6/27/2007	T07-03-10	39.2917	40.7157	86.2215	85.7728
76	6/27/2007	T08-42-00	44.7803	45.5775	59.6758	59.3878
77	6/28/2007	T09-25-18	10.9408	26.515	57.7885	54.2028
78	6/29/2007	T08-29-36	35.6154	36.7739	65.6889	65.3524
79	6/30/2007	T07-33-59	37.3368	40.5415	79.0935	78.1061
80	6/30/2007	T09-12-49	12.1499	18.8861	60.618	59.112
81	7/3/2007	T08-04-43	35.6539	36.6791	71.8649	71.567

A total of 81 potential heavy aerosol cases are identified. Among the 81 cases, 43 of them are optically thin dust/smoke events over elevated terrains (e.g., near the Himalayan and Tibeten plateaus) that have strong OMI AI signals due to high elevations. Because HAIS is designed to detect heavy aerosol plumes, only the remaining 38 potential heavy aerosol cases are used for further evaluation.

Of the 38 heavy dust and smoke aerosol cases, HAIS is able to successfully identify 27 of them, including 3 heavy aerosol cases (one dust aerosol and two smoke aerosol cases) that are misclassified by CALIOP as clouds. Of the 11 heavy smoke

and dust aerosol cases that are misidentified by HAIS, 7 of them have aerosol plumes touching the ground. When an aerosol layer is very close to the ground, strong ground signals can be misidentified as clouds by HAIS and this causes HAIS to fail. The remaining four cases are dust aerosol cases for which dust plumes are misidentified as clouds.

Note that HAIS is designed to detect heavy smoke aerosol cases. If we separate the 38 heavy aerosol cases into 8 smoke aerosol cases and 30 dust aerosol cases, HAIS could successfully detect 7 of the 8 cases. The only failed case is due to ground contamination. Those case studies suggest that HAIS is functioning well in detecting heavy smoke aerosol plumes, but it has a limitation in detecting heavy aerosol plumes that are near the ground.

It is worth mentioning that although CALIOP data can be used to identify aerosol plumes with a relatively high successful rate (78 of 81 cases), CALIOP data cannot be used alone to detect heavy aerosol plumes for two reasons. First, as indicated earlier, there are cases in which heavy smoke/dust aerosols plumes are misidentified as clouds by CALIOP. Also, for a heavy aerosol scene, CALIOP-measured backscattering values can be significantly attenuated by the aerosol layer. For example, as shown in Figure 42, very low CALIOP AODs of less than 0.2 are reported over heavy aerosol polluted regions. Also, for the 38 heavy aerosol cases as identified in this section, the averaged CALIOP case-maximum AODs is 0.85, while a much higher averaged AOD of 2–4 is expected as discussed subsequently. Thus, by simply evaluating CALIOP data, it is difficult to single out heavy aerosol cases from medium to low aerosol-loading cases due to the strong attenuation of CALIOP signals

by the heavy aerosol plumes. Thus, HAIS is needed to identify and study heavy aerosol plumes.

7.4 Results

7.4.1 Investigation of the misclassification-induced low bias in DT and DB aerosol products

In this section, the newly developed HAIS is applied to all collocated OMI, CALIOP and MODIS data pairs over Asia (70°–180° E and -15° S–80° N) for 2007. The number of heavy aerosol CALIOP scenes, as identified by HAIS, is obtained for regions with OMI AI > 2.

Of a total of ~100,000 CALIOP detected aerosol pixels, only 1,213 potential clear-sky heavy-aerosol (PCSHA) pixels are identified by HAIS. Thus, from a climatology perspective, the misclassification introduced low bias is statistically insignificant (1.6%). However, those heavy aerosol events are important for aerosol modeling studies and thus need to be further evaluated.

Among the 1,213 PCSHA cases (hereafter referred to all cases), 782 of them are CALIPSO identified non-dust cases. Here non-dust cases include cases such as smoke and polluted continental aerosol contaminated scenes. Only 40% (57%) of all (non-dust) HAIS identified heavy aerosol cases have valid MODIS DT retrievals and the corresponding numbers are 66% (59%) for MODIS DB retrievals.

Note that for heavy aerosol polluted regions with no valid DT and/or DB retrievals, the above-mentioned misclassification is not the only cause. For example, The MODIS DT retrievals are only applied to 10 × 10 km areas that have at least 10%

138

of the dark pixels (Levy et al., 2005). No MODIS DT retrievals are available over bright surfaces such as desert regions (Levy et al., 2005; Levy et al., 2010). Similarly, MODIS DB retrievals are not performed over complicated terrain surfaces (Hsu et al., 2013). To estimate the fractions of such cases, seasonally-based spatial distributions of retrieval density (number of retrievals) are constructed using one year of MODIS DT and DB data at a spatial resolution of 0.17° Lat/Lon (Figure 46). Here we assume that surface characteristics remain constant within a season, and thus the 0.17° Lat/Lon bins that have more than two valid DT/DB retrievals are considered to be the regions that are suitable for DT/DB algorithms.

Upon removing 0.17° Lat/Lon bins that have less than two DT/DB retrievals, for the remaining regions, we assume that the missing retrievals over heavy aerosol polluted regions, as indicated by HAIS, are from the misclassification of aerosol plumes as clouds. It is estimated that around 34% (42%) of all (non-dust) heavy aerosol cases, as indicated by HAIS, are misclassified as clouds by MODIS DT retrievals, and corresponding numbers are 33% (40%) for MODIS DB data.

Lastly, uncertainties exist in these estimates. First of all, CALIOP and MODIS observations have different fields of views and pixel sizes, which could introduce a sampling related bias. To exclude regions that are not suitable for MODIS DT/DB retrievals, seasonal-based retrieval density maps were constructed by assuming surface characteristics are rather invariant within a given season. However, surface characteristics may vary within a given season due to issues such as regional snow events. Still, this is the first time the misclassification-induced bias has been evaluated.
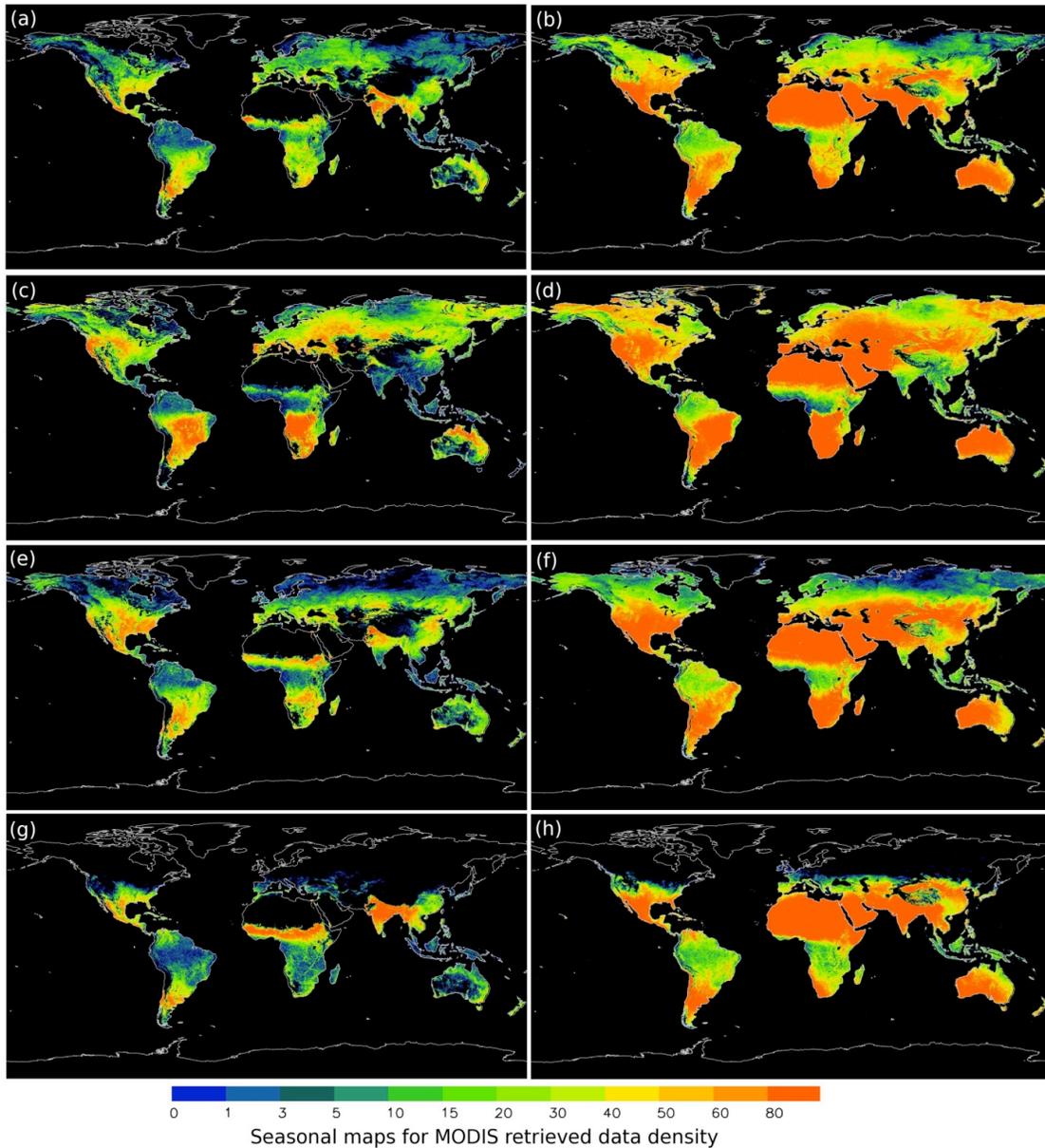
Figure 46. Seasonal distributions of retrieval density (number of retrievals) per 0.17 ° Lat/Lon for DT and DB from 2007. From the top to bottom, the four panels show retrieval densities for four seasons: spring, summer, autumn, and winter. The left column is for DT and the right column is for DB.

7.4.2 Study observing conditions that trigger the misclassification

As a follow-up question, it is important to study the observing conditions under which this misclassification occurs. One direct way of assessing this problem is to use CALIOP AOD, which was computed by integrating total extinction through

140

a column. However, as shown in Figure 47, a significant low bias is found in CALIOP AOD relative to MODIS DT and DB AOD. This low bias is understandable and expected. This is because CALIOP signals can be attenuated by an aerosol or cloud layer. Thus, when computing CALIOP AOD values, especially for optically thick aerosol plumes, this attenuation needs to be considered; however, it is not accounted for in this study.

Attempts have also been made to estimate AODs from OMI AIs. This was done by stratifying OMI AI as a function of AOD_{DT} or AOD_{DB} for various observation conditions as shown in Figure 48. The estimated average AOD values from this AI-AOD based relationships are 2.05 (2.64) and 2.14 (2.39) for MODIS DT and DB products for the misclassified cases with values for non-dust cases in the parenthesis. Still, converting OMI AI to AOD is a problem with large uncertainties because OMI AI is also sensitive to other atmospheric and surface properties such as the vertical distribution of an aerosol plume, surface reflectance, etc. Thus, the numbers computed from the OMI AI-AOD relationship can only provide a very rough estimate.

As an alternative approach, for an observed scene with aerosol plumes misclassified as clouds, the closest valid AOD retrievals may be used to estimate the AOD threshold that triggers the misclassification. This approach was applied at the granule (observed scene) level. By applying HAIS over Asia for 2007, a total of 61 misclassified MODIS scenes were identified. After excluding scenes that are either significantly contaminated by clouds or dusty cases, there are a total of seven
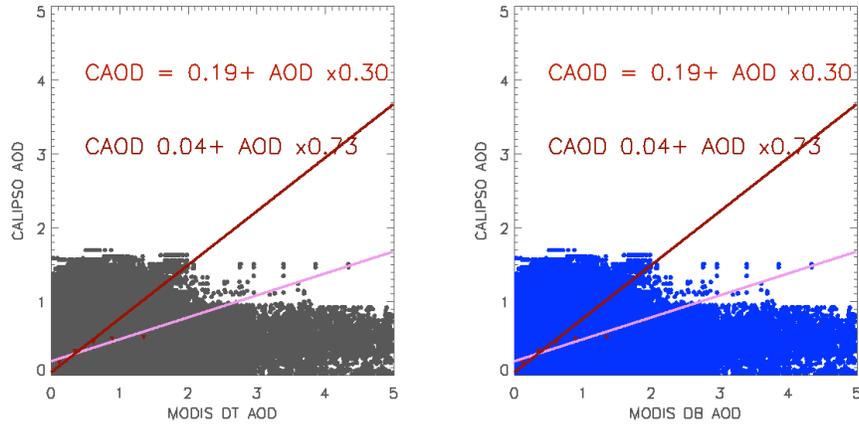
Figure 47. Comparisons between CALIOP AOD and c6 DT (a) and DB (b) AOD for 2007. The red line indicates a linear fit with all data and the pink line indicates a linear fit using averaged CALIOP AOD within each MODIS AOD bins.
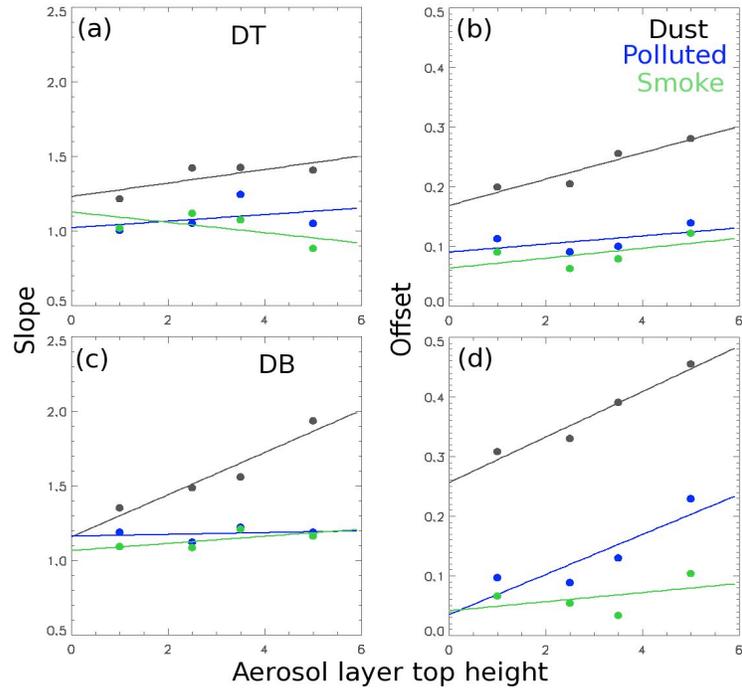
Figure 48. Slopes and offsets from AOD versus AI comparisons as functions of aerosol types and aerosol layer top height from CALIOP cloud and aerosol products using collocated MODIS, OMI, and CALIOP products from 2007. The left column is for slopes and the right column is for offsets. The top row is for DT and the bottom row is for DB.

142

Scenes remained for further analysis. Table 11 lists the dates and overpass times of these seven scenes. Of the seven selected heavy smoke aerosol scenes, the misclassification is found in all cases for DT retrievals. Misclassification also occurred for two of the seven scenes for DB retrievals.

Table 11 Locations and satellite overpass times of seven identified misclassification (misidentified aerosol plumes as clouds) cases. Also included are the causes for the misclassification, as well as the nearest available AOD retrievals.

Julian day/Year	72/2007	79/2007	88/2007	92/2007	92/2007	93/2007	205/2006
Time	0645	0655	0645	0620	0625	0705	0610
Cause A	DT 2.87		DT 2.07	DT 1.99	DT 2.81	DT 2.43	
Cause B		DT 3.20					DT 4.43
Cloud contamination	DB > 3.0		DB (1.5–3.0)				

For DT retrievals, the misidentification of aerosol plumes as clouds can be categorized into two scenarios: (1) high spatial variance in visible reflectance near emission source regions (cause A); (2) very optically thick homogenous aerosol plumes (cause B). The first scenario is illustrated in Figure 49. Similar as Figure 42, Figure 49 shows the MODIS RGB, AOD_{DT}, AOD_{DB}, and OMI AI (with CALIOP track over-plotted) over 93º–110º E and 18º–23º N for 6:20 UTC, April 2nd, 2007. A smoke plume is visible with clouds present in the top right corner. The OMI AI plot suggests that aerosol plumes are above a cloud deck around 102 ºE and 20 ºN. Also, at the center of the image, smoke emission sources are visible. Correspondingly, no AOD_{DT} retrievals are found near some of the emission sources, and a part of the reason is due to cloud contamination. Still, for the region around 97 ºE and 21.5 ºN, where no clouds are apparent, no retrievals are reported from the DT products,

possibly due to high variability in visible reflectance over that region. Besides the 2 April, 2007 case, similar situations are found for other three scenes (13 March, 2007, 29 March, 2007, and 3 April, 2007). The closest AOD retrievals to the missing-data region are found to be around 2.0–2.8 (0.55μm).

Figure 42 shows a case where misclassification is caused by a very optical thick smoke plume. As mentioned before, no retrieval is performed at the center of the plume for the DT products. The largest reported AOD_{DT} near the bottom left branch of the smoke plume is 4.43. A similar situation occurred on 20 March, 2007, when the closest available AOD retrieval is 3.2.

Due to rather limited cases, it is unclear under what observing conditions misclassification occur for DB data, such as the case shown in Figure 49. In Figure 49, no DB retrievals are reported in the top right corner near 104º E and 21º N. However, the aerosol plume is rather homogeneous with the reported AOD_{DT} values of 2–3. Still, there are two cases (13 Marc, 2007 and 29 Marc, 2007) for which above cloud aerosols are misclassified as cloud-free aerosol events. Since OMI AI values are used to rescue heavy aerosol cases in the DB algorithm (Hsu et al., 2013), it is possible that some of the above cloud aerosol events, which have high OMI AI values, are misidentified as cloud-free aerosol cases (e.g. Figure 50). Lastly, details of the seven selected cases, as well as the thresholds found, both for DB and DT products, are listed in Table 11.
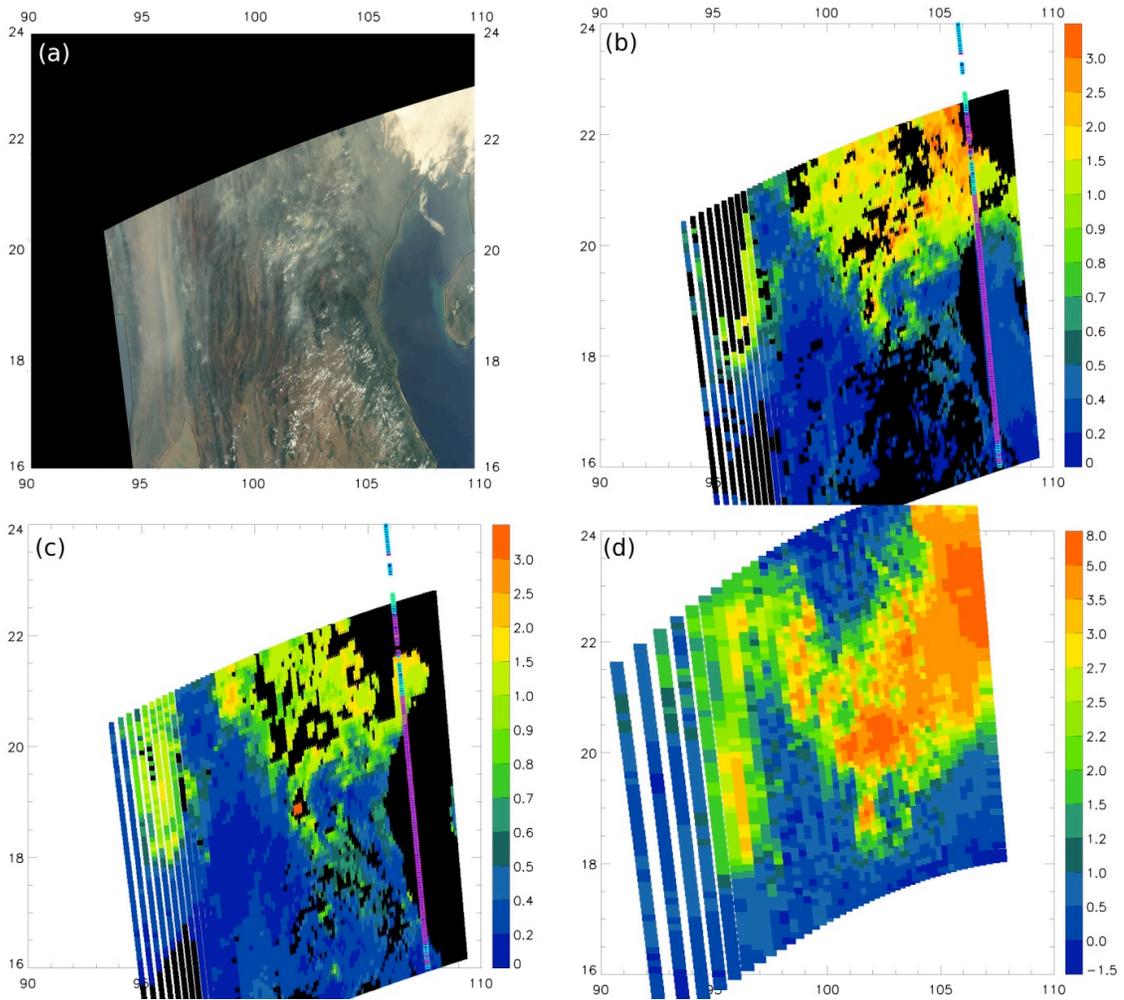
Figure 49. Similar to Figure 42 but for 2 April, 2007 (092–0620) over 93 °–110 ºE and 18 °–23 ºN.

7.5 Conclusion

Both passive-based and active-based satellite studies may misclassify thick aerosol plumes as clouds and thus introduce a low bias in satellite AOD estimations. In this study, a heavy aerosol identifying system (HAIS) was developed with the use of CALIOP level 1B data, CALIOP cloud and aerosol product, and OMI AI to distinguish heavy aerosol plumes from clouds for CALIOP observations. HAIS has been tested with case studies and extensive manual-checks. These evaluation steps
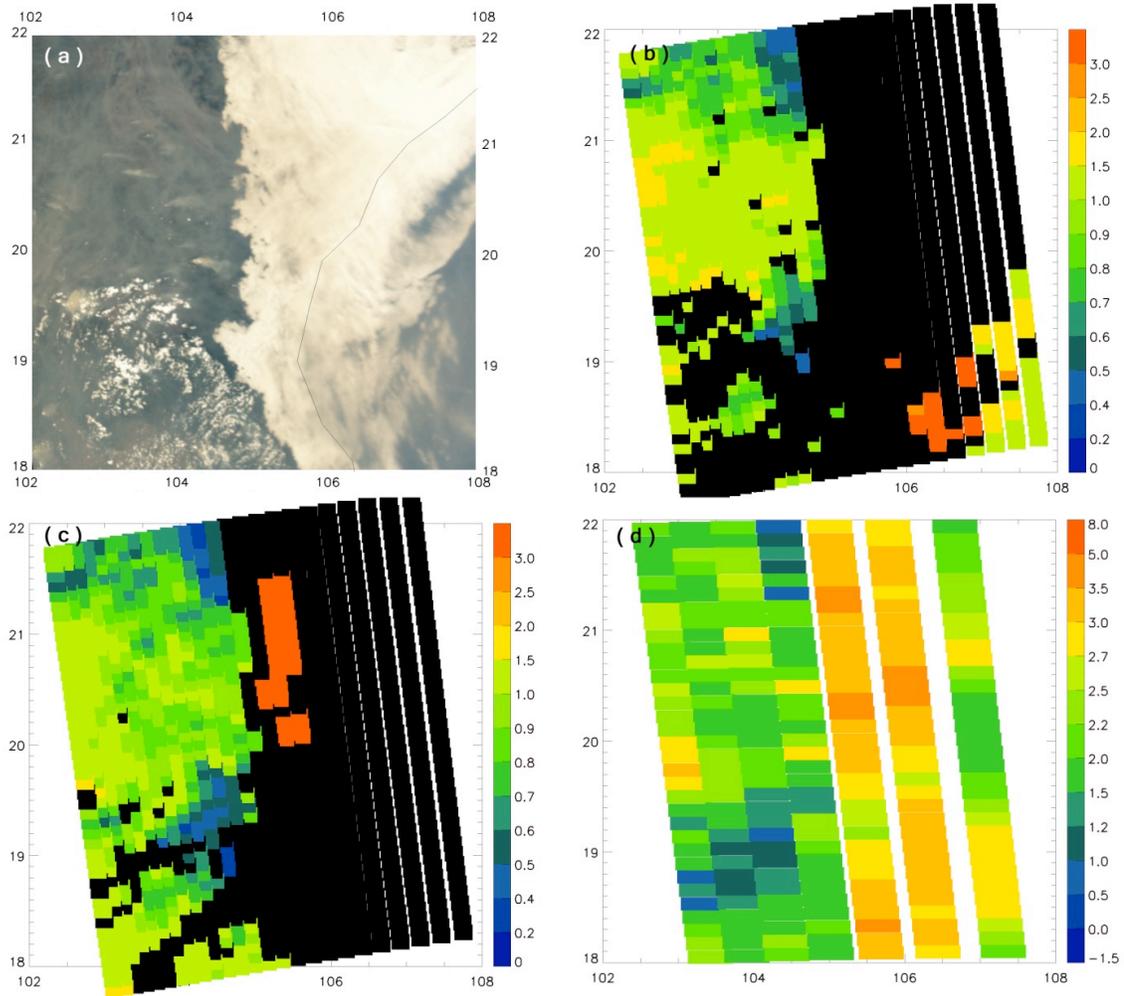
Figure 50. Similar to Figure 42 but for 13 March, 2007 (072–0645) over 102º–108 ºE and 18º–22 ºN.

suggest that HAIS is capable of distinguishing thick smoke aerosol plumes from clouds for CALIOP observations. This study also suggests that due to strong attenuation, CALIOP data cannot be used alone to single out heavy smoke aerosol events.

Applying the newly developed HAIS over Asia, this study suggests that heavy aerosol events are rather infrequent and the corresponding AOD low bias does not have a significant contribution to the regional AOT climatology over Asia. However,

it is necessary to study the misclassification of heavy aerosol plumes as clouds for aerosol modeling efforts.

This study also shows that of the HAIS identified PCSHA smoke cases, about 42% (40%) are misclassified by DT (DB) retrievals as clouds. The misclassified cases can be categorized into two scenarios: (1) inhomogeneous smoke plumes near emission-source regions and (2) very optically thick smoke plumes. Correspondingly, the misclassification thresholds with respect to AOD (0.55μm) are found to be 2.0–2.8 and 3.2–4.4 for DT respectively. The misclassification rate is low for DB retrievals. However, there are cases in which above cloud aerosol events are misidentified as cloud-free aerosol cases with erroneous high AOD values reported.

CHAPTER VIII

CONCLUSIONS

In an effort to construct quality-assured and bias-reduced datasets for aerosol analyses and forecasts, this study investigated uncertainties in MODIS DT, DB, and MISR aerosol products. Beyond the M.S. study completed by this author, which focused on evaluating the c5 DT over-ocean aerosol products, this research effort emphasized c5 and c6 DB (Aqua only for c6) products and MISR v22 aerosol products, with the use of ground-based observations. In addition, inter-comparisons were conducted among products to evaluate performance of those products over regions with limited or none ground-based observations. Upon gaining an improved understanding of uncertainties and bias in each product, procedures were developed to construct DA-quality level 3 aerosol products with reduced noise and bias for potential use in satellite aerosol data assimilation. In addition, very optically thick aerosol plumes, which have high visible albedoes and may be misclassified as clouds by both active- and passive-based aerosol retrievals, could be excluded from the operational MODIS and MISR products. Being able to identify and predict such events are critical to modeling related studies. Thus, in the last section of the study, this misclassification-related low bias was studied.

As a first step, three years of collocated c5 MODIS DT, DB, and version 22 MISR aerosol products were spatially compared. While similar spatial distributions of major aerosol features are found from all satellite aerosol products,

large discrepancies are also observable in reported AOD values. In particular, significant differences in AODs are found between satellite aerosol products over China and Southeast Asia. Clearly, those are the regions that deserve further attention in later studies.

Evaluations of selected products, starting with the MODIS c5 DB aerosol products were conducted. Empirically correctable biases, such as uncertainties related to aerosol microphysical properties and surface characteristics, were identified. Observing conditions that led to large AOD uncertainties were also identified. Both of these were used to develop procedures for constructing bias- and noise- reduced level 3 DA-quality AOD data over North Africa and the Arabian Peninsula for modeling applications. Last year, the new collection 6 Aqua MODIS DT and DB products were released, and thus, updates were also made to generate DA-quality c6 DT over-ocean and DB aerosol products.

Similar procedures were also applied on the MISR v22 AOD product, with a focus on developing a method for cloud clearing of MISR AOD data using MODIS observations. This is needed as MISR lacks thin cirrus cloud-sensitive channels. Onboard the same satellite platform, MODIS has the 1.38-μm channel that can be used to detect optically thin clouds. Thus, MODIS data can be used for further cloud clearing of MISR data. It is found that thin-cirrus cloud contamination exists in the MISR aerosol product and introduces an AOD bias of ~0.01 over global oceans, with a higher bias of ~0.015–0.02 over mid- to high- latitude oceans.

In regions such as Asia, heavy aerosol plumes are rather frequent. However, those heavy aerosol features could be misidentified as clouds by satellite aerosol

retrieval algorithms, thus introducing a low bias in both passive- and active-based satellite AOD climatologies. To evaluate this issue, HAIS was developed to "rescue" misclassified aerosol features using OMI AI, CALIOP cloud and aerosol products and CALIOP level 1b data. Evaluated through case studies and extensive hand checks, it is found that although HAIS has difficulty in identifying near surface aerosol plumes, HAIS is capable of detecting elevated thick smoke aerosol plumes with a high successful rate, and is able to identify elevated smoke aerosol features that are misclassified as clouds by CALIOP. With the use of HAIS, the low bias that is related to the misclassification of smoke aerosol plumes as clouds was investigated using one year of collocated OMI, CALIOP, and MODIS data. This study suggests that the frequency of occurrence of such misclassified events is rather low, and thus introduces an insignificant low bias to the passive-based satellite AOD climatology over Asia. However, these heavy aerosol events influence regional air quality and visibility, which further have impacts on public health and could introduce economic impacts. These optically thick smoke events may also alter the regional 3-D radiation budget, which directly affect weather forecasts and possibly meso- and synoptic scale atmospheric circulations. Thus, "rescuing" those misclassified aerosol features is critical for accurate aerosol forecasts of major aerosol events. Thresholds that trigger misclassification events were estimated.

Lastly, the c6 Terra MODIS DT and DB products were released early this year. Thus, as a part of a future study, research approaches and knowledge gained from this study will be applied to c6 Terra MODIS aerosol products. With the development of quality assured aerosol products from MODIS and MISR, it is

possible to construct a combined aerosol product for both climate and modeling applications. The developments of quality assured aerosol products from MODIS and MISR will also enable further study of true uncertainties and limitations in current satellite-data related aerosol climate studies.

REFERENCES

Al-Saadi, J., Szykman, J., Pierce, R. B., Kittaka, C., Neil, D., Chu, D. A., ... & Fishman, J. (2005). Improving national air quality forecasts with satellite aerosol observations. Bulletin of the American Meteorological Society, 86(9), 1249-1261.

Ackerman, S. A., Strabala, K. I., Menzel, W. P., Frey, R. A., Moeller, C. C., & Gumley, L. E. (1998). Discriminating clear sky from clouds with MODIS. Journal of Geophysical Research: Atmospheres (1984–2012), 103(D24), 32141-32157.

Ackerman, S. A., Holz, R. E., Frey, R., Eloranta, E. W., Maddux, B. C., & McGill, M. (2008). Cloud detection with MODIS. Part II: validation. Journal of Atmospheric and Oceanic Technology, 25(7), 1073-1086.

Balkanski, Y. J., Jacob, D. J., Gardner, G. M., Graustein, W. C., & Turekian, K. K. (1993). Transport and residence times of tropospheric aerosols inferred from a global three-dimensional simulation of 210_Pb.

Bellouin, N., O. Boucher, J. Haywood, and M. S. Reddy, (2005), Global Estimate of Aerosol Direct Radiative Forcing from Satellite Measurements, Nature Vol 438|22/29 December 2005|DOI:10.1038/nature 04348.

Benedetti, A., Morcrette, J. J., Boucher, O., Dethof, A., Engelen, R. J., Fisher, M., ... & Suttie, M. (2009). Aerosol analysis and forecast in the European centre for medium-range weather forecasts integrated forecast system: 2. Data assimilation. *Journal of Geophysical Research: Atmospheres (1984–2012),114*(D13).

Blifford, I. H., Lockhart, L. B., & Rosenstock, H. B. (1952). On the natural radioactivity in the air. Journal of Geophysical Research, 57(4), 499-509.

Bond, T. C., Doherty, S. J., Fahey, D. W., Forster, P. M., Berntsen, T., DeAngelo, B. J., ... &Zender, C. S. (2013). Bounding the role of black carbon in the climate system: A scientific assessment. Journal of Geophysical Research: Atmospheres, 118(11), 5380-5552.

Bull et al. (2010) MISR Data Products Specifications Document, JPL D-13963, Revision S.

Campbell, J. R., Reid, J. S., Westphal, D. L., Zhang, J., Hyer, E. J., and Welton, E. J. (2010) CALIOP aerosol subset processing for global aerosol transport model data assimilation, IEEE Journal of Selected Topics in Applied Earth Observations and Remote Sensing, Volume: 3, Issue: 2, pp.203-214, 10.1109/JSTARS.2010.2044868.

Campbell, J. R., Tackett, J. L., Reid, J. S., Zhang, J., Curtis, C. A., Hyer, E. J., ... & Winker, D. M. (2012). Evaluating nighttime CALIOP 0.532 μm aerosol optical depth and extinction coefficient retrievals. *Atmos. Meas. Tech. Discuss*, *5*(2), 2747-2794.

CCSP, (2009). Atmospheric aerosol properties and climate impacts, A report by the U.S. Climate Change Science Program and the Subcommittee on Global Change Research. [Mian Chin, Ralph A. Kahn, and Stephen E. Schwartz (eds.)]. National Aeronautics and Space Administration, Washington, D.C., USA, 128 pp.

Chan, C. K., & Yao, X. (2008). Air pollution in mega cities in China. Atmospheric environment, 42(1), 1-42.

Charlson, R. J., Schwartz, S. E., Hales, J. M., Cess, R. D., COAKLEY, J. J., Hansen, J. E., & Hofmann, D. J. (1992). Climate forcing by anthropogenic aerosols. Science, 255(5043), 423-430.

Chew, B. N., Campbell, J. R., Reid, J. S., Giles, D. M., Welton, E. J., Salinas, S. V., & Liew, S. C. (2011). Tropical cirrus cloud contamination in sun photometer data. Atmospheric Environment, 45(37), 6724-6731.

Christopher, S. A., Zhang, J., Kaufman, Y. J., & Remer, L. A. (2006). Satellite-based assessment of top of atmosphere anthropogenic aerosol radiative forcing over cloud-free oceans. Geophysical research letters, 33(15).

Di Girolamo, Larry, and Davies, R. (1994). A Band-Differenced Angular Signature technique for cirrus cloud detection. Geoscience and Remote Sensing, IEEE Transactions on 32, no. 4: 890-896.

Diner, D. J., Abdou, W. A., Bruegge, C. J., Conel, J. E., Crean, K. A., Gaitley, B. J., ... &Holben, B. N. (2001). MISR aerosol optical depth retrievals over southern Africa during the SAFARI‐2000 dry season campaign. Geophysical Research Letters, 28(16), 3127-3130.

Diner, D. J., Beckert, J. C., Reilly, T. H., Bruegge, C. J., Conel, J. E., Kahn, R., ... & Verstraete, M. M. (1998). Multi-angle Imaging SpectroRadiometer (MISR) instrument description and experiment overview. Geoscience and Remote Sensing, IEEE Transactions on, 36(4), 1072-1087.

Dubovik, O., & King, M. D. (2000). A flexible inversion algorithm for retrieval of aerosol optical properties from Sun and sky radiance measurements. Journal of Geophysical Research: Atmospheres (1984–2012), 105(D16), 20673-20696.

Dubovik, O., Holben, B., Eck, T. F., Smirnov, A., Kaufman, Y. J., King, M. D., ... & Slutsker, I. (2002). Variability of absorption and optical properties of key aerosol types observed in worldwide locations. Journal of the atmospheric sciences, 59(3), 590-608.

Duce, R. A., Unni, C. K., Ray, B. J., Prospero, J. M., & Merrill, J. T. (1980). Long-range atmospheric transport of soil dust from Asia to the tropical North Pacific: Temporal variability. *Science*, *209*(4464), 1522-1524.

Eck, T. F., Holben, B. N., Reid, J. S., Dubovik, O., Smirnov, A., O'neill, N. T., ... & Kinne, S. (1999). Wavelength dependence of the optical depth of biomass burning, urban, and desert dust aerosols. Journal of Geophysical Research: Atmospheres (1984–2012), 104(D24), 31333-31349.

Eck, T. F., Holben, B. N., Dubovik, O., Smirnov, A., Goloub, P., Chen, H. B., ... & Slutsker, I. (2005). Columnar aerosol optical properties at AERONET sites in central eastern Asia and aerosol transport to the tropical mid‑Pacific. Journal of Geophysical Research: Atmospheres (1984–2012), 110(D6).

Eck, T. F., Holben, B. N., Sinyuk, A., Pinker, R. T., Goloub, P., Chen, H., ... & Xia, X. (2010). Climatological aspects of the optical properties of fine/coarse mode aerosol mixtures. *Journal of Geophysical Research: Atmospheres (1984–2012)*, *115*(D19).

Frey, R. A., Acherman,S. A., Liu,Y.,Strabala, K. I., Zhang,H., Key, J. R., and Wang, X. (2008) Cloud detection with MODIS. Part I: Improvements in the MODIS cloud mask for Collection 5. J. Atmos. Oceanic Technol., 25, 1057–1072.

Gao, B. C., Yang, P., Han, W., Li, R. R., &Wiscombe, W. J. (2002). An algorithm using visible and 1.38-μm channels to retrieve cirrus cloud reflectances from aircraft and satellite data. Geoscience and Remote Sensing, IEEE Transactions on, 40(8), 1659-1668.

Gao, B. C., & Kaufman, Y. J. (2003). Water vapor retrievals using Moderate Resolution Imaging Spectroradiometer (MODIS) near‑infrared channels. Journal of Geophysical Research: Atmospheres (1984‑2012), 108(D13).

Gautam, R., Liu, Z., Singh, R. P., & Hsu, N. C. (2009). Two contrasting dust-dominant periods over India observed from MODIS and CALIPSO data. *Geophysical Research Letters*, *36*(6).

Ginoux, P., Garbuzov, D., & Hsu, N. C. (2010). Identification of anthropogenic and natural dust sources using Moderate Resolution Imaging Spectroradiometer (MODIS) Deep Blue level 2 data. Journal of Geophysical Research: Atmospheres (1984–2012), 115(D5).

Giorgi, F., &Chameides, W. L. (1986). Rainout lifetimes of highly soluble aerosols and gases as inferred from simulations with a general circulation model. *Journal of Geophysical Research: Atmospheres (1984–2012)*, *91*(D13), 14367-14376.

Haxel, O., & Schumann, G. (1955). Selbstreinigung der atmosphäre. Zeitschrift für Physik, 142(2), 127-132.

Haywood, J., & Boucher, O. (2000). Estimates of the direct and indirect radiative forcing due to tropospheric aerosols: A review. REVIEWS OF GEOPHYSICS-RICHMOND VIRGINIA THEN WASHINGTON-, 38(4), 513-543.Charlson, R. J., Schwartz, S. E., Hales, J. M., Cess, R. D., COAKLEY, J. J., Hansen, J. E., & Hofmann, D. J. (1992). Climate forcing by anthropogenic aerosols. Science, 255(5043), 423-430.

Hogan, T. F., and Rosmond, T. E. (1991), The Description of the Navy Operational Global Atmospheric Prediction Systems Spectral Forecast Model, Mon. Weather Rev., 119(8), 1786-1815,DOI:10.1175/1520-0493(1991)119<1786: TDOTNO>2.0.CO:2.

Holben, B. N., T. F. Eck, I. Slutsker, D. Tanré, J. P. Buis, A. Setzer, E. Vermote, J. A. Reagan, Y. J. Kaufman, T. Nakajima, F. Lavenu, I. Jankowiak, and A. Smirnov, (1998), AERONET-A Federated Instrument Network and Data Archive for Aerosol Characterization Remote Sens. Environ. 66:1-16 PI1 s003-4257(98)00031-5.

Holben, B. N., Eck, T. F., Slutsker, I., Smirnov, A., Sinyuk, A., Schafer, J., ... & Dubovik, O. (2006, December). AERONET's version 2.0 quality assurance criteria. In Asia-Pacific Remote Sensing Symposium (pp. 64080Q-64080Q). International Society for Optics and Photonics.

Hollingsworth, A., Engelen, R. J., Textor, C., Benedetti, A., Boucher, O., Chevallier, F., ... & Simmons, A. (2008). The Global Earth-system Monitoring using Satellite and in-situ data (GEMS) Project: Towards a monitoring and forecasting system for atmospheric composition. Am. Meteorol. Soc, 89(8), 1147-1164.

Hsu, N. C., Tsay, S. C., King, M. D., & Herman, J. R. (2004). Aerosol properties over bright-reflecting source regions. Geoscience and Remote Sensing, IEEE Transactions on, 42(3), 557-569.

Hsu, N. C., Tsay, S. C., King, M. D., & Herman, J. R. (2006). Deep blue retrievals of Asian aerosol properties during ACE-Asia. Geoscience and Remote Sensing, IEEE Transactions on, 44(11), 3180-3195.

Hsu, N. C., M. J. Jeong, C. Bettenhausen, A. M. Sayer, R. Hansell, C. S. Seftor, J. Huang, and S.-C. Tsay (2013), Enhanced Deep Blue aerosol retrieval algorithm: The second generation, J. Geophys. Res. Atmos., 118, 9296–9315, doi:10.1002/jgrd.50712 Sayer, A. M., N. C. Hsu, C.

Hunt, W. H., Winker, D. M., Vaughan, M. A., Powell, K. A., Lucker, P. L., & Weimer, C. (2009). CALIPSO lidar description and performance assessment. Journal of Atmospheric and Oceanic Technology, 26(7), 1214-1228.

Husar, R. B., Prospero, J. M., & Stowe, L. L. (1997). Characterization of tropospheric aerosols over the oceans with the NOAA advanced very high resolution radiometer optical thickness operational product. Journal of Geophysical Research: Atmospheres (1984–2012), 102(D14), 16889-16909.

Husar, R. B., Tratt, D. M., Schichtel, B. A. B. A., Falke, S. R., Li, F., Jaffe, D., ...&Malm, W. C. (2001). Asian dust events of April 1998. *Journal of Geophysical Research*, *106*(D16), 18317-18330.

Hyer, E. J., Reid, J. S., & Zhang, J. (2011). An over-land aerosol optical depth data set for data assimilation by filtering, correction, and aggregation of MODIS Collection 5 optical depth retrievals. Atmospheric Measurement Techniques, 4(3), 379-408.

Jaffe, D., Anderson, T., Covert, D., Kotchenruther, R., Trost, B., Danielson, J., ...& Uno, I. (1999).Transport of Asian air pollution to North America.*Geophysical Research Letters*, *26*(6), 711-714.

Johnson, D. W., Kilsby, C. G., McKenna, D. S., Saunders, R. W., Jenkins, G. J., Smith, F. B., & Foot, J. S. (1991). Airborne observations of the physical and chemical characteristics of the Kuwait oil smoke plume. *Nature*, *353*(6345), 617-621.

Kahn, R. A., Gaitley, B., Martonchik, J., Diner, D., Crean, K., & Holben, B. (2005). MISR global aerosol optical depth validation based on 2years of coincident Aerosol Robotic Network (AERONET) observations. J. Geophys. Res, 110, D10S04.

Kahn, R. A., Li, W.-H., Moroney, C., Diner, D. J., Martonchik, J. V., and Fishbein, E. (2007), Aerosol source plume physical characteristics from space-based multiangle imaging, J. Geophys. Res., 112, D11205, doi:10.1029/2006JD007647.

Kahn, R., Nelson, D. L., Garay, M. J., Levy, R. C., Bull, M., Diner, D. J., ... & Remer, L. (2009). MISR aerosol product attributes and statistical comparisons with MODIS. Geoscience and Remote Sensing, IEEE Transactions on, 47(12), 4095-4114.

Kahn, R. A., Gaitley, B. J., Garay, M. J., Diner, D. J., Eck, T. F., Smirnov, A., & Holben, B. N. (2010). Multiangle Imaging SpectroRadiometer global aerosol product assessment by comparison with the Aerosol Robotic Network. Journal of Geophysical Research: Atmospheres (1984–2012), 115(D23).

Kaufman, Y. J., & Nakajima, T. (1993). Effect of Amazon smoke on cloud microphysics and albedo: Analysis from satellite imagery.

Kaufman, Y. J., and R. S. Fraser, Control of the effect of smoke particles on clouds and climate by water vapor, Science, 277, 1636 –1639, 1997.

Kaufman, Y. J., Boucher, O., Tanré, D., Chin, M., Remer, L. A., &Takemura, T. (2005). Aerosol anthropogenic component estimated from satellite data. *Geophysical Research Letters*, *32*(17).

Kaufman, Y. J., Tanré, D., & Boucher, O. (2002). A satellite view of aerosols in the climate system.Nature, 419(6903), 215-223.

Lelieveld, J., Berresheim, H., Borrmann, S., Crutzen, P. J., Dentener, F. J., Fischer, H., ... & Ziereis, H. (2002). Global air pollution crossroads over the Mediterranean. Science, 298(5594), 794-799.

Levelt, P. F., Hilsenrath, E., Leppelmeier, G. W., J. van den Ooord, G. H., Bhartia, P. K., Taminnen, J., de Haan, J. F., and Veefkind J. P. (2006), Science objectives of the Ozone Monitoring Instrument, IEEE Trans. Geo. Remote Sens., 44(5), 1093–1101.

Levy, R. C., L. A. Remer, D. Tanré, Y. J. Kaufman, C. Ichoku, B. N. Holben, J. M. Livingston, P. B. Russell, and H. Maring (2003), Evaluation of the Moderate-Resolution Imaging Spectroradiometer (MODIS) retrievals of dust aerosol over the ocean during PRIDE, J.Geophys. Res., 108(D19), 8594, DOI: 10.1029/2002JD002460.

Levy, R. C., Remer, L. A., Martins, J. V., Kaufman, Y. J., Plana-Fattori, A., Redemann, J., & Wenny, B. (2005). Evaluation of the MODIS aerosol retrievals over ocean and land during CLAMS. Journal of the Atmospheric Sciences, 62(4), 974-992.

Levy, R. C., Remer, L. A., Kleidman, R. G., Mattoo, S., Ichoku, C., Kahn, R., & Eck, T. F. (2010), Global evaluation of the Collection 5 MODIS dark-target aerosol products over land. Atmospheric Chemistry and Physics, 10(21), 10399-10420.

Levy, R. C., Mattoo, S., Munchak, L. A., Remer, L. A., Sayer, A. M., & Hsu, N. C. (2013). The Collection 6 MODIS aerosol products over land and ocean. Atmos. Meas. Tech. Discuss, 6, 159-259.

Li, Qian, Li, C., Mao, J,: Evaluation of Atmospheric Aerosol Optical Depth Products at Ultraviolet Bands Derived from MODIS Products. Aerosol Science and Technology 46:9, 1025-1034, 2012

Loeb, N.G., and Manalo-Smith, N (2005), Top-of-Atmosphere Direct Radiative Effect of Aerosols over Global Oceans from Merged CERES and MODIS Observations, J. Climate, 18, 3506-3526, 2005.

Lohmann, U., &Feichter, J. (2005). Global indirect aerosol effects: a review. Atmospheric Chemistry and Physics, 5(3), 715-737.

Martonchik, J. V., D. J. Diner, B. Pinty, M. M. Verstraete, R. B. Myneni, Y. Knyazikhin, and H. R. Gordon, (1998), Determination of Land and Ocean Reflective, Radiative and Biophysical Properties Using Multi-angle Imaging, IEEE Trans. Geosci. Remote Sens., 36, 1266-1281, 1998.

Martonchik, J. V., Diner, D. J., Crean, K., & Bull, M. (2002). Regional aerosol retrieval results from MISR. Geoscience and Remote Sensing, IEEE Transactions on, 40(7), 1520-1531.

Martonchik, J. V., Diner, D. J., Kahn, R., Ackerman, T. P., Verstraete, M. M., Pinty, B., & Gordon, H. R. (1998). Techniques for the retrieval of aerosol properties over land and ocean using multiangle imaging.Geoscience and Remote Sensing, IEEE Transactions on, 36(4), 1212-1227.

Martonchik, J. V., Kahn, R. A., & Diner, D. J. (2009). Retrieval of aerosol properties over land using MISR observations. In Satellite Aerosol Remote Sensing Over Land (pp. 267-293). Springer Berlin Heidelberg.

McCormick, M. P., Thomason, L. W., &Trepte, C. R. (1995). Atmospheric effects of the Mt Pinatubo eruption. *Nature*, *373*(6513), 399-404.

Minnis, P., Harrison, E. F., Stowe, L. L., Gibson, G. G., Denn, F. M., Doelling, D. R., & Smith, W. L. (1993). Radiative climate forcing by the Mount Pinatubo eruption. *Science*, *259*(5100), 1411-1415.

Nakajima, T., Lavenu, F., Jankowiak, I., and Smirnov, A.: AERONET – a federated instrument network and data archive for aerosol characterization, Remote Sens. En- viron. 66, 1–16, 1998.

O'Neill, N. T., Eck, T. F., Smirnov, A., Holben, B. N., & Thulasiraman, S. (2003). Spectral discrimination of coarse and fine mode optical depth. Journal of Geophysical Research: Atmospheres (1984–2012), 108(D17).

Park, R. J., Jacob, D. J., Chin, M., & Martin, R. V. (2003). Sources of carbonaceous aerosols over the United States and implications for natural visibility. Journal of Geophysical Research: Atmospheres (1984–2012), 108(D12).

Penner, J. E., Charlson, R. J., Schwartz, S. E., Hales, J. M., Laulainen, N. S., Travis, L., ... &Radke, L. F. (1994). Quantifying and minimizing uncertainty of climate forcing by anthropogenic aerosols. Bulletin of the American Meteorological Society, 75(3), 375-400.

Pierce, J. R., Kahn, R. A., Davis, M. R., & Comstock, J. M. (2010). Detecting thin cirrus in Multiangle Imaging Spectroradiometer aerosol retrievals. Journal of Geophysical Research: Atmospheres (1984–2012), 115(D8).

Platnick, S., King, M. D., Ackerman, S., Menzel, W. P., Baum, B., Riédi, J. C., & Frey, R.(2003). The MODIS cloud products: Algorithms and examples from Terra. Geoscience and Remote Sensing, IEEE Transactions on, 41(2), 459-473.

Quaas, J., Boucher, O., &Lohmann, U. (2006).Constraining the total aerosol indirect effect in the LMDZ and ECHAM4 GCMs using MODIS satellite data.*Atmospheric Chemistry and Physics*, *6*(4), 947-955.

Quaas, J., Boucher, O., Bellouin, N., &Kinne, S. (2008).Satellite-based estimate of the direct and indirect aerosol climate forcing.*Journal of Geophysical Research: Atmospheres (1984–2012)*, *113*(D5).

Ramanathan, V., & Carmichael, G. (2008).Global and regional climate changes due to black carbon.Nature geoscience, 1(4), 221-227.reflecting source regions, IEEE T. Geosci. Remote, 42, 557–569, 2004.

Reid, J. S., Hobbs, P. V., Ferek, R. J., Blake, D. R., Martins, J. V., Dunlap, M. R., & Liousse, C. (1998). Physical, chemical, and optical properties of regional hazes dominated by smoke in Brazil. Journal of Geophysical Research: Atmospheres (1984–2012), 103(D24), 32059-32080.

Reid, J. S., Prins, E. M., Westphal, D. L., Schmidt, C. C., Richardson, K. A., Christopher, S. A., ... & Hoffman, J. P. (2004). Real‐time monitoring of South American smoke particle emissions and transport using a coupled remote sensing/box‐model approach. Geophysical Research Letters, 31(6).

Reid, J. S., Eck, T. F., Christopher, S. A., Koppmann, R., Dubovik, O., Eleuterio, D. P., ... & Zhang, J. (2005). A review of biomass burning emissions part III: intensive optical properties of biomass burning particles. Atmospheric Chemistry and Physics, 5(3), 827-849.

Reid, J. S., Hyer, E. J., Prins, E. M., Westphal, D. L., Zhang, J., Wang, J., ... & Hoffman, J. P. (2009). Global monitoring and forecasting of biomass-burning smoke: Description of and lessons from the Fire Locating and Modeling of Burning Emissions (FLAMBE) program. Selected Topics in Applied Earth Observations and Remote Sensing, IEEE Journal of, 2(3), 144-162.

Remer, L. A., Y. J. Kaufman, D. Tanré, S. Matoo, D. A. Chu, J. V. Martins, R.-R. Li, C. Ichoku, R. C. Levy, R. G. Kieidman, T. F. Eck, E. Vermote, and B. N. Holben, (2005), The MODIS Aerosol Algorithm, Products, and Validation, Journal of Atmospheric Sciences, vol. 62, Issue 4, pp.947-973 DOI: 10.1175/JAS3385.1.

Remer, L. A., Chin, M., DeCola, P., Feingold, G., Halthore, R., Kahn, R. A., Quinn, P. K., Rind, D., Schwartz, S. E., Streets, D., and Yu, H. (2009) Executive summary, atmospheric aerosol properties and climate impacts. A report by the U.S. climate change science program and the subcommittee on global change research, edited by: Chin, M., Kahn, R. A., and Schwartz, S. E., National Aeronautics and Space Administration, Washington, D.C., USA.

Rodhe, H. (1999). Human impact on the atmospheric sulfur balance. Tellus A, 51(1), 110-122.

Saide, P. E., G. R. Carmichael, Z. Liu, C. S. Schwartz, H. C. Lin, A. M. da Silva, and E. Hyer (2013), Aerosol optical depth assimilation for a sizeresolved sectional model: Impacts of observationally constrained, multi-wavelength and fine mode retrievals on regional scale analyses and forecasts, Atmos. Chem. Phys., 13, 10,425–10,444, doi:10.5194/acp-13-10425-2013.

Sassen, K., and Cho, B. S.: Subvisual-thin cirrus lidar dataset for satellite verification and climatological research, Journal of Applied Meteorology 31, no. 11 (1992): 1275-1285.

Sayer, A. M., Hsu, N. C., Bettenhausen, C., &Jeong, M. J. (2013). Validation and uncertainty estimates for MODIS Collection 6 "Deep Blue" aerosol data. Journal of Geophysical Research: Atmospheres, 118(14), 7864-7872.

Sayer, A. M., Hsu, N. C., Bettenhausen, C., Jeong, M. J. & Meister, G. (2015), Effect of MODIS Terra radiometric calibration improvements on Collection 6 Deep Blue aerosol products: validation and Terra/Aqua consistency. Journal of Geophysical Research: Atmospheres, submitted.

Schafer, J. S., Eck, T. F., Holben, B. N., Thornhill, K. L., Anderson, B. E., Sinyuk, A., Giles, D. M., Winstead, E. L., Ziemba, L. D., Beyersdorf, A. J., Kenny, P. R., Smirnov, A., and Slutsker, I.(2014), Intercomparison of aerosol single scattering albedo derived from AERONET surface radiometers and LARGE in-situ aircraft profiles during the 2011 DRAGON-MD and DISCOVER-AQ experiments, J. Geophys. Res.-Atmos., 119, 7439–7452

Sekiguchi, M. T., K. Suzuki, K. Kawamoto, A. Higurashi, D. Rosenfeld, I. Sano, and S. Mukai (2003), A study of the direct and indirect effects of aerosols using global satellite data sets of aerosol and cloud parameters, J. Geophys. Res., 108(D22), 4699, doi:10.1029/2002JD003359.

Sekiyama, T. T., Tanaka, T. Y., Shimizu, A., & Miyoshi, T. (2010). Data assimilation of CALIPSO aerosol observations. Atmospheric Chemistry and Physics, 10(1), 39-49.

Shi, Y., Zhang, J., Reid, J. S., Holben, B., Hyer, E. J., & Curtis, C. (2011a) An analysis of the collection 5 MODIS over-ocean aerosol optical depth product for its implication in aerosol assimilation. Atmospheric Chemistry and Physics, 11(2), 557-565.

Shi, Y., Zhang, J., Reid, J. S., Hyer, E. J., Eck, T. F., Holben, B. N., and Kahn, R. A. (2011b) A critical examination of spatial biases between MODIS and MISR aerosol products – application for potential AERONET deployment, Atmos. Meas. Tech., 4, 2823–2836, doi:10.5194/amt-4- 2823-2011.

Smirnov, A., Holben, B. N., Giles, D. M., Slutsker, I., O'Neill, N. T., Eck, T. F., ... & Diehl, T. L. (2011). Maritime Aerosol Network as a component of AERONET-first results and comparison with global aerosol models and satellite retrievals. Atmospheric Measurement Techniques Discussion, 4, 1-32.

Smirnov, A., Holben, B. N., T., Eck, Dubovik, O., Slutsker, I. (2000). Cloud-Screening and Quality Control Algorithms for the AERONET Database. Remote Sensing of Environment. 09/2000; 73(3):337-349. DOI: 10.1016/S0034-4257(00)00109-7

Stephens, G. L., Vane, D. G., Boain, R. J., Mace, G. G., Sassen, K., Wang, Z., et al. (2002), The CloudSat mission and the A-train,Bull. Am.Meteorol. Soc.,83, 1771–1790.

Sun, Y., Zhuang, G., Wang, Y., Han, L., Guo, J., Dan, M., ...&Hao, Z. (2004).The air-borne particulate pollution in Beijing—concentration, composition, distribution and sources.Atmospheric Environment, 38(35), 5991-6004.

Tackett, J. L., & Di Girolamo, L. (2009). Enhanced aerosol backscatter adjacent to tropical trade wind clouds revealed by satellite‐based lidar. Geophysical Research Letters, 36(14).

Tanré, D., Y.J. Kaufman, M. Herman, and S. Mattoo, (1997), Remote Sensing of Aerosol Properties Over Oceans Using the MODIS/EOS Spectral Radiances, J. Geophys. Res., VOL 102, No.D14, Page 16,971-16,988, July 27. 1997.

Technol.,26,1214–1228, 2009.

Tie, Xuexi, and Junji Cao. "Aerosol pollution in China: Present and future impact on environment." *Particuology* 7, no. 6 (2009): 426-431.

Torres, O., Bhartia, P. K., Herman, J. R., Sinyuk, A., Ginoux, P., &Holben, B. (2002). A long-term record of aerosol optical depth from TOMS observations and

comparison to AERONET measurements. Journal of the atmospheric sciences, 59(3), 398-413.

Torres, O., Tanskanen, A., Veihelman, B., Ahn, C., Braak, R., Bhartia, P. K.,Veefkind, P., and Levelt, P.: Aerosols and surface UV products from Ozone Monitoring Instrument observations (2007), An overview, J. Geophys. Res., 112, D24S47, doi:10.1029/2007JD008809.

Tosca, M. G., Randerson, J. T., Zender, C. S., Nelson, D. L., Diner, D. J., & Logan, J. A. (2011). Dynamics of fire plumes and smoke clouds associated with peat and deforestation fires in Indonesia. *Journal of Geophysical Research: Atmospheres (1984–2012)*, *116*(D8).

Toth, T. D., Zhang, J., Campbell, J. R., Reid, J. S., Shi, Y., Johnson, R. S., Smirnov, A., Vaughan, M. A., and Winker, D. M. (2013). Investigating Enhanced Aqua MODIS Aerosol Optical Depth Retrievals over the Mid-to-High Latitude Southern Oceans through Intercomparison with Co-Located CALIOP, MAN, and AERONET Datasets. J. Geophys. Res. Atmos., 118, 4700–4714, doi:10.1002/jgrd.50311.

Uno, I., K. Yumimoto, A. Shimizu, Y. Hara, N. Sugimoto, Z. Wang, Z. Liu, and D. M. Winker (2008), 3D structure of Asian dust transport revealed by CALIPSO lidar and a 4DVAR dust model, Geophys. Res. Lett., 35, L06803, doi:10.1029/2007GL032329.

Vadrevu, K. P., Ellicott, E., Giglio, L., Badarinath, K. V. S., Vermote, E., Justice, C., & Lau, W. K. (2012). Vegetation fires in the himalayan region–Aerosol load, black carbon emissions and smoke plume heights. *Atmospheric Environment*, *47*, 241-251.

Van Donkelaar, A., Martin, R. V., Brauer, M., Kahn, R., Levy, R., Verduzco, C., & Villeneuve, P. J. (2010). Global estimates of ambient fine particulate matter concentrations from satellite-based aerosol optical depth: development and application. Environmental health perspectives, 118(6), 847-855.

Van Donkelaar, A., Martin, R. V., Levy, R. C., da Silva, A. M., Krzyzanowski, M., Chubarova, N. E., ... & Cohen, A. J. (2011). Satellite-based estimates of ground-level fine particulate matter during extreme events: A case study of the Moscow fires in 2010. Atmospheric Environment, 45(34), 6225-6232.

VanCuren, R. A., & Cahill, T. A. (2002). Asian aerosols in North America: Frequency and concentration of fine dust. *Journal of Geophysical Research: Atmospheres (1984–2012)*, *107*(D24), AAC-19.

Wan, Z. (2008). New refinements and validation of the MODIS land-surface temperature/emissivity products. Remote Sensing of Environment, 112(1), 59-74.

Wang, J., Xu, X., Spurr, R., Wang, Y., & Drury, E. (2010). Improved algorithm for MODIS satellite retrievals of aerosol optical thickness over land in dusty atmosphere: Implications for air quality monitoring in China. Remote Sensing of Environment, 114(11), 2575-2583.

Weaver, C., da Silva, A., Chin, M., Ginoux, P., Dubovik, O., Flittner, D., ...& Gregg, W. (2007). Direct insertion of MODIS radiances in a global aerosol transport model.Journal of the atmospheric sciences, 64(3), 808-827.

Williams, J., Reus, M. D., Krejci, R., Fischer, H., &Ström, J. (2002). Application of the variability-size relationship to atmospheric aerosol studies: estimating aerosol lifetimes and ages. *Atmospheric Chemistry and Physics*,*2*(2), 133-145.

Winker, D. M., Hunt, H. H., and McGill, M. J. (2007) Initial performance assessment of CALIOP, Geophys. Res. Lett., 34, L19803, doi:10.1029/2007GL030135.

Winker, D. M., Vaughan, M. A., Omar, A., Hu, Y., Powell, K. A., Liu, Z., ... & Young, S. A. (2009). Overview of the CALIPSO mission and CALIOP data processing algorithms. Journal of Atmospheric and Oceanic Technology, 26(11), 2310-2323.

Witek, M. L., Garay, M. J., Diner, D. J., & Smirnov, A. (2013). Aerosol optical depths over oceans: A view from MISR retrievals and collocated MAN and AERONET in situ observations. Journal of Geophysical Research: Atmospheres, 118(22), 12-620.

Witte, J. C., Douglass, A. R., da Silva, A., Torres, O., Levy, R., and Duncan, B. N.: NASA A-Train and Terra observations of the 2010 Russian wildfires, Atmos. Chem. Phys., 11, 9287–9301, doi:10.5194/acp-11-9287-2011, 2011.

Yu, H., Dickinson, R. E., Chin, M., Kaufman, Y. J., Holben, B. N., Geogdzhayev, I. V., & Mishchenko, M. I. (2003). Annual cycle of global distributions of aerosol optical depth from integration of MODIS retrievals and GOCART model simulations. Journal of Geophysical Research: Atmospheres (1984–2012), 108(D3).

Yu, H., Kaufman, Y. J., Chin, M., Feingold, G., Remer, L. A., Anderson, T. L., ... & Zhou, M. (2006). A review of measurement-based assessments of the aerosol direct radiative effect and forcing. *Atmospheric Chemistry and Physics*, *6*(3), 613-666.

Zhang, J., Christopher, S. A., & Holben, B. N. (2001). Intercomparison of smoke aerosol optical thickness derived from GOES 8 imager and ground‐based Sun photometers. Journal of Geophysical Research: Atmospheres (1984‐2012), 106(D7), 7387-7397.

Zhang, J., and Christopher, S. A. (2003). Longwaveradiative forcing of Saharan dust aerosols estimated from MODIS, MISR, and CERES observations on Terra. *Geophysical Research Letters*, *30*(23).

Zhang, J., Reid, J. S., & Holben, B. N. (2005). An analysis of potential cloud artifacts in MODIS over ocean aerosol optical thickness products. Geophysical Research Letters, 32(15).

Zhang, J., and J. S. Reid (2006), MODIS aerosol product analysis for data assimilation: Assessment of level 2 aerosol optical thickness retrievals, J. Geophys. Res., Vol.111, D22207, doi:10.1029/2005JD006898.

Zhang, J., Reid, J. S., Westphal, D. L., Baker, N. L., & Hyer, E. J. (2008a). A system for operational aerosol optical depth data assimilation over global oceans. Journal of Geophysical Research: Atmospheres (1984–2012), 113(D10).

Zhang, J., Reid, J. S., Miller, S. D., & Turk, F. J. (2008b). Strategy for studying nocturnal aerosol optical depth using artificial lights. International Journal of Remote Sensing, 29(16), 4599-4613.

Zhang, J., and J. S. Reid (2009), An analysis of clear sky and contextual biases using an operational over ocean MODIS aerosol product, Geophys. Res. Lett., 36, L15824, doi:10.1029/2009GL038723.

Zhang, J., & Reid, J. S. (2010). A decadal regional and global trend analysis of the aerosol optical depth using a data-assimilation grade over-water MODIS and Level 2 MISR aerosol products. Atmospheric Chemistry and Physics, 10(22), 10949-10963.

Zhang, J., Campbell, J. R., Reid, J. S., Westphal, D. L., Baker, N. L., Campbell, W. F., & Hyer, E. J. (2011). Evaluating the impact of assimilating CALIOP‐derived aerosol extinction profiles on a global mass transport model. Geophysical Research Letters, 38(14).

Zhao, T. X. P., Chan, P. K., & Heidinger, A. K. (2013). A global survey of the effect of cloud contamination on the aerosol optical thickness and its long‐term trend derived from operational AVHRR satellite observations. Journal of Geophysical Research: Atmospheres, 118(7), 2849-2857.